Doctoral theses at NTNU, 2017:295

Anton Akulichev

Elastomer viscoelasticity and performance of seals in cold-climate applications

ISBN 978-82-326-2658-8 (printed ver.)
ISBN 978-82-326-2659-5 (electronic ver.)
ISSN 1503-8181

NTNU
Norwegian University of Science and Technology

NTNU
Norwegian University of Science and Technology
Thesis for the Degree of
Philosophiae Doctor
Faculty of Engineering
Department of Mechanical and Industrial Engineering

Doctoral theses at NTNU, 2017:295

NTNU
Norwegian University of Science and Technology

Anton Akulichev

Elastomer viscoelasticity and performance of seals in cold-climate applications

Thesis for the Degree of Philosophiae Doctor

Trondheim, December 2017

Norwegian University of Science and Technology
Faculty of Engineering
Department of Mechanical and Industrial Engineering

NTNU
Norwegian University of
Science and Technology

NTNU
Norwegian University of Science and Technology

Thesis for the Degree of Philosophiae Doctor

Faculty of Engineering
Department of Mechanical and Industrial Engineering

ISBN 978-82-326-2658-8 (printed ver.)
ISBN 978-82-326-2659-5 (electronic ver.)
ISSN 1503-8181

Doctoral theses at NTNU, 2017:295

Printed by NTNU Grafisk senter

Preface

This thesis has been submitted to the Norwegian University of Science and Technology (NTNU) for partial fulfilment of the requirements for the degree of Philosophiae Doctor (Ph.D.). The research has been chiefly carried out at the Department of Mechanical and Industrial Engineering (MTP) under supervision of Professor Andreas T. Echtermeyer and co-supervisor Professor Nuria Espallargas over a period from October 2014 to August 2017. Some work has been conducted by the author during his visits to Jülich research centre and SINTEF Materials and Chemistry in Oslo in 2015-2017.

This research is part of the collaborative project "Thermo Responsive Elastomer Composites for cold climate application (TREC)" financed by the Research Council of Norway (Project 234115 in the Petromaks2 programme), FMC Kongsberg Subsea AS and STATOIL Petroleum AS, with the research partners Norwegian University of Science and Technology (NTNU) and SINTEF Materials and Chemistry. This work was also supported in part by EU COST Action MP1303.

Abstract

The Ph.D. thesis addresses the issues of elastomer seals operating in cold climate areas like Arctic. The work is devoted to a better understanding of low-temperature behaviour of elastomer seals near the glass transition T_{g}. The main objective of the work is to understand the causes for seal failures in cold environment and to establish a correlation between the low-temperature performance of hydrogenated nitrile butadiene rubber (HNBR) seals and the composition and the properties of the material. The basic material studied is HNBR with 96 % saturated polybutadiene with 36 % acrylonitrile content and varied carbon black (CB) content from 0 to 50 phr (parts per hundred rubber). A set of material and seal experiments was designed and carried out together with a finite element analysis (FEA) approach in order to accomplish the set goal. The major findings and novel results are as follows:

1. The relaxation function of the HNBR is found to be independent of strain at low temperatures down to $-15\,^{\circ}\mathrm{C}$ ($\approx T_{\mathrm{g}} + 8\,^{\circ}\mathrm{C}$) or times higher than $\approx 10^{-3}$ s. Therefore, the relaxation function of HNBR needed for FEA or other modelling can be measured at one single strain relevant for the application using the most convenient deformation mode. The relaxation function is also unaffected by the CB at the indicated temperatures and times, however it exhibits an increasing strain or CB dependency if the material is brought deeper into the glass transition region.

2. Compression set as a measure of elastic recovery in HNBR is found to increase with cooling. Below T_{g}, the HNBR compression strain field in HNBR is "frozen-in", i.e. the HNBR compounds demonstrate no recovery regardless of the presence of CB. Equivalence of time and temperature on the cold compression set is also shown. A viscoelastic model for prediction of the cold compression set using the stress relaxation data is proposed and validated against the FEA and experimental results.

3. The effect of cold adhesion is studied using a pull-off test set-up at ambient and low temperatures. The adhesion of HNBR to clean and smooth steel substrate is found to be low (e.g. pull-off force per unit length of O-ring $f_c \approx 0.04$ N/mm for 10 % initial compression) at ambient temperature, while it dramatically increases below T_{g} and the pull-off force might reach 1-2 N/mm. The explanation is as follows. When the separation between HNBR and its counter-surface occurs at ambient temperature, the elastic deformation energy stored at the interface is given back during pull-off and helps to break the adhesive bonds resulting in the very small pull-off force values. When the contact pair formed at room temperature is cooled down below the T_{g} of HNBR, the elastic deformation imposed on the HNBR is "frozen-in" and the stored-up elastic energy is not given back during separation at the low temperature. This results in a giant pull-off force. It is also found that the contaminated or roughened contacting surfaces reduce f_c to about 0.2 N/mm due to incomplete contact (lower relative contact area).

4. The cold performance of O-ring seals made of the HNBR compounds is studied using a vacuum test fixture. The seal failure temperatures under freezing conditions depend on the surface finish of the counter-face, seal compression ratio, lubrication and additions of CB in HNBR. The main reason for the seal failures is believed to be detachment of the elastomer seals from their mating sealing parts due to :

    - breakage of the adhesion bond induced by the elastomer thermal contraction in case of a rather strong adhesion bond and negligible recovery of the HNBR below T_{g}
    - or due to the thermal contraction and the negligible recovery when the strong adhesion bond is not formed.

5. It is shown that most of the cold failures can be modelled by the effective medium leakage theory and a simple FEA approach using thermo-mechanical material data the most important of which are the thermal expansivity and small-strain viscoelasticity of the elastomer compounds. The CB filled HNBR has a lower thermal expansion which results in a better retention of the sealing force and lower leakage temperatures if compared to the seals made of the unfilled HNBR. Hence, it can be inferred that better low-temperature serviceability in static applications can be achieved using elastomer compounds with low coefficients of thermal expansion (CTE) ideally close to the one of the seal housing material.

6. The low-CTE HNBR can be produced by adding negative thermal expansion

(NTE) materials into the base elastomer composition. Low-CTE composites of $\mathrm{HNBR} - \mathrm{ZrW_2O_8}$ are produced and characterised in this work. The NTE effect in the composite is found to be stronger in the glassy state than in the rubbery plateau of the base elastomer. The reduction of CTE with the $\mathrm{ZrW_2O_8}$ content is well described by the simple rule of mixture at temperatures above T_g, while Kerner and the upper bound of the Schapery models as well as a FEA homogenisation approach fit the CTE results below T_g better. The models can, thus, be used for prediction of the CTE of other elastomer composites.

Acknowledgement

First and foremost, I would like to express my gratitude to my supervisor Professor Andreas Echtermeyer and my co-supervisor Professor Nuria Espallargas for giving me the opportunity to enter into the Ph.D. programme and gain this enormous knowledge over the last 3 years. Their invaluable encouragement, inspiration and support both technical and administrative were essential for the completion of my project. In addition, I would like to thank Dr. Ben Alcock at SINTEF M&K for his immense support in preparation of the TREC materials, guidance on the characterisation techniques and fruitful intellectual discussions.

Second, I thank the doctoral and post-doctoral fellows and the permanent staff at the Department of Mechanical and Industrial Engineering (MTP) for various support and assistance. Special mention is given to Abedin Gagani, Avinash Tiwari, Børge Holen, Carl Magnus Midtbø, Cristian Torres Rodriguez, Fahmi Mubarok, Gaute Stenerud, Søren Heinze, Szymon Bernat and Yun Deng for their time and help with consumables, workshop, various lab and office equipment as well as software. I am also deeply grateful to Mr. Halvard Støwer for his continuous assistance with electric parts and electronics I used. I would also like to acknowledge significant support and lots of useful advices in FEM I received from Dr. Nils Peter Vedvik and Sergey Shubin (IPME RAS, St. Petersburg). In addition, I would like to thank Andrejs Krauklis for proofreading the thesis.

Third, I would like to express my sincere gratitude to Dr. Bo Persson for excellent hosting at Jülich research centre, guiding me through the world of multi-scale contact mechanics and theoretical seal leakage and allowing me to use his codes.

Fourth, the project financial support from the Research Council of Norway, FMC Kongsberg Subsea AS and STATOIL Petroleum AS is gratefully acknowledged. In particular, I would like to thank Mr. Brede Thorkildsen at FMC for his excellent technical support, prompt feedback and great interest in this work. I would also like to acknowledge the travel support provided by EU Cost Action MP 1303.

Finally, my special appreciation is given to my beloved wife Natalia and my daughter Sofia for their support and patience over these years.

Contents

List of Tables

List of Figures

Nomenclature

List of Abbreviations

CoF	Coefficient of friction
CS	Compression set
CSR	Compression stress relaxation
CTE	Coefficient of thermal expansion
DMTA	Dynamic mechanical thermal analysis
DSC	Differential scanning calorimetry
FEA	Finite element analysis
HNBR	Hydrogenated nitrile butadiene rubber
LB	Lower bound
LT	Low temperature
NTE	Negative thermal expansion
phr	parts per hundred rubber
PSD	Particle-size distribution
ROM	Rule of mixtures
RT	Room temperature

SR	Stress relaxation
TGA	Thermal gravimetric analysis
TR	Temperature retraction
TTS	Time-temperature superposition
UB	Upper bound
WLF	Williams-Landel-Ferry

List of Symbols

α	linear thermal expansion coefficient
δ	O-ring axial compression
Λ	wave length
λ	stretch ratio
ν	Poisson's ratio
ψ	normalised relaxation function
ε	nominal strain
ζ	magnification
A	area of contact
a_T	horisontal shifting TTS parameter
b_T	vertical shifting TTS parameter
C	surface roughness power spectrum
C_{10}	material parameter
D	diameter
D_g	glassy compliance
D_1	material parameter
E	Young's modulus
E'	storage modulus

E''	loss modulus
E_∞	long-term (low-frequency) modulus
F	force
F_c	pull-off force
f_c	pull-off force per unit length
I_1	first strain invariant
J	volume ratio
K	bulk modulus
L_x	contact width
L_y	contact length
P	fluid pressure
P_0	nominal contact pressure
Q	leak rate
q	wave vector
R	radius
S	nominal (engineering) stress
T	temperature
t	time
T_g	glass transition temperature
V	volume
W	strain energy density function
w	work of adhesion
μ	fluid viscosity
ρ	relaxation time
σ	fluid conductivity of interface
τ	retardation time

Chapter 1

Introduction

1.1 Background

Elastomer seals like O-rings are utilized in almost any industrial pressure retaining equipment operating at low or high pressure, e.g. in automotive, oil and gas or aerospace applications. These seals possess many unique advantages such as excellent flexibility, resilience and recovery properties, a low ratio between the shear and bulk moduli [1]. They in general do not require very fine surface finish to make a good seal, as, for example, thermoplastic seals would demand. There are, however, natural factors under which the pressure integrity of elastomer seals can be compromised. One of these influencing factors is exposure to low temperatures near and below the glass transition point T_{g} of the elastomers. A cold environment is known to pose a major threat to elastomers and might, in fact, lead to catastrophic consequences, as, for instance, in the Challenger shuttle explosion which occurred due to a leaking O-ring seal [1, 2].

One particular concern with the cold service of elastomer seals is their considerable thermal contraction with cooling, as the Coefficient of Thermal Expansion (CTE) of engineering elastomers is typically at least an order of magnitude higher than that of steel [1, 3–6]. Due to this, an elastomer seal compressed in its groove gradually shrinks when the service temperature decreases, and it might eventually lose interference with the mating steel surface to form a leak path for the contained fluid. The thermal contraction alone might result in a 50 % decrease of the sealing force [7].

Another very important phenomenon to consider when it comes to the seals for the freezing service is the loss of the resilience and recovery properties at temperatures

approaching the glass transition T_g. The molecular and segmental movements in elastomers slow down with cooling. At low temperatures near T_g, the molecules loose their thermal energy needed to overcome local potential barriers [8] in addition to the increased molecular congestion caused by the aforementioned thermal contraction. On the macroscopic level, these phenomena are manifested in an increase of the time required to observe a particular effect like stress relaxation (SR) to the equilibrium (long-term) state or the shape recovery after load release in compression set (CS) experiments. CS is one of the most common measures of elastic recovery in sealing applications and it directly relates to the ability of an elastomer seal to follow any sudden structural deformation in the seal joint [1]. At temperatures below T_g, the molecular rearrangement processes become so slow that the relaxation time exceeds any experimentally feasible time period. Thus, it has been found that CS increases to 100 % meaning no recovery below T_g in many elastomers [9–16]. An example of the cold compression set in elastomers cooled below the T_g [16] is given in Figure 1.1.

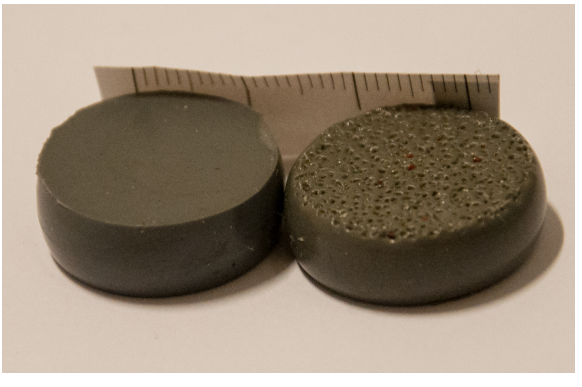

Figure 1.1: Unfilled HNBR CS specimens photographed 3 min after load release at -25 °C. 20 % nominal compression was imposed, and the specimen on the right was compressed against sandpaper (photo courtesy of Natalia Akulicheva).

These issues with low-temperature extremes mentioned can be overcome to some extent if a suitable elastomer material with a sufficiently low T_g is selected. Therefore, sealing a single clean fluid at a low temperature is a rather trivial engineering task. However, as the service conditions of the seal material become more diverse and difficult (e.g. also include elevated temperatures, a long design life and exposure to a wide range of aggressive fluids), the choice of elastomers capable to comply with the whole set of requirements has been narrowing. For example, the non-metallic seals used in the oil and gas industry shall sustain low and high temperature extremes at low and high fluid pressure as well as numerous aggressive chemicals injected into the wells and pipelines. All of these

might be exacerbated by strict requirements of NORSOK M710 [17] for rapid gas decompression in gas systems and the prolonged design life of 20+ years in contact with the aggressive media. Therefore, hydrogenated nitrile butadiene rubber (HNBR) has become a primary choice of base elastomer in the oilfield applications [18] due to its proven versatility.

Among all fluids, sealing of gases represents the most difficult task for engineers due to their extremely low viscosity. The gas leakage in elastomer seals arises from gas permeation through the materials and from the interfacial (or contact) leakage. The permeation of gases through elastomers is known to decline with temperature decrease (see, for instance, [1, 19, 20]) and is, thus, not as significant at low temperatures as the interfacial leaks [19, 21].

The Challenger catastrophe triggered scientists and engineers from a variety of industries to study the low-temperature behaviour of elastomer seals to be used in gas containing systems. Their efforts have led to a number of publications [21–32]. The sealing experiments undertaken in different conditions and using different equipment show some similarities. Thus, the majority of seals leaked at temperatures approximately 10-35 °C below T_{g} depending on their compression level and the exerted pressure difference. Hence, T_{g} does not accurately define the low-temperature limit of serviceability of elastomer seals. Furthermore, T_{g} can be determined by several methods, which in general does not give the same results.

Another interesting observation can be made considering the effect of gas pressure: high ($\geq$ 100 bar) pressure difference, if applied prior to cooling of the sealed joint, might result in lower leakage temperatures [26, 27]. Higher failure temperatures were obtained in low-pressure ($<$ 100 bar) systems [23, 24, 28, 30], or in high-pressure systems pressurized after the cooling step [27]. Furthermore, there are indications that not only the sequence of cooling and pressurisation is important, but also cycling of pressure and temperature from low to high values might yield increased leak temperatures [33]. However, not much experimental data are available to public for these cases.

1.2 Motivation

Despite of its importance the low-temperature behaviour of elastomer seals has not been thoroughly studied and understood since questions of the cold serviceability of elastomer seals still arise [34]. Most of the earlier investigators used commercial seals and fixtures with scarcely reported sealing surface properties and low-temperature properties of the seal materials (typically only the glass transition T_{g} and sometimes 10 % retraction TR-10 temperatures are given). Therefore, no links between cold sealing performance and the material composition and

the material properties are established, except for the seal failure cases when an artificial increase of the sealing gap is induced by a partial release of compression [16, 29, 32].

The major emphasis of research and testing of seal suppliers and the end-users of the seals is usually placed in the field of high-temperature and ageing resistance or strengthening the mechanical properties of their products. As a result, the low-temperature performance and cold leakage mechanisms of elastomer seals have received much less attention and in many cases remained unclear. The problem is also recognised by the European sealing association [35] and some actions are now undertaken by its members. This Ph.D. work aims to contribute to bridging the knowledge gap.

1.3 Objectives and scope

In view of the lack of knowledge of the cold performance of elastomer seals and its relation to the material properties, a set of material and seal experiments using a model HNBR compound was designed and carried out and supplemented by a finite element analysis (FEA) simulation approach for a better understanding of the physics of the elastomer and the seals made thereof. The main purpose of the Ph.D. work is to understand the low-temperature behaviour of static elastomer seals and find a correlation between cold seal failures and the relevant seal material properties to be able to predict such failures in future. As parts of the main goal, the following work objectives are set:

- to elucidate the effects of fillers in the HNBR on the thermal expansivity of the HNBR compound in the glassy and rubbery states;
- to investigate the effects of low temperatures, imposed strain and filler (carbon black) on the stress relaxation (SR) in the HNBR;
- to understand the effects of low temperatures, time and filler (carbon black) on the compression set (CS) of in elastomer and elucidate the link between SR and CS at low temperatures;
- to explore the adhesion of HNBR to a metal counter-surface at low temperatures and study the effects of the different surface conditions on the strength of the adhesion bond;
- to study the low-temperature leakage of static low-pressure elastomer seals against sealing faces with different surface finish and establish a correlation between the cold seal leakage and the thermo-mechanical properties of the HNBR

It should be noted that the thesis does not purport to address all aspects of low-temperature sealing with elastomers due to limited resources and time constraints. As such, high-pressure and/or dynamic sealing, seal design and geometrical effects, wear, ageing and chemical degradation of HNBR and temperature cycling are excluded from the scope. Very limited attention is also given to seal lubrication at low temperatures.

1.4 Thesis structure

The thesis is made as a compendium of five scientific articles together with four preceding chapters. Chapter 1 introduces the reader to the scientific problem to be addressed and provides motivation for the research, the chief objectives posed and a description of the scientific papers. Chapter 2 gives a full description of the materials used and the experimental procedures, test and simulation methods employed. Chapter 3 provides a summary of the results, and Chapter 4 outlines the main conclusions and recommendations for future work. The five scientific articles incorporated in the appendix A of this thesis are:

I. A.G. Akulichev, B. Alcock, A.T. Echtermeyer. Compression stress relaxation in carbon black reinforced HNBR at low temperatures. *Polymer Testing*. 2017;63:226-235.

II. A.G. Akulichev, B. Alcock, A.T. Echtermeyer. Elastic recovery after compression in HNBR at low and moderate temperatures: Experiment and modelling. *Polymer Testing*. 2017;61:46-56.

III. A.G. Akulichev, A. Tiwari, L. Dorogin, A.T. Echtermeyer, and B.N.J. Persson. *Rubber adhesion below the glass transition temperature: role of frozen-in elastic deformations* (submitted) (2017).

IV. A.G. Akulichev, A.T. Echtermeyer, and B.N.J. Persson. *Interfacial leakage of elastomer seals at low temperatures* (submitted) (2017).

V. A.G. Akulichev, B. Alcock, A. Tiwari, and A.T. Echtermeyer. Thermomechanical properties of zirconium tungstate/hydrogenated nitrile butadiene rubber (HNBR) composites for low-temperature applications. *Journal of Material Science*. 2016;51(24):10714-10726.

The relation between the papers can be represented by a simple diagram in Figure 1.2. Paper I studies various effects on the SR in HNBR at low and moderately elevated temperatures. It also provides the viscoelastic material data for Paper II and insight for Paper IV. Paper II discusses the elastic recovery (CS)

in HNBR and its modelling. Paper II also provides insight for Paper III and IV. Paper III focuses on cold adhesion of HNBR to a metallic substrate and its theoretical description. Paper IV investigates leakage of static HNBR seal and factors affecting it. It uses the results generated in Papers I-III and Paper V. Paper V reports the effect of NTE filler (ZrW_2O_8) on the thermo-mechanical properties of HNBR with the focus on the thermal expansivity of HNBR and the composites.

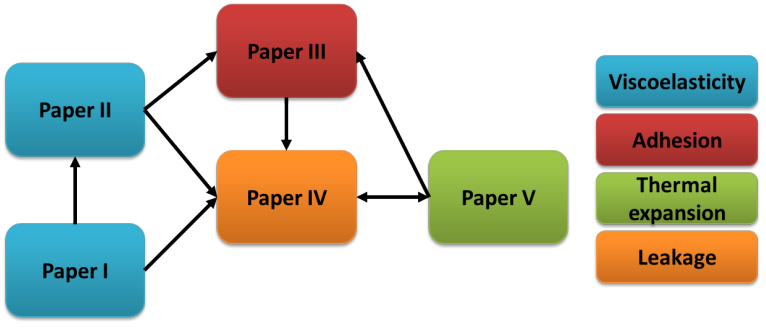

Figure 1.2: Schematic of the relation between the papers in the thesis. The colour codes indicate the central topics of the papers.

The contribution of the author and the co-authors is as follows:

- **A.G. Akulichev** has formulated the objectives and defined the test program, designed and assembled the customised test rigs in Paper I, IV and V, produced the test specimens and O-rings, developed test methods in Papers II-IV, carried out most experiments and all FEA simulations, developed the MATLAB codes for TTS, viscoelastic analysis and CS prediction in Paper I,II, analysed and interpreted the data and written papers I,II, IV,V and the experimental part of paper III;

- **B. Alcock** has performed TGA, DSC, density measurements in Paper V and hardness measurements in Paper II, participated in compounding and moulding of the test pieces, advised on the experiments and test procedures and contributed with comments and editing of paper I, II and V ;

- **A. Tiwari** has conducted the qualitative adhesion tests in Paper III, participated in compounding and moulding of the test pieces, contributed with comments and editing of paper III and V;

- **L. Dorogin** has conducted the qualitative adhesion tests in Paper III, contributed with suggestions, comments and editing of paper III;

- **B.N.J. Persson** has provided the theoretical foundation for the low-temperature adhesion of rubber and written the theoretical part of paper III, contributed with advices, comments and editing of paper IV;
- **A.T. Echtermeyer** has contributed with intellectual discussions, guidance, suggestions and comments to all papers;

Chapter 2

Methodology

2.1 Materials

The elastomer used in the work represents an elastomer formulation typical of that which might be found in the oil and gas sealing applications. The material composition is shown in Table 2.1 and is based on hydrogenated nitrile butadiene rubber (HNBR) with 96 % saturated butadiene units with 36 % acrylonitrile content. This HNBR was selected because previous work yielded that it has a combination of good ageing resistance, hydrocarbon resistance [36] and necessary barrier property [20, 36]. The compound formulations contained varied concentration of fillers: N-330 HAF carbon black (CB) and zirconium tungstate (ZrW_2O_8) as described in Table 2.2.

A zirconium tungstate powder was acquired for the experiments from Alfa Aesar.

Table 2.1: Composition of the generic HNBR used in the research work

Component	Content, phr
HNBR	100
Antioxidant	3
Stearic acid	0.5
Zinc oxide	5
Magnesium oxide	10
Plasticizer	20
Peroxide	10
Filler	Varies (see Table 2.2)

Table 2.2: Filler volume fraction in HNBR

No.	Filler volume fraction, %	
	CB (Papers I-IV)	ZrW_2O_8 (Paper V)
1	0	0
2	20.4	8.6
3		17.3
4		25.3
5		35.8
6		39.7

The ZrW_2O_8 powder has a Gaussian-like particle size distribution (PSD) with filler particles varying in size from less than 0.3 μm to about 100 μm [37].

The compound described in Table 2.1 (except the peroxide and zirconium tungstate) was combined in an internal mixer to yield a single HNBR masterbatch which was used for subsequent production of all of the materials used in the Ph.D. work. This HNBR masterbatch was then combined with the peroxide (and ZrW_2O_8 in Paper V) using a Schwabenthan Polymix 110P open two roll mill. Each formulation was subjected to continuous mixing on the mill for 10 minutes. After compounding, the materials were compression moulded into 2 mm thick sheets and test-specific specimens using a hot press. The materials were cured at 170 °C (443 K) for 20 min in the press, followed by post-curing at 150 °C (423 K) for 4 h in an oven. Figure 2.1 gives an overview of the specimens used in the research work.

The vulcanised unfilled HNBR has Shore A hardness of 70 ± 5. The glass transition temperature T_g of the cured rubber compound was determined by DSC using a Perkin Elmer DSC 8500 at a heating rate of 20 °C per minute and appeared to be -23 °C (250 K). The glass transition temperature was not affected by the fillers used in this work.

2.2 Experimental methods

With a few exceptions, the experiments described in this section were carried out at Department of Mechanical and Industrial Engineering, NTNU. CTE, TGA, DSC and density measurements together with the uniaxial tensile tests were conducted at SINTEF Materials and Chemistry in Oslo. Temperature-frequency DMTA data for unfilled and 20.4 vol.% CB filled HNBR were obtained at FZ Jülich, and surface topography measurements of the parts used in sealing experiments were performed at NTNU NanoLab.

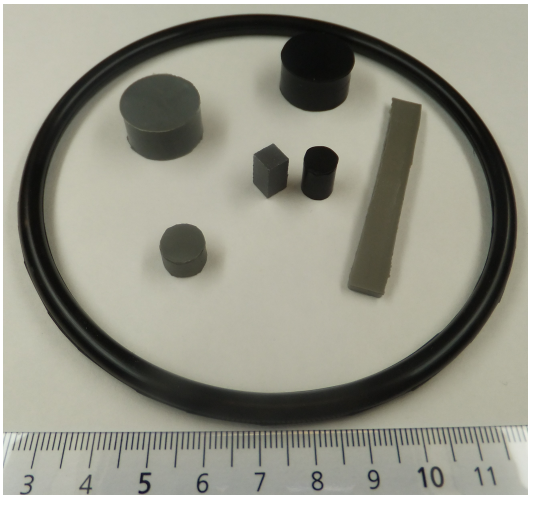

Figure 2.1: Photograph of some elastomer specimens moulded in this work.

2.2.1 Material Characterisation

Scanning Electron Microscopy

A Quanta FEG 650 scanning electron microscope (SEM) operated in a low-vacuum mode at 80 Pa chamber pressure and 5 kV accelerating voltage was employed to observe the microstructure of the $\mathrm{HNBR} - \mathrm{ZrW_2O_8}$ composites in Paper V at various magnifications and qualitatively evaluate the distribution of the $\mathrm{ZrW_2O_8}$ filler particles. The specimens fractured in tensile tests were examined in the microscope. No specific surface treatment was applied to the specimens.

Dilatometry

Thermal expansion measurements were carried out on a Netzsch DIL402C dilatometer during heating from -80 to 200 °C (193 to 473 K) at a heating rate of 2 °C per minute. The specimens for dilatometry were 6x6x10 mm moulded-to-shape bricks. The linear CTE α is computed by linear regression of the thermal dilatation data in the ranges from -80 to -40 °C and from 25 to 130 °C for the glassy and rubbery regions of HNBR respectively.

Volumetric compression

The HNBR bulk modulus K was measured on a special test set-up tailored for volumetric compression measurements. It comprises a steel pressure vessel and a pump system with a Quizix C-5000 pump cylinder, a set of hoses and two valves. The test stand is demonstrated in Figure 2.2. A specimen was inserted into the

pressure vessel which was then fully filled with distilled water and connected to the pump by a short metallic tube. The pump cylinder provides the system with high pressure monitored by a pressure gauge. The measurement is performed by tracking the change of external pressure in the system against the amount of hydraulic fluid (distilled water) supplied to the vessel when the delivery valve is open. The water supply rate was 3 ml/min.

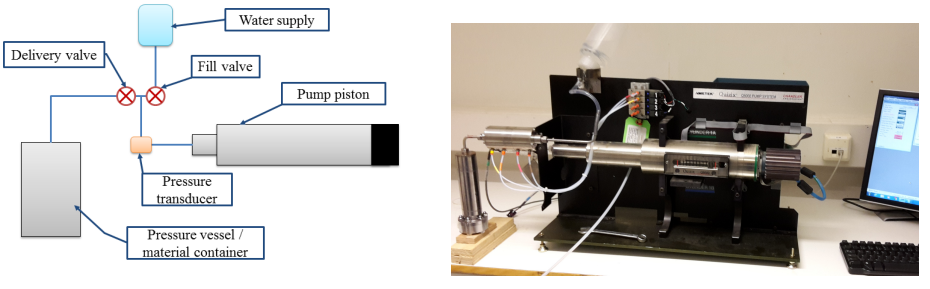

Figure 2.2: The volumetric compression test set-up: left - schematic; right - photograph

The outcome of the measurement is given as a pressure versus supplied volume curve. Only the linear part of the curve is used in the calculation of the bulk modulus via the well-known expression:

$$K = V\frac{\mathrm{d}P}{\mathrm{d}V} \tag{2.1}$$

Where K is the bulk modulus; P is the external pressure and V is the compressed volume. Water compressibility and any expansion of the equipment are also taken into account by making a separate measurement in the system solely filled with water. Separation of the specimen compressibility and the contribution arising from the system can be done using the effective bulk modulus K_{eff} obtained in the measurement. The final equation for calculating the specimen bulk modulus is

$$K_{\mathrm{s}} = \frac{V_{\mathrm{s}}}{\frac{V_{\mathrm{eff}}}{K_{\mathrm{eff}}} - \frac{V_{\mathrm{eff}}-V_{\mathrm{s}}}{K_{\mathrm{sys}}}} \tag{2.2}$$

Where V_{eff} is the effective (total) volume inside the pressure vessel which includes the specimen volume V_{s}, K_{s} is the sought specimen bulk modulus and K_{sys} is the system expansion modulus computed from the abovementioned water compression experimental data.

Uniaxial Tensile Testing

The mechanical behaviour in uniaxial extension was investigated using a Zwick universal testing machine equipped with a contact extensometer and a 2.5 (or 1) kN

load cell. The specimen geometry was in accordance with ISO 37 type 2. Each specimen was fixed in the machine by mechanical grips and pre-loaded to 0.5 N before stretching. For testing at temperatures other than ambient, the specimens were exposed to the testing temperature for 30 min prior to the test commenced. The values of Young's modulus in Paper V were computed by linear regression of the stress-strain curves over the range strain of 0.0025 to 0.005.

Uniaxial Compression Testing

The step-strain instantaneous and relaxation behaviour in uniaxial compression at room and other temperatures was investigated using a Netzsch-Gabo Eplexor 150 DMTA machine equipped with a 1.5 kN load cell, thermal chamber and parallel plate holders. Cylindrical specimens with 20 (or 10) mm nominal diameter and 10 (or 6) mm height were used in the testing. Molykote 33 Medium silicone grease was applied to the faces of specimens to minimise barrelling. The strain rate here is approximately 0.005 s^{-1}. The studied range of nominal compressive strain is 0.05-0.35 with a strain step length of 0.05.

Low-temperature compression stress relaxation (CSR)

Sub-zero compression stress relaxation (CSR) experiments were carried out on a special test rig illustrated in Figure 2.3 (herein called the "manual method"). The main principle is that a specimen is manually compressed between lubricated steel plates by a screw to a predefined deformation. The applied deformation was controlled by means of the screw rotation. The specimens were maintained at the constant strain and temperature while the force was recorded. Test times were chosen to observe stress decay preferably until attaining the equilibrium where possible. The times were, thus, between 3 hours and 15 days.

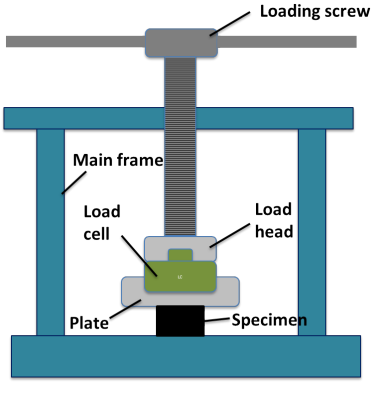

Figure 2.3: Schematic of the compression stress relaxation rig used in the "manual method".

Prior to loading the rigs, the specimens were positioned in a freezing cabinet and kept there at the desired temperature for at least 12 hours. The temperature fluctuations inside the freezing cabinet were ± 0.4 °C. The experiments at most conditions except for temperatures lower than -20 °C were repeated to ensure reproducibility. The accuracy of the experimental data obtained by compressing specimens using the "manual method" was checked for a few cases by a more conventional test method using the Zwick testing machine. The discrepancy between these two set-ups was $\leq$ ca. 3 %. This small discrepancy is believed to be caused by the imperfect control of the loading rate in the "manual method".

The compression specimens had a cylindrical shape with 20 mm nominal diameter and 10 mm height. For measurements below -20 °C, smaller specimens of 10 mm diameter and 6 mm height were used due to the increased level of stiffness of the material and the limited capacity of the force sensors.

The investigated range of nominal compressive strains was 0.10-0.40. The loading and subsequent relaxation was performed stepwise with a nominal strain step length of 0.05 as in the Eplexor DMTA machine. The maximum degree of compression at temperatures near and lower than the T_{g} was, however, reduced to 0.15-0.30 due to the high stiffness of the materials in the glassy state. Prior to the relaxation experiments, the specimens were pretreated with 4 full deformation cycles in order to minimise the Mullins effect [38]. The specimens were left unloaded to recover their original shape for at least 48 hours after the pre-treatment and prior to each test.

Compression set

Compression set (CS) in HNBR was measured by two methods: manual at room temperature and automatised in the Eplexor DMTA machine at different temperatures.

Manual method
The CS measurements in Paper V were performed at room temperature using a special mechanical fixture with the design similar to the one recommended in ISO 815-1. Cylindrical specimens of 20 mm diameter and 10 mm height were placed between thick steel plates of the fixture and mechanically compressed by 4 bolts to 80 % of the initial height defined by inserted steel spacers. The specimen height after the load release was measured manually with a calliper. The test methodology followed ISO 815-1 and CS values were calculated in accordance with the standard.

Automatic method
The automatic CS measurements at various temperatures were conducted using

the Eplexor 150 machine with a 1500 N load cell operated in the compression mode. The specimens for CS tests were of the same size as the CSR specimens. The procedure illustrated in Figure 2.4 was automatized in the machine. First, an

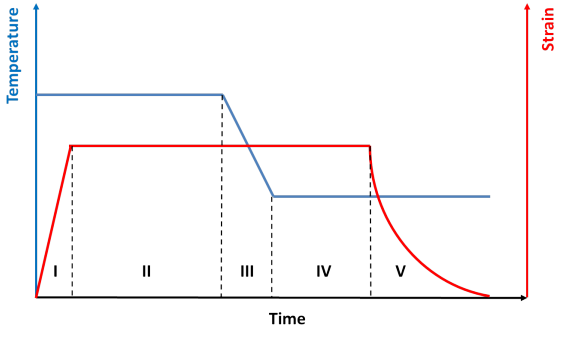

Figure 2.4: Schematic of the low-temperature strain recovery (compression set) test procedure.

elastomer specimen was compressed to 85 % of its initial height (step I) and left to relax at room temperature for 6 hours (step II). After the compression step, the elastomer specimen was exposed to the required temperature and held under load over 30 min (steps III and IV). Then the compression load was quickly removed keeping, however, 2 N compressive force in order to maintain the contact with the specimen. The specimen height change was recorded over time starting from the point of unloading (step V).

Dynamic mechanical thermal analysis

Dynamic mechanical thermal analysis (DMTA) was carried out using TA Instruments and Eplexor 150 DMTA apparatuses in tension mode in air at ambient pressure. The frequency scan was made over a wide range of temperatures from -70 to +120 °C with a temperature increment of 5 °C (2.5 °C in the region from -30 to +30 °C) at 10 frequencies with the strain amplitude of 0.04 %. In this Ph.D. work, temperature-frequency sweep was only performed for unfilled and 20.4 vol.% CB filled HNBR compounds.

2.2.2 Seal experiments

For the experiments in paper III and IV, O-rings of ca. 108 mm inner diameter and 5.3-5.5 mm cross section diameter were manufactured in lab environment by compression moulding. Two compounds were used: unfilled HNBR and 20.4 vol.%) carbon black filled HNBR.

Cold sealing experiments

The cold sealing experiments were performed using a custom-built thermal chamber coupled with heat exchanger piping connected to a recirculating coolant bath manufactured by Julabo. A photograph of the set-up is given in Figure 2.5. The interiors of the chamber with test rigs can be cooled down to about -52 °C in the experimental set-up.

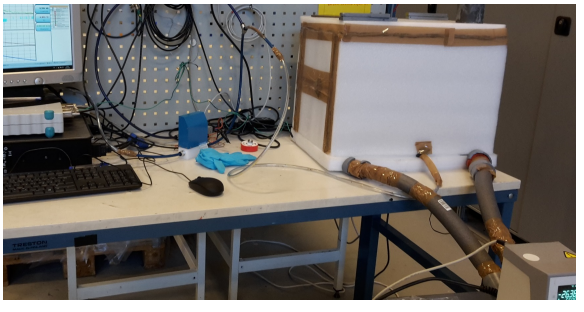

Figure 2.5: Photograph of the leak test set-up in operation.

Two configurations of test fixture were utilized in the experiment. The first one was based on the compression rig concept used in CSR experiments and features compression (sealing) force measurements by a 25 kN compression load cell, see Figure 2.6(left). Pre-defined compression is exerted to an O-ring by a screw in this concept. The sealing counter-faces have root mean square (RMS) surface roughness of 0.95 μm. The main purpose of the measurements with this rig was to measure the sealing force variation with cooling. Vacuum creates additional compressive force to the seal estimated to be about 800 N leading to lower failure temperatures, especially if the pressure difference is applied at temperatures above the T_g. As a result, another rig was also utilized for measurement of leak rates in cold environment.

The second rig is schematically illustrated in Figure 2.6(right) and represents a simple flange arrangement accommodating an O-ring and exchangeable flange parts having different sealing surface topography as will be described later. A set of spacers was selected to fix the desired seal compression. The temperature of the tested O-rings was measured by two thermocouples positioned near the seals; the average values of the thermocouple readings are reported. The sealing surfaces were cleaned with ethanol prior to each test, and the seals were mounted dry at a temperature of 24 ± 1 °C. In addition, several experiments were carried out with application of the Molykote 33 Medium silicone grease.

A vacuum pump connected to the leak port in the test fixtures was used to create

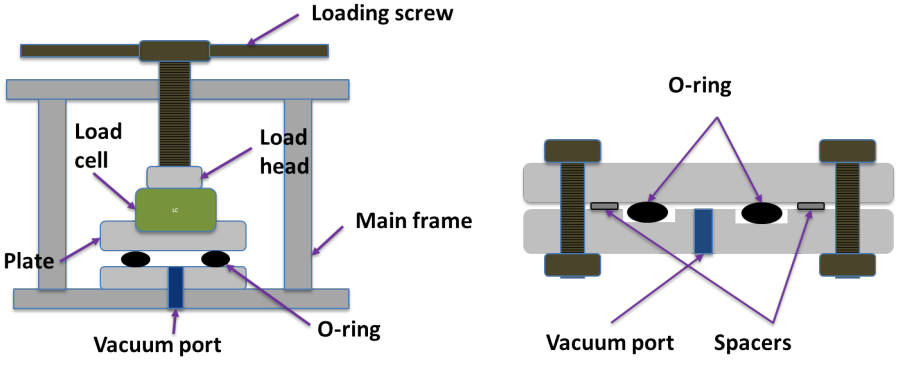

Figure 2.6: Leak test fixtures used in the experiment: left - compression fixture; right - flange based fixture

a pressure difference between the system and ambient environment. The system (vacuum) pressure and leak rate was continuously measured during each test by a vacuum pressure transducer and supplemented by a flow meter with a resolution of $10^{-3}\,\mathrm{cm}^3/\mathrm{min}$. The overall system leakage (which includes the leakage in the fittings and air permeation through the polymer parts) was measured to be approximately 3.5 $\mathrm{Pa}\cdot\mathrm{cm}^3\cdot\mathrm{s}^{-1}$ (or $2\times10^{-3}\,\mathrm{cm}^3/\mathrm{min}$) by the pressure decay method.

Surface characteristics of the sealing parts

Three flange parts with different surface finish were used in the leak measurements. The sealing areas were prepared by milling, turning and grinding processes and exhibited rather different surface roughness. The topography was characterised by a Veeco Dektak 150 stylus profilometer using a line scan in the direction orthogonal to the leakage path with a lateral resolution of 0.56 μm and track length of 10 mm. A summary of the roughness properties is given in Table 2.3.

The surface roughness in the case of milling is somewhat higher than usually specified in engineering documentation, however that was made intentionally to promote leakage. The sealing area topography of the flange parts is depicted in Figure 2.7(left), while Figure 2.7(right) shows the computed one-dimensional (1D) surface roughness power spectra. It should be noted that the surface roughness is anisotropic in all cases studied here.

Table 2.3: Surface roughness properties of the sealing surfaces used in the flange experiments.

Surface finish	Surface roughness parameters				
	R_a, μm	R_q, μm	R_v, μm	R_p μm	RMS slope
Milling	1.7806	2.1588	-6.189	5.38	0.1807
Turning	0.4081	0.5069	-1.043	1.212	0.0083
Grinding	0.4788	0.6471	-3.812	2.517	0.0928

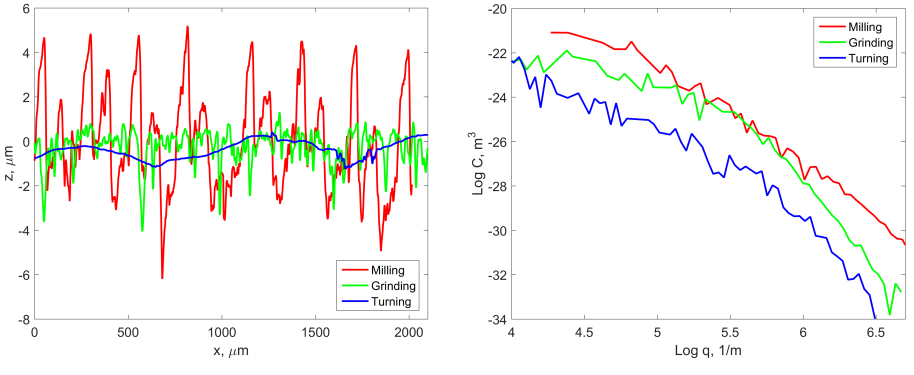

Figure 2.7: Topography (left) and 1D surface roughness power spectra (right) of the indicated sealing surfaces

Adhesion experiments

For the adhesion experiments, use was made of the Explexor DMTA machine operated in the compression mode and cylindrical specimens of $26 \pm 1\,\mathrm{mm}$ length cut from the unfilled HNBR O-rings. The set-up is schematically depicted in Figure 2.8. The compression clamps were cleaned with ethanol prior to each experiment. Three HNBR specimens were roughened with a coarse sand paper to study the effect of rough surface on adhesion.

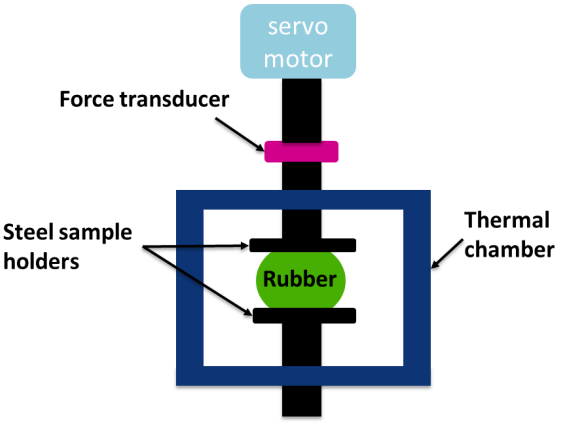

Figure 2.8: Schematic of the pull-off test set-up.

The experiment procedure was as follows. The specimens were compressed in the radial direction and let relax for 1000 s under the constant deformation. Then the chamber was cooled down to -50 °C keeping the strain constant until failure of the adhesion bond occurred due to the thermal shrinkage of HNBR. The force, the distance between the clamps and the chamber temperature were recorded during the course of each experiment. In experiments at room temperature, the clamps were separated after the initial compression and relaxation steps at a rate of 140 μm/s. The maximum pull-off force recorded was taken as a value of the adhesion strength. Three measurements were made for each test condition.

2.3 Simulation

2.3.1 FEA simulation

FEA is used in this work to predict the time-temperature dependent behaviour of HNBR seals in Paper IV and CS specimens in Paper II as well as the thermo-mechanical properties of $\mathrm{HNBR} - \mathrm{ZrW_2O_8}$ composites in Paper V using a homogenisation method. The commercial FEA software package Abaqus was used in all FEA simulation experiments.

The detailed description of the FEA approaches are given in the corresponding papers. It should be noted that the neo-Hookean form of the material strain energy density function was chosen in all cases because of its physical significance [39, 40] and the moderate strains involved. Furthermore, the difference between neo-Hookean and other widespread hyperelastic models in the quality of fitting the material stress response of the HNBR compounds is rather small as demonstrated in Figure 2.9.

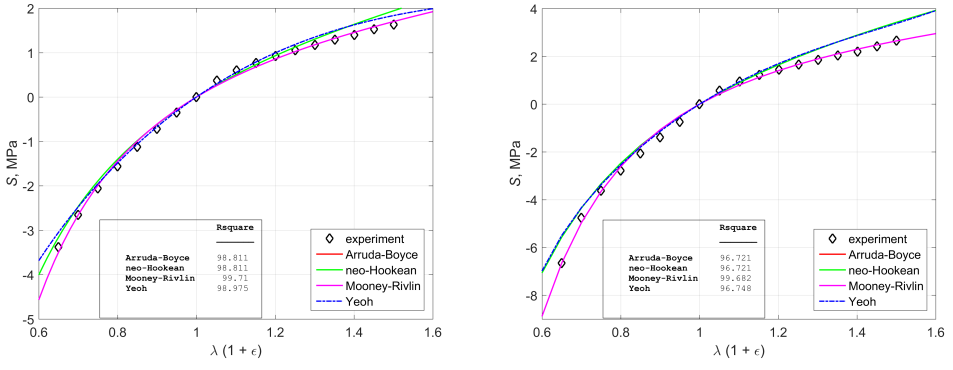

Figure 2.9: Experimental and fitting curves of nominal stress vs. stretch ratio: left - unfilled HNBR; right - 20.4 vol.% CB filled HNBR. The experimental data are obtained by step-strain relaxation in uniaxial tension and compression at +60 °C. The inset shows the R^2 fitting parameters for the indicated models

The strain energy density function for a compressible neo-Hookean material in Abaqus is formed of the deviatoric and the volumetric terms [41,42] and expressed as:

$$W = C_{10}(\bar{I}_1 - 3) + \frac{1}{D_1}(J-1)^2,$$

where C_{10} and D_1 are material parameters representing the resistance to shear and the compressibility of the material respectively; $\bar{I}_1 = J^{-2/3} I_1$ is the first deviatoric strain invariant; $J = \lambda_1 \lambda_2 \lambda_3$ and $I_1 = \lambda_1^2 + \lambda_2^2 + \lambda_3^2$ is the first strain invariant expressed in terms of the principal stretch ratios λ_i. Parameter D_1 can be found from the bulk modulus through the following expression:

$$D_1 = \frac{2}{K}.$$

2.3.2 Persson's contact mechanics and the effective medium seal leakage theory

Leakage experiments of HNBR seals exposed to low temperatures at various compression levels were carried out using sealing surfaces with different topography. In order to understand the effects of compression and the counter-surface topography on leakage, a multi-scale approach based on the Persson contact mechanics [43–45] is undertaken.

It is generally accepted that the real contact area of two contacting bodies is smaller than the nominal one. In the Persson's contact mechanics [43,44], magnification ζ is introduced in order to quantify the effect of roughness at different length scales on the contact area and, consequently, seal leakage. The apparent contact area $A(\zeta)$ can be then studied as a function of magnification ζ or length scale $\Lambda = L/\zeta$ with L being the macroscopic contact width. The contact between a rubber block and a rigid surface appears to be complete $A(1) = A_0$ at the lowest magnification $\zeta = 1$. At higher magnifications surface roughness can be observed and, thus, the apparent contact area decreases ($A(\zeta) < A_0$). The apparent relative contact area $A(\zeta)/A_0$ at the magnification ζ can be obtained according to the theory [44–46] via

$$\frac{A(\zeta)}{A_0} = \mathrm{erf}\left(\frac{P_0}{2\Phi^{\frac{1}{2}}}\right) \tag{2.3}$$

where $\mathrm{erf}(x)$ is the error function, P_0 is the nominal contact pressure and the function Φ is expressed as

$$\Phi(\zeta) = \frac{\pi}{4}\left(\frac{E}{1-\nu^2}\right)\int_{q_L}^{\zeta q_L} \mathrm{d}q q^3 C(q) \tag{2.4}$$

where $C(q)$ is the 2D surface roughness power spectrum, E and ν are the elastomer Young's modulus and the Poisson's ratio, $q = \zeta q_L$ (with $q_L = 2\pi/L$) is the wave vector.

Estimation of the interfacial leak rate through a seal-rigid substrate contact can be done using the critical junction theory [47,48] or the Bruggeman effective medium leakage theory [49, 50]. The latter is used here since it takes into account the leak rate through multiple channels, not only the critical constriction channel as in the former approach. The effective medium theory treats a multi-component medium (e.g. a porous medium in the fluid flow studies) as a single phase medium with

effective (averaged) properties. Assuming incompressible laminar flow, the leak rate is calculated using the effective conductivity of the contact interface σ_{eff} in accordance with [49, 50]

$$Q = \frac{L_y}{L_x}\sigma_{\text{eff}}\Delta P \tag{2.5}$$

where

$$\frac{1}{\sigma_{\text{eff}}} = \int_1^{\zeta} \left(-\frac{A'(\zeta)}{A_0}\right) \frac{2}{\sigma_{\text{eff}} + \sigma(\zeta)} \mathrm{d}\zeta \tag{2.6}$$

and

$$\sigma(\zeta) = \frac{[u_1(\zeta)]^3}{12\mu} \tag{2.7}$$

Here $u_1(\zeta)$ is a function dependent on the average effective separation between surfaces, μ is the sealed fluid viscosity. For more details on the theoretical foundation of the leak rate calculations, the reader is referred to the original publications [43–46, 49, 50]. The contact mechanics and leakage codes developed by Persson were utilised in this work. Here, no correction for the elastomer adhesion or surface anisotropy was made in order to simplify the contact and leakage analyses.

Chapter 3

Key findings

3.1 Stress relaxation in HNBR at low temperatures (Paper I)

Compression stress relaxation (CSR) measurements were performed in HNBR at temperatures below and above the T_g and at compression ratios relevant for the sealing applications [51]. The experimental measurements successfully showed changes in the stiffness of carbon black filled (20.4 vol.%) and unfilled HNBR due to SR. It is experimentally demonstrated that the elastomers can attain the equilibrium state even near the glass transition temperature provided there is enough time for the relaxation to take place [51].

The SR significantly affects the mechanical behaviour of HNBR at low temperatures. The stiffness of the material at temperatures above the glass transition and at moderate compressive strains is determined by two phenomena which have opposing impacts on it. The first effect is related to the entropic nature of rubber elasticity, and, thus, manifested in a decrease of the modulus with temperature reduction down to the T_g. The second effect consists of a steady increase of the transient component of stress (or the time-dependent part of the modulus) with cooling. As a result of these two competing processes, the temperature variation of the strain energy function of the HNBR has a complex concave-downward shape with an inflection point above the T_g, see Figure 3.1. Generally, HNBR exhibits relaxation-dominated stiffness below the inflection point of the strain energy curve and the entropy-dominated stiffness above. The inflection point is shifted to higher temperatures in the carbon black reinforced HNBR.

The stiffness changes with time and temperature cannot be fully predicted by

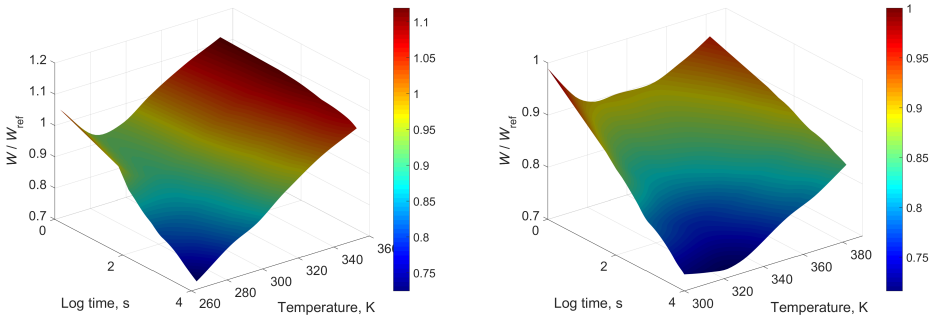

Figure 3.1: The time-temperature contour plot of the normalised strain energy density function for: left - unfilled HNBR; right - 20.4 vol.% CB filled HNBR. The strain energy density data are interpolated by cubic splines and normalized by the values of the instantaneous strain energy density obtained at ambient temperature

simple time-temperature superposition. Due to the entropic elasticity effect, a temperature correction factor (vertical shifting) needs to be introduced for a more accurate application of the time-temperature superposition principle. These vertical correction factors are found to relate with temperature as 0.0038 and 0.0026 K^{-1} for the unfilled and carbon black filled HNBR compounds respectively when the reference temperature is taken as 298 K (+25 $^{\circ}C$). The relaxation master curves demonstrated in Figure 3.2 are produced by horizontal and vertical translation of the time segments obtained in CSR measurements. The temperature relation of a_T can be well fitted by WLF equation [52].

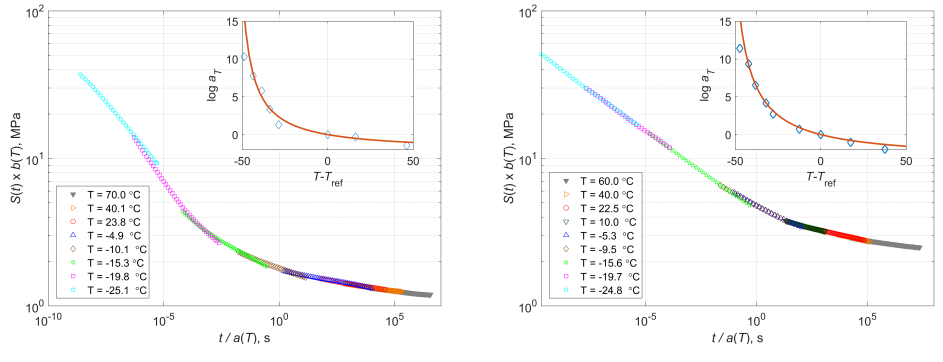

Figure 3.2: Representative CSR master curve for the unfilled (left) and 20.4 vol.% CB filled (right) HNBR. 20 % nominal compression. The insets depict the variation of the horizontal shifting factors with temperature and its fitting by the WLF equation (solid lines)

The effects of carbon black and compressive strain on the relaxation dynamics of HNBR are evaluated using a normalized relaxation function ψ computed as [53]:

$$\psi = \frac{S(t) - S_\infty}{S(t_1 = t_{\min}) - S_\infty} \tag{3.1}$$

where S_∞ is the equilibrium (long-term) stress, $S(t)$ is the stress at time t.

Carbon black imparts greater long-term stiffness and also larger relaxation strength to the HNBR at times longer than 10^{-4}. On the other hand, the relaxation dynamics of HNBR at times from 10^{-3} to 10^{4} s are found to be unaffected by the addition of carbon black, see Figure 3.3. At the T_g or deeper into the glassy region, the relaxation rates are found to be lower in the carbon black filled HNBR than in the unfilled HNBR. On the contrary, the relaxation rates in the filled HNBR appeared greater at elevated temperatures (or at times $> 10^4$ s).

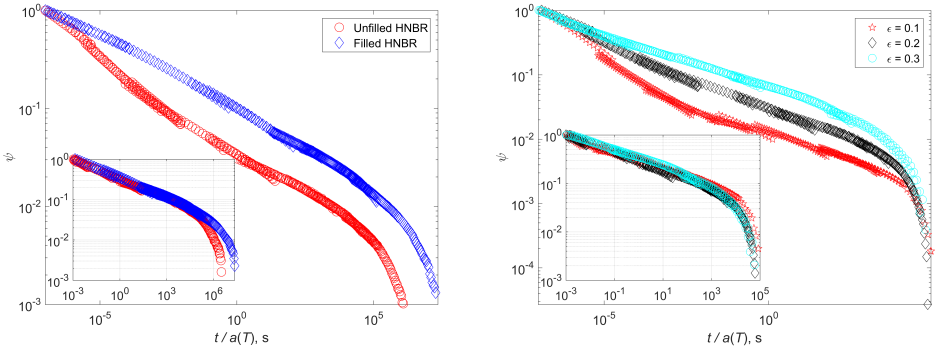

Figure 3.3: The effect of 20.4 vol.% CB loading (left) and imposed compressive strain ε (right) on the relaxation function ψ of HNBR. The insets show the same at times $\geq 10^{3}$ s.

The relaxation function is also found to be unaffected by the compression strains at times $\geq 10^{-3}$ (which corresponds to $\gtrapprox -15\,^{\circ}\mathrm{C}$ in the relaxation experiments). The results, thus, confirm that the time-strain separability in elastomer mechanical behaviour might extend to down to $\approx T_g$ which was not apparent from the earlier publications on the subject [53, 54]. This can greatly simplify the analysis of the elastomers and has a large impact on the modelling of elastomer articles (e.g. seals) in practice. In this work, the SR master curves and the TTS factors were used in section 3.2 to obtain the viscoelastic parameters for prediction of cold compression set in HNBR.

3.2 Elastic recovery after compression in HNBR at low temperatures (Paper II)

Elastic recovery after compression or compression set (CS) is an important property for a sealing material which reflects its ability to restore its undeformed shape after unloading. This, for instance, can be very useful in cases where the structural framework around an elastomer seal is not fully fixed and allows for some displacements. If an elastomer has a large CS at low temperatures it might fail to close a sudden increase in the sealing gap as schematically depicted in Figure 3.4. The results of a study of the cold CS in HNBR and its modelling (paper II) are presented in this section

Figure 3.4: Schematic of compressed O-ring seal (black) in a flange: left - at ambient temperature; right - upper part lift-off at low temperature and leakage due to "frozen" seal.

CS is found to increase with cooling reaching $\approx 100\,\%$ near T_{g} in unfilled and 20.4 vol.% CB filled HNBR. CS might, however, approach zero even at such low temperatures provided there is substantial time for the shape recovery. The duration of the initial compression has a significant effect on the elastic recovery in the CS experiments conducted at ambient temperature, while the effect becomes minimal at sub-zero conditions once the glass transition region is reached.

Since the compression set in the studied materials has a clear viscoelastic origin at low and moderate temperatures, and the neighbouring time segments have similar shapes and overlap quite well near their edges, the postulate of time and temperature equivalence can be applied to construct compression set master curves. The TTS principle has been successfully applied to the HNBR compression set data measured at various temperatures. The CS master curves are depicted in Figure 3.5. The variation of the horizontal shifting parameter a_{T} with temperature is well fitted by the WLF expression [52] with the parameters being similar to the "universal" values for polymers regardless of whether the HNBR compound is reinforced or not.

CB imparts inferior low temperature recovery properties to HNBR compared to

the unfilled HNBR, although the negative effect is not substantial at ambient conditions. The largest difference of about 20 % between the CS values in the 20.4 vol.% CB filled and unfilled HNBR is observed near the T_g region. Below this temperature both compounds demonstrate no or minimal elastic recovery (see Figure 3.5).

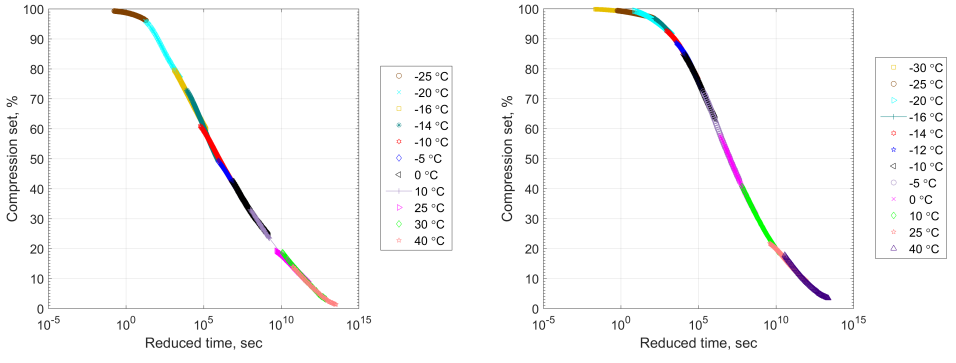

Figure 3.5: CS Master curve with $T_{\text{ref}} = -20\,^{\circ}\text{C}$: left - for unfilled HNBR; right - for 20.4 vol.% CB filled HNBR.

As shown above, the shape recovery after compression is a viscoelastic process, therefore the recovery can be modelled based on the viscoelastic characteristics of the elastomers. Using the Boltzmann superposition principle [55] and generalised Maxwell and Voigt models for approximation of stress relaxation and creep processes respectively [55–57], it is possible to derive the following expression for the strain ε at any time t after release of the compressive load [16]:

$$\begin{aligned}\varepsilon(t) =& \varepsilon_0 \left(1 - \left(E_\infty + \sum_{i=1}^{m} E_i \exp^{-\left(\frac{t_c}{\rho_i}\right)}\right)\right) \times \cdots \\ \cdots \times & \left[D_g + \sum_{j=1}^{n} D_j \left(1 - \exp^{-\left(\frac{t}{a_T(T)\tau_j}\right)}\right)\right]\end{aligned} \tag{3.2}$$

where ε_0 is the initial compressive strain imposed at ambient temperature, E_∞ is the equilibrium elastic modulus, t_c is the time under compressive load, E_i are the relaxation strengths and ρ_i are the corresponding relaxation times, D_j are the retardation strengths and τ_j are the corresponding retardation times, a_T is the horizontal shifting TTS factor. The glassy compliance D_g is found by:

$$D_g = \frac{1}{\left(E_\infty + \sum_{i=1}^{m} E_i\right)} \tag{3.3}$$

The expression consists of two terms in the parentheses. The first of which accounts for the compression stress relaxation history while the second determines the actual recovery behaviour at any time (or reduced time t/a_{T}). The strain recovery can be converted to the compression set using

$$\mathrm{CS} = \frac{\varepsilon(t)}{\varepsilon_0}. \tag{3.4}$$

By virtue of the relaxation data with the TTS shifting factors from section 3.1, CS was computed using Equation 3.2 and Equation 3.4. The results of the CS model prediction are presented in Figure 3.6 and Figure 3.7 together with FEA simulation output against the experimental CS data in HNBR.

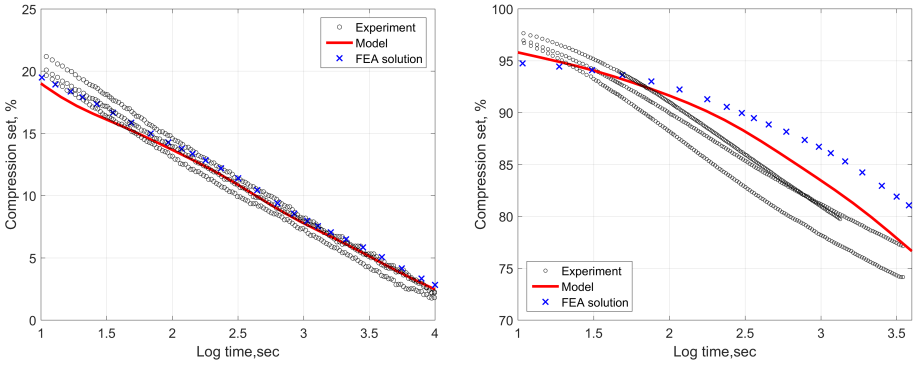

Figure 3.6: Experimental and modelling results of the compression set as function of time for the unfilled HNBR: left - at $+25\,^{\circ}\mathrm{C}$; right - at $-20\,^{\circ}\mathrm{C}$.

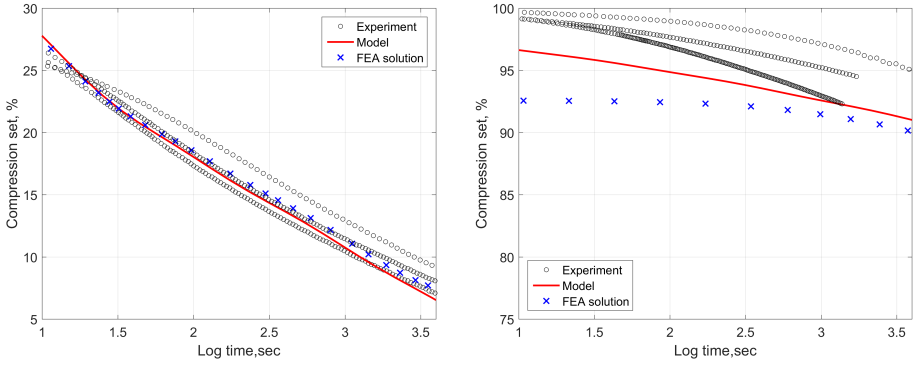

Figure 3.7: Experimental and modelling results of the compression set as function of time for 20.4 vol.% CB filled HNBR: left - at $+25\,^{\circ}\mathrm{C}$; right - at $-20\,^{\circ}\mathrm{C}$.

Both models predict the elastic recovery of HNBR quite well at $+25\,°C$ and acceptably at $-20\,°C$ which is near the glass transition temperature of the HNBR. The deviation between the FEA solution and the proposed model is rather small and presumably related to the difference in fitting of the relaxation data and the limited number of the Prony elements in Abaqus. Another potential source of this small discrepancy is the necessary use of the hyperelastic material model in FEA dictated by the finite strains in the FEA model.

The largest differences between the experiment and modelling results of about 5 % are observed close to T_g in both compounds. In general, the thermo-mechanical behaviour of elastomers becomes more complex in the vicinity of T_g, and there can be several reasons for the noticeable deviation. The first and foremost reason of the deviation is the increasing strain dependency of the HNBR relaxation function (and, thus, creep and recovery) on temperature below $-15\,°C$ described in section 3.1. Another explanation is the known temperature dependency of the elastomer modulus which has not been accounted for in the modelling approach (application of the vertical shifting factor $b_T(T)$). A small contribution for the deviation can arise from the finite cooling (or heating) time during which some incomplete relaxation processes may still take place at rates varying with the temperature.

The modelling approach can be used to predict the HNBR elastic recovery at low and moderately elevated temperatures provided that only physical relaxation processes occur in the studied material and the temperature relation of time-temperature superposition factor a_T is available. The mechanical behaviour of HNBR at finite strains in the glassy state is no longer described by the simple models used in this work [51]. As such, both FE and analytical approaches might fail to give accurate estimates of CS below T_g. Nonetheless, as demonstrated by this Ph.D. work and many other experiments, e.g. [9, 14, 15], the deformation field in elastomers pre-loaded in ambient conditions is "frozen-in" at temperatures below T_g, i.e. they exhibit no or very limited recovery manifesting in CS values of about 100 %.

3.3 HNBR adhesion below the glass transition temperature (Paper III)

Adhesion of soft materials put into contact with a rigid substrate might change their contact mechanics and frictional behaviour, hence it might also affect the leakage behaviour in elastomer seals. This section reports the experimental results of HNBR-substrate adhesion in cold environment and explains the origin of the adhesion phenomenon. The specimens were compressed to desired deformation

and cooled down below T_g while monitoring the compressive force, clamp distance and the chamber temperature as described in section 2.2.2.

At some temperature, below the glass transition point of the HNBR, the compressive force gradually decreased down to zero (due to the entropic nature [51] and thermal contraction of the material as well as the negligible recovery, as will be explained below), and even to negative values due to the adhesive strength of the HNBR-steel contact; see Figure 3.8. Once the tensile stress in the elastomer near the interface reached the elastomer-steel bond strength, breakage of the adhesive bonds (opening crack propagation) occurs and the force abruptly vanish. Several experiments with different compression of HNBR O-ring sections

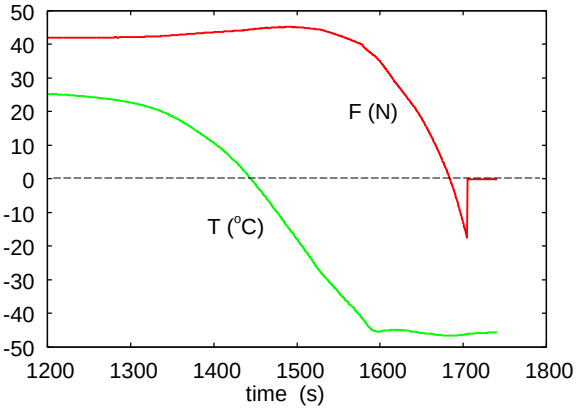

Figure 3.8: The compressive force imposed on a specimen (red line) and the temperature (green line) as a function of time. Note that the temperature plot indicates the temperature inside the chamber, but not the specimen internal temperature.

are conducted for smooth and rough elastomer surfaces; see Table 3.1 for a summary.

The phenomenon of adhesion of HNBR to a rigid substrate can be explained considering 2 limiting cases: adhesion in a room temperature contact and adhesion in the contacting pair cooled to temperatures below T_g.

3.3.1 Adhesion in a room temperature contact

Low pull-off force values of about 0.04 N/mm are measured when separation between the HNBR ring section and the clamp counter-surface occurs at room temperature. The elastic deformation of the solids at the interface (as a result of the adhesive forces) leads to stored elastic energy. During pull-off this elastic energy is given back, and helps to break the atomic interactions. It results in the vanishing pull-off force observed in ambient conditions. In spite of the small

Table 3.1: The change in force (pull-off force) during the abrupt detachment induced by the thermal contraction of HNBR at temperatures below T_g (LT), and due to pull-off action at room temperature (RT). The results are given for smooth and sand paper roughened HNBR surfaces.

surface condition	10 % compression	20 % compression
smooth, LT	$20.4 \pm 3.0\,N$	$31.4 \pm 8.8\,N$
rough, LT	$4.8 \pm 0.2\,N$	..
smooth, RT	$0.9 \pm 0.2\,N$	..
rough, RT	$0.015 \pm 0.015\,N$	..

values, the adhesion can be still sufficient to sustain the weight of the specimens, see Figure 3.9.

Figure 3.9: HNBR ring section adhering to one of the holders after the pull-off test.

The strength of adhesion can be estimated quantitatively. The adhesive interaction between an elastic cylinder and a flat surface is a straightforward extension of the classical theory of the interaction between a spherical body and a flat surface known as Johnson-Kendel-Roberts (JKR) theory [58]. If the applied pull-off force is orthogonal to the flat contact region, the pull-off force per unit length is given by [59–61]

$$f_c = -\frac{3\pi E_0^* a_c^2}{4R},$$

where the half-width of the rectangular contact region at the pull-off instability is

given by

$$a_{\mathrm{c}} = \left(\frac{2wR^2}{\pi E_0^*} \right)^{1/3},$$

where the effective low-frequency modulus $E_0^* = E_0/(1-\nu^2)$ (where E_0 and ν are the elastomer long-term (low-frequency) modulus and Poisson ratio, respectively).

The work of adhesion $w \approx 0.1\,\mathrm{J/m^2}$ was previously measured for the HNBR against smooth glass surface using an opening crack at the pull-off velocity of $\approx 1\,\mu\mathrm{m/s}$ [62]. However, the pull-off rate in these experiments is ~ 100 times higher, and, for this case, theory predicts a ~ 10 times higher work of adhesion because of the viscoelastic enhancement factor [63–67]. Assuming $w \approx 1\,\mathrm{J/m^2}$ for HNBR against a steel surface (at the pull-off speed $\approx 100\,\mu\mathrm{m/s}$) one gets $a_{\mathrm{c}} \approx 0.1\,\mathrm{mm}$ and the pull-off force $F_{\mathrm{c}}/L = f_{\mathrm{c}} = 40\,\mathrm{N/m}$ or for $L = 26\,\mathrm{mm}$ long O-ring section, about $F_{\mathrm{c}} \approx 1\,\mathrm{N}$. This low pull-off force is close to the value measured at room temperature ($0.9\,\mathrm{N}$).

3.3.2 Adhesion in the contact cooled below the glass transition temperature

For the contact pair engaged at room temperature and then cooled below T_{g}, a very strong adhesion is observed manifesting in the large pull-off force values (Table 3.1). This phenomenon can be understood qualitatively as follows. When the system is cooled to $T = -50^{\circ}\mathrm{C}$, the elastic deformation field in HNBR is frozen-in, and the stored elastic energy (which helps to break the adhesion bonds at ambient temperature) is not given back during separation of the elastomer from the mating clamp surfaces. Thus, the absence of the elastic deformation energy can result in very strong adhesive bonds.

It is also possible to make quantitative estimates of the force required to separate the glassy HNBR from its substrate using linear fracture mechanics. Consider the limiting case where the HNBR ring section is in full contact with the counter-surface and assume that no elastic energy is given back during pull-off. In this case, the pull-off force in the direction orthogonal to the contact region (mode I crack propagation):

$$f_{\mathrm{c}} \approx (2\pi w a E_g^*)^{1/2}, \tag{3.5}$$

where $E_g^* = E_g/(1-\nu_g^2)$ is the effective elastic modulus of the elastomer in the glassy region (or high-frequency modulus). Knowing that $a \approx (R\delta)^{1/2}$ (where δ is the ring compression) one can get $a \approx 0.5\,\mathrm{mm}$ for $\sim 10\,\%$ compression. Taking $L = 26\,\mathrm{mm}$ and $E_g^* = 2\,\mathrm{GPa}$, the pull-off force is estimated to be $F = Lf \approx 17\,\mathrm{N}$, which is close to what was found for the smooth clean O-ring section

(see Table 3.1). It was assumed that $w = 0.07\,\mathrm{J/m^2}$ because when the HNBR is in the glassy region it behaves as an elastic solid, and there is no viscoelastic enhancement factor [68]. If the contact is incomplete within the nominal contact area, the work of adhesion and, hence, the calculated pull-off force will be smaller, as, for instance, in the case of roughened HNBR.

In the cold adhesion experiments and experiments on the sealing force decay in section 3.4, the separation of HNBR from the substrate at low temperatures was induced not by a pulling action, but rather the thermal contraction of HNBR. Thus, from the glass transition temperature to $T = -50\,°\mathrm{C}$, HNBR contracts with $\approx 0.2\,\%$, or (for the $2R = 5.5\,\mathrm{mm}$ O-ring cross section) $\Delta R \approx 11\,\mu\mathrm{m}$ in the radial direction. If no contraction would be possible (e.g. by adhesion to the confining steel plates), one would instead expect a stress of order $S \approx E_g \times 0.002 \approx 4\,\mathrm{MPa}$ to develop, and a normal force $F \approx L2aS \approx 100\,\mathrm{N}$, which is larger than the cold adhesive force measured. Hence, the adhesive bond will break when the temperature decreases below as indeed observed in the experiments. These results are crucial for sealing applications, and particularly used for describing the low-temperature phenomena in section 3.4.

3.4 Leakage of elastomer seals at low temperatures (Paper IV)

Interfacial leakage of air in hydrogenated nitrile butadiene rubber (HNBR) O-ring seals subjected to different compression ratios and exposed to sub-zero temperatures is studied in this section. The leakage experiments are supplemented with analysis of the soft seal-rigid substrate contact by FEM and leakage prediction using a multiscale contact mechanics approach proposed by Persson [43, 45, 46] and the effective medium leakage theory [49, 50] described in section 2.3.2 taking the counter-face surface properties (detailed in section 2.2.2) as input.

The leak rates of the studied seals do not change much with cooling to temperatures approximately above $-25\,°\mathrm{C}$. At a certain temperature below it an abrupt increase in the air leakage occurs. This finding is in accordance with the cold seal failures experienced before [19,21,24,28]. The temperature at which the leak rate abruptly increases ($> 10^{-2}\,\mathrm{cm^3/min}$) reflecting the seal failure is referred to as leakage (or failure) temperature. The variation of the leakage temperature with O-ring compression is shown in Figure 3.10 for all studied counter-surfaces.

The leak data feature a wide distribution of leak temperatures depending on the filler content, the sealing surface topography and the seal compression level. The leak temperature of the seals is found to decrease with increase of O-ring compression for all types of surface finish and regardless of CB content in HNBR. The effect of larger seal compression is, however, more pronounced in the CB

filled HNBR seals. Furthermore, the seals made of CB filled HNBR in general demonstrate lower leak temperatures as compared to the unfilled HNBR seals. The highest leak temperature (about $-28\,^{\circ}\mathrm{C}$) was observed in the unfilled HNBR seals at $\approx 7\,\%$ compression with the roughest counter-surface, while the lowest leak temperatures below $-45\,^{\circ}\mathrm{C}$ were found in the filled HNBR seals at $\approx 30\,\%$ compression against the most smooth sealing counter-surface in the experiment.

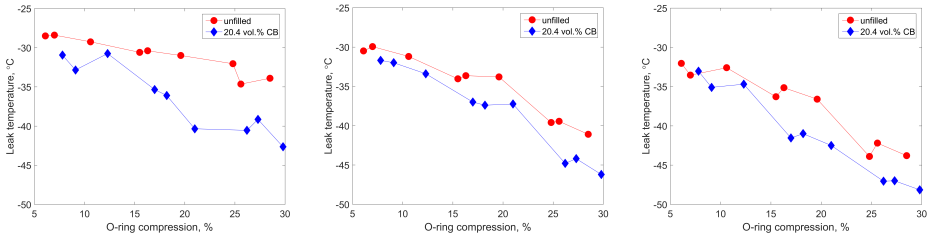

Figure 3.10: Leak temperature as function of seal compression for 20.4 vol.% CB filled and unfilled HNBR seals for the indicated surface treatment.

The difference between leak temperatures at various surface finish conditions is illustrated in Figure 3.11. The positive effect of a smoother sealing surface on the seal failure temperature is quite apparent for seals made of both elastomers. However, the effect of roughness at relatively low $(7-10\,\%)$ seal compression ratios is not as significant as at high $(25-30\,\%)$ compression ratios.

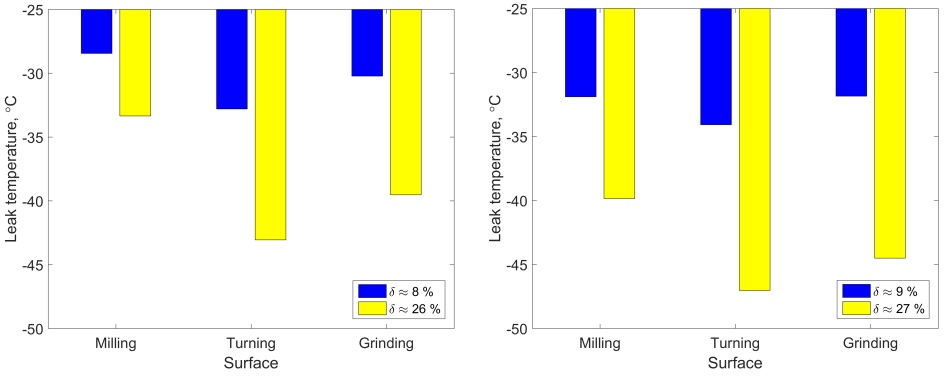

Figure 3.11: The effect of surface finish on leak temperature at the indicated seal compression δ: right - in unfilled HNBR and left - in 20.4 vol.% CB filled HNBR seals.

Low temperatures have a profound effect on the retention of the sealing force of the tested O-rings as depicted in Figure 3.12. The O-ring sealing force decays with cooling to nearly zero at sub-zero temperatures. A similar behaviour of sealing

force decline during cooling was noticed earlier in fluoroelastomer [23–25] and HNBR [30, 69] seals. In addition, experiments were carried out on CB filled O-rings, and the effect of filler on the sealing force is quite apparent here. A higher amount of carbon black makes the retention of the sealing force at low temperatures better. This positive effect of the filler is in a good agreement with the results of the flange-based leak experiments and attributed to a lower thermal contraction of the filled elastomers [37] as well as a lower contribution of the entropy elasticity [51].

Another interesting phenomenon, which was not discovered in the earlier studies, is the abrupt force increase observed in these experiments at temperatures below the glass transition (see Figure 3.12). These force jumps led, in turn, to a drastic increase of the leak rates in every experiment, except for the seals lubricated by a silicone grease. This peculiar effect is believed to be related to breakage of the adhesive bond between the elastomers and the metal substrates at low temperatures when the thermal stresses in the elastomer near the interface reach a critical value due to the thermal shrinkage as described in section 3.3.

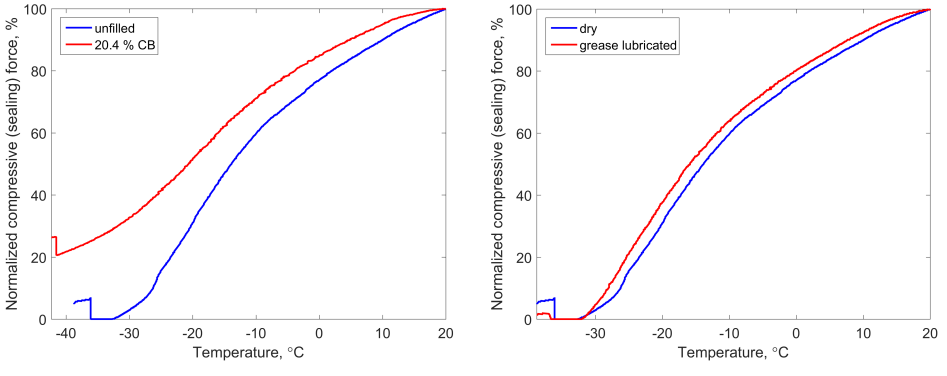

Figure 3.12: The effect of CB loading (left) and grease lubrication (right) on the temperature variation of the O-ring compressive force normalised to the compressive force at room temperature. The seals were compressed ($\delta = 0.1 \pm 0.005$) and left to relax under the constant strain for approximately 16-17 hours in ambient conditions before the cooling step in order to minimise the effect of stress relaxation during the experiment.

No significant increase of the leak rates was observed in grease lubricated seals, even though the seals detached from the counter-surface manifested in similar force jumps as in the dry O-rings, see Figure 3.12. The silicone grease is likely to fill up the gap between the HNBR and its counter-surface and, thus, to impede the air permeation through the contact.

An approach combining FEA and the effective medium leakage theory is used to

predict cold failures in HNBR seals [70]. The predicted seal failure temperature is plotted against the initial compression of the seal together with the experimental leak data for the two studied compounds in Figure 3.13. The simplified FEA model is seen to capture the onset of air leakage in HNBR seals at temperatures below the T_g quite well, considering the data scatter and the assumptions used in the modelling approach. The difference between experimental and predicted leakage temperatures can also be attributed to quality of the data fitting with 13 Prony elements (maximum in Abaqus) and also the cold adhesion phenomenon described in detail in section 3.3.

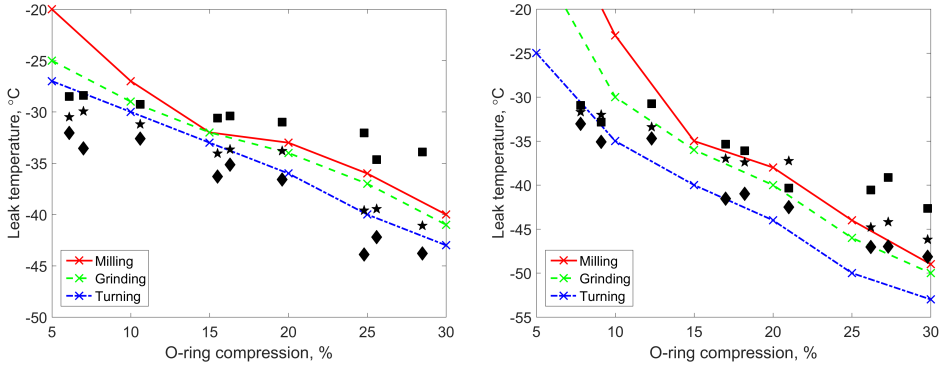

Figure 3.13: Simulated and experimental leak temperatures as functions of seal initial compression in unfilled HNBR (left) and 20.4 vol.% CB filled HNBR (right). The experimental data are for surfaces after milling (■), grinding (★) and turning (♦) listed in the direction of roughness decrease. The FEA was performed using a cooling rate of -0.01 °C/s attained in the flange-based leak tests and CoF = 5.0

The adhesion bond between HNBR seal and its steel substrate might break at low temperatures due to thermal stresses in elastomer at the interface leading to the premature onset of air leakage. The thermal stresses are generated in the elastomer rings due to thermal contraction both in radial and circumferential directions (the O-ring cross section and the circumference decrease with cooling). As soon as the normal or shear stresses exceed the adhesion strength at a critical temperature T_{crit}, the detachment of a glassy elastomer takes place. In turn, a large leakage might immediately develop since the deformation field in the elastomer seal is frozen-in in the initial compressed state (i.e. it has a negligible recovery), as schematically illustrated in Figure 3.14. The leak will be sustained if the seal is not able to recover within the experiment time as most likely the case for with the leakage experiments at temperatures below T_g. Only external heating can help the elastomer to recover and close up the gap between the HNBR seal and its counter-surface.

A quantitative estimation of the thermal stress in the direction orthogonal to the

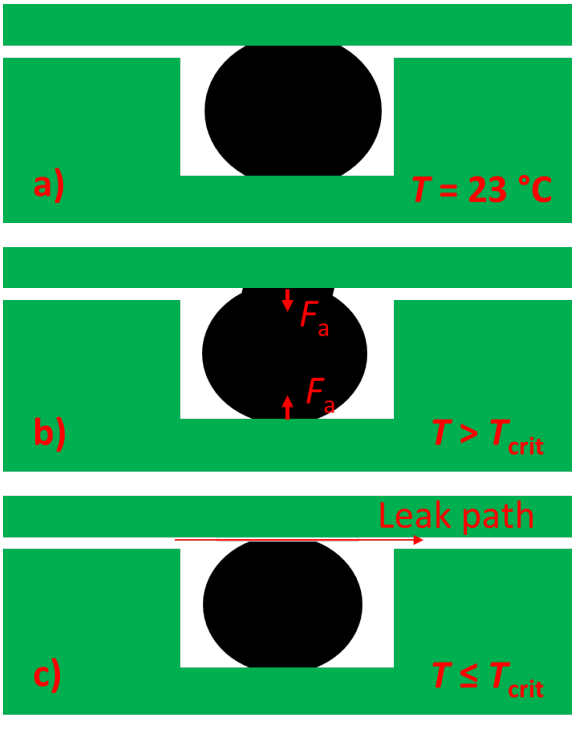

Figure 3.14: Schematic of the O-ring compressed in a flange joint a) at room temperature, b) cooled down to a low temperature (HNBR-steel adhesion increases with cooling down to T_{g}), c) cooled down to the critical temperature ($T_{\mathrm{crit}} < T_{\mathrm{g}}$) at which debonding and subsequent leakage occur.

contact area and its implication for adhesion-related seal failures can be made. The condition for the adhesion bond breakage is

$$S > S_{\mathrm{adh}}$$

where the normal thermal stress $S = E\alpha\Delta T$ and the bond strength $S_{\mathrm{c}} = F_{\mathrm{c}}/(2aL_y) = f_{\mathrm{c}}/(2a)$ with f_{c} being the adhesion (pull-off) force per unit length of O-ring. Hence, the temperature interval that the adhesion bond in glassy elastomer can sustain without failure (assuming no recovery) is

$$\Delta T = \frac{f_{\mathrm{c}}}{2aE\alpha}$$

Consider two limiting cases of weak and strong cold adhesion measured using unfilled HNBR O-ring sections observed in section 3.3, i.e. the pull-off force per unit length of 0.2 N/mm and 1 N/mm respectively in the case of 10 % initial compression. Thus, using the glassy modulus E of 2 GPa and $\alpha \approx 8 \times 10^{-5}\,°\mathrm{C}^{-1}$ the lower and upper bounds of ΔT are $\approx 1.2\,°\mathrm{C}$ and $\approx 6\,°\mathrm{C}$. Since f_{c} increases with $\sqrt{a}$ (or $\approx \delta^{1/4}$) (see Equation 3.5) while the contact area linearly grows with a (or $\approx \sqrt{\delta}$), it can be concluded that the adhesion bond might fail earlier (at lower ΔT) when higher compression ratios δ are involved. The opposite is also true at lower δ, e.g. 5 %. Similar observations can be made taking the elastic modulus (f_{c} scales with $\sqrt{E}$ while the thermal stress has a linear relationship with E).

The results also signify the effect of the thermal contraction of static seal material at the point where the frozen seal cannot recover within the experimental time scale. The importance of the elastomer CTE at and below T_{g} is much higher than estimated before [71]. It is clear that the CB filled HNBR seals with CTE $\alpha \approx 6 \times 10^{-5}\,°\mathrm{C}^{-1}$ in the glassy state yielded a better cold leakage performance than the unfilled counterparts with $\alpha \approx 8 \times 10^{-5}\,°\mathrm{C}^{-1}$, in spite of the inferior cold-recovery properties of the filled HNBR [16]. This is also supported by the experimental data of the sealing force decay rate which is significantly lower in CB filled HNBR seals. Therefore, having an elastomer with a small CTE (ideally $\leq 1 \times 10^{-5}\,°\mathrm{C}^{-1}$ for contact with steel counter-parts) would be very beneficial for sealing applications where permanent or periodic exposure to temperatures reaching the glass transition and below is foreseen.

3.5 Thermo-mechanical properties of zirconium tungstate / HNBR composites (Paper V)

As demonstrated in section 3.4, controlling the coefficient of thermal expansion of sealing elastomers turns out to be very important in static applications with freezing environment. This section reports the properties of HNBR filled with

zirconium tungstate ZrW_2O_8 exhibiting a negative thermal expansion (NTE) effect over a wide range of temperatures ($\alpha \approx -9 \times 10^{-6}\,°C^{-1}$ [72]). The emphasis of this research work was on the thermal expansivity of the prepared composites and its modelling.

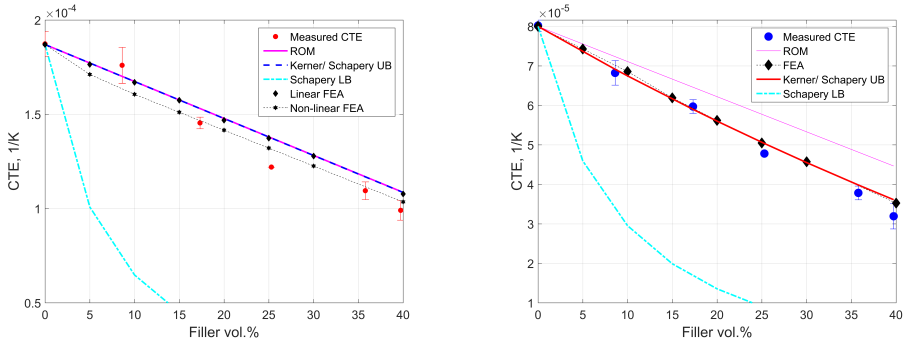

Figure 3.15: Linear CTE of the composites as a function of ZrW_2O_8 content : left - at temperatures between 298 K and 403 K ($25 \div 130\,°C$); right - at temperatures between 193 K to 233 K ($-80 \div -40\,°C$).

Figure 3.15 illustrates the experimentally determined relationship between the CTE of the composite material in the rubbery state and ZrW_2O_8 volume fraction above and below the glass transition of the HNBR. As expected, the CTE of HNBR-ZrW_2O_8 composites has a downward trend if plotted against the ZrW_2O_8 volume fraction in both the rubbery and glassy states. The peak CTE reduction of almost half of the original value in the unfilled HNBR is observed in the elastomer filled with approximately 40 vol.% ofZrW_2O_8. An even larger decrease in CTE to 0.4 of the initial CTE value is measured in the same compound, when it is cooled down below the glass transition of the HNBR.

All prediction models used in the work, except the lower bound (LB) of the Schapery model [73], capture the CTE reduction of HNBR in the rubbery state reasonably well and can be used for engineering purposes. The rule of mixtures (ROM), however, fails to provide a good estimate for the effective CTE in the glassy state. A simple FEA homogenisation approach as well as Kerner's expression [74] and the upper bound (UB) of the Schapery model [73] yielded much more accurate predictions of the composite CTE below the T_g.

The addition of ZrW_2O_8 to HNBR also changes the mechanical characteristics of the material. The effect is observed in volumetric compression and uniaxial tensile tests. The bulk modulus is found to increase with ZrW_2O_8 content as depicted in Figure 3.16. The largest bulk modulus measured in the HNBR filled

with 35.8 vol.% of zirconium tungstate is ≈ 1.45 times greater than that observed in the unfilled HNBR compound. The bulk modulus results are in agreement with previously reported theoretical prediction derived in [71].

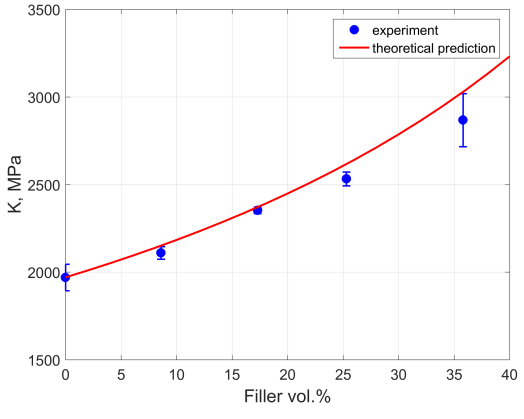

Figure 3.16: Bulk modulus of HNBR-ZrW_2O_8 composites as function of ZrW_2O_8 content. Solid line indicates the theoretical prediction of the bulk modulus. The graph points are averages of three samples with error bars showing the standard deviation.

The small-strain tensile modulus increases with the concentration of zirconium tungstate as well which is demonstrated in Figure 3.17. Like many other inorganic fillers, the inclusion of ZrW_2O_8 leads to lower failure strains in the filled HNBR (see Figure 3.17). Nevertheless, the lowest strain at failure values recorded is still well above the strains expected in sealing applications.

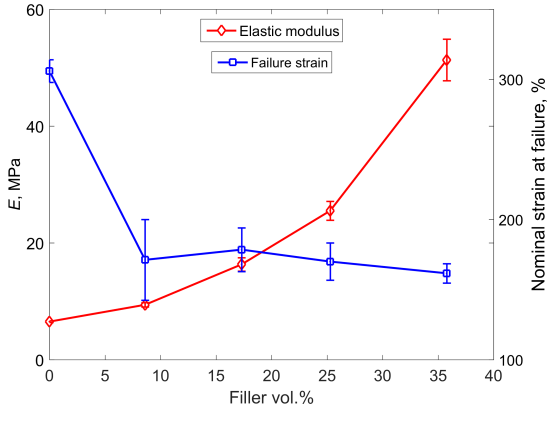

Figure 3.17: Tensile failure strain and small-strain elastic modulus E as a function of ZrW_2O_8 content. The graph points are averages of five tests with error bars showing the standard deviation.

Chapter 4

Conclusions and future work

4.1 Conclusions

The elastomer seal capability to quickly recover or adjust its shape in accordance with any structural deformation of the seal housing is of great importance for pressurised equipment where such deformations are possible. The most common measure of this recovery property is compression set (CS). CS in hydrogenated nitrile butadiene rubber (HNBR) is found to increase with cooling, but decrease with time reflecting its viscoelastic origin. At temperatures approaching the glass transition point T_{g} and deeper into the glassy region ($\leq -25\,^{\circ}\mathrm{C}$) the initial compressive deformation state in HNBR is "frozen-in", i.e. the material demonstrates no recovery manifesting in CS of $100\,\%$ regardless of additions of filler. Carbon black (CB) as a reinforcing filler imparts a higher stiffness, however at the same time it has a negative impact on the CS: the filler effect on CS is small at ambient temperature, but steadily increases with cooling. The maximum difference between CS in CB filled and unfilled HNBR of $\approxeq 20\,\%$ is found near T_{g} (at $\approx -15\,^{\circ}\mathrm{C}$).

A viscoelastic model for prediction of the time variation of the elastic strain recovery (or CS) is proposed. The model links the basic relaxation characteristics of a rubbery material, such as the relaxation spectrum obtained in stress relaxation (SR) experiments, with the compression set in the material. Such link has been missing so far, despite some researchers empirically noticed a correlation between SR and CS. It is demonstrated that the CS model prediction matches finite element analysis (FEA) solution and it successfully captures the recovery behaviour of the studied HNBR at ambient temperature. The modelling approach can also be used to predict CS at low and moderately elevated temperatures with a good accuracy

provided that only physical relaxation processes occur in the studied material and the temperature relation of time-temperature superposition factor is available.

The relaxation function of HNBR needed for CS and other viscoelastic modelling can be determined at any strain used in sealing application at temperatures down to $\approx T_{\mathrm{g}}+1 \div 8\,^{\circ}\mathrm{C}$ (i.e. $-15\,^{\circ}\mathrm{C}$) or at times higher than 10^{-3} s. At temperatures below that, the relaxation function has an increasing strain dependency which renders the slight deviation between CS model prediction and experimental results at $-20\,^{\circ}\mathrm{C}$.

The behaviour of elastomer seals in static immovable joints is not solely determined by the viscoelastic properties of the sealing elastomer. Here, the thermal contraction of the material and adhesive interaction in the contact zone might be crucial for the cold performance. In this work, leak rates of static HNBR O-rings at various compression are investigated using a vacuum test fixture. When cooling down to temperatures below T_{g} of HNBR, an abrupt increase of air leakage ($> 10^{-2}\,\mathrm{cm}^3/\mathrm{min}$) is observed. The experimental results demonstrate that the seal failure temperatures are affected by surface finish conditions, variation of the compression ratio of the seals and additions of carbon black (CB) in the HNBR.

The seal compression force is also found to decrease with cooling, and the rate of the compression force decay depends on the CB content. In addition, an abrupt increase of compression force followed by a sudden increase of the leak rate in HNBR seals was observed at low temperatures $< T_{\mathrm{g}}$. This effect is believed to be caused by failure of the HNBR-substrate adhesion bond induced by the thermal shrinkage of the elastomer. The strong adhesion of HNBR to its substrate at low temperatures was confirmed by small-scale experiments with sections of O-rings. When the elastomer seal-substrate contact formed in ambient conditions is cooled down below the glass transition temperature, the elastic deformation imposed on the elastomer at room temperature is "frozen-in", and the stored-up elastic energy is not given back during separation at low temperatures. This results in the strong adhesion manifested as a large pull-off force.

The main cause for the seal failures is believed to be detachment of the elastomer seals from their mating sealing parts due to a) breakage of the adhesion bond induced by the elastomer thermal contraction in case of a rather strong adhesion bond and negligible recovery of the HNBR below T_{g} or b) due to the thermal contraction and the negligible recovery when the strong adhesion bond is not formed. It is demonstrated that most of the cold failures can be modelled by the effective medium leakage theory and a simple FEA approach using thermo-mechanical material data, the most important of which are the thermal expansivity and small-strain viscoelasticity of the elastomer compounds. Despite the worse recovery properties, the CB filled HNBR has a lower thermal

expansion which results in a better retention of the sealing force and lower leakage temperatures if compared to the seals made of the unfilled HNBR. Hence, it can be inferred that better low-temperature serviceability in static joints can be achieved using elastomer compounds with low coefficients of thermal expansion (CTE) ideally close to the one of the seal housing material.

Rigid filler inclusions with low or negative thermal expansion (NTE) can be utilized to minimise the CTE of sealing elastomers. In this work, composites of HNBR and zirconium tungstate ZrW_2O_8 having CTE of $\approx -9 \times 10^{-6}\,°C^{-1}$ were produced and characterised. The CTE of HNBR filled with approximately 40 vol.% ZrW_2O_8 is shown to be reduced by a factor of 2 in the rubbery state and by a factor of 2.5 in the glassy state. The reduction of CTE with the ZrW_2O_8 content is well described by the simple rule of mixture at temperatures above T_g, while Kerner and the upper bound of the Schapery models as well as a FEA homogenisation approach fit the CTE results below T_g better. The models can, thus, be used for prediction of the CTE of other elastomer composites.

4.2 Recommendations for future work

This thesis addresses the problem of cold leakage in static elastomer seals subjected to moderate compressive deformations and its relationship with the material properties. Nevertheless, there are related research topics that were scarcely covered or not investigated at all in this Ph.D. work. The unresolved questions include:

- Time and temperature variation of the bulk modulus K (and, thus, Poisson's ratio) of elastomers in cold environment should be thoroughly studied to be able to improve the seal performance prediction. This is especially important for high-pressure applications since a proper transmission of the fluid pressure to the contact face is required. Furthermore, high pressure introduces more molecular congestion and, as a result, might change the viscoelastic response of the materials and shift the onset of the glass transition towards higher temperatures as reported elsewhere [75–77].
- The effect of fillers and plasticisers on adhesion at ambient and low temperatures should be investigated since most of the soft seals are made of elastomers containing these constituents. Lubrication with industrial oils or greases might also change the cold pull-off characteristics depending on their viscosity, wetting and other properties. Therefore, it is necessary to understand and characterise this effect on adhesion.
- The effect of lubrication on seal leakage should be examined in greater detail

over longer periods. Fluids tend to squeeze out of the contact zone with time [50, 78, 79], or they can be washed away by the service media.

- The materials in this work were tested soon after their production, whereas years of service in the real-world applications can lead to a different cold performance. Therefore, the effects of ageing and degradation on the viscoelasticity, adhesion and cold leakage of HNBR should also be evaluated.
- Alternative materials with even larger NTE effect (e.g. those described in [80, 81]) can yield further reduction of the CTE of HNBR and other elastomers.

Bibliography

[1] H. K. Müller and B. S. Nau. *Fluid sealing technology : principles and applications*. Mechanical engineering. Marcel Dekker, New York, 1998.

[2] D. Baker. Why Challenger failed. *New Scientist*, 1525(Sep. 11):52, 54–56, 1986.

[3] R. F. Robbins, Y. Ohori, and D. H. Weitzel. Linear thermal expansion of elastomers in the range 300 to 76 K. *Rubber Chemistry and Technology*, 37 (1):154–168, 1964.

[4] G. Kraus and J. T. Gruver. Thermal expansion, free volume, and molecular mobility in a carbon black-filled elastomer. *Journal of Polymer Science Part A-2-Polymer Physics*, 8(4):571–581, 1970.

[5] D. W. Brazier and G. H. Nickel. Application of TMA for rapid evaluation of low-temperature properties of elastomer vulcanizates. *Thermochimica Acta*, 26(1-3):399–413, 1978.

[6] L. Nikiel, H. Yang, M. Gerspacher, and G. Hoang. Electrical resistivity and thermal expansion coefficient of carbon black filled compounds around T-g. *Kautschuk Gummi Kunststoffe*, 57(10):538–540, 2004.

[7] R.P. Campion, D. Derham, G.J. Morgan, and M.V. Lewan. Effects of time, temperature, and fluids on the long-term service durability of elastomers and elastomeric components. In *Current Topics in Elastomers Research*. CRC Press, 2008.

[8] C. M. Roland. Glass transition in rubbery materials. *Rubber Chemistry and Technology*, 85(3):313–326, 2012.

[9] R. E. Morris, J. W. Hollister, and P. A. Mallard. The cold-compression sets of natural and synthetic vulcanizates. *Rubber Chemistry and Technology*, 19 (1):151–162, 1946.

[10] B. M. Gorelik and M. F. Bukhina. Crystallization of rubber at low temperatures in compression (in russian). *Kauchuk i Rezina*, (11):11–15, 1961.

[11] B. M. Gorelik and M. F. Bukhina. Effect of degree of compression of rubber on strain recovery and contact pressure (in russian). *Kauchuk i Rezina*, (9): 22–26, 1961.

[12] N. S. Baranov and A. I. El'kin. Loss of resilience of rubber seals at low temperatures (in russian). *Kauchuk i Rezina*, (5):33–37, 1974.

[13] M. F. Bukhina and M. D. Parizenberg. Temperature-strain superposition of elastomer properties near the transition from rubberlike into glassy state (in russian). *Vysokomolekulyarnye Soedineniya Seriya B*, 23(6):456–460, 1981.

[14] M. Jaunich, W. Stark, and D. Wolff. A new method to evaluate the low temperature function of rubber sealing materials. *Polymer Testing*, 29(7): 815–823, 2010.

[15] M. Jaunich, W. Stark, and D. Wolff. Low temperature properties of rubber seals. *Kgk-Kautschuk Gummi Kunststoffe*, 64(3):52–55, 2011.

[16] A. G. Akulichev, B. Alcock, and A. T. Echtermeyer. Elastic recovery after compression in HNBR at low and moderate temperatures: Experiment and modelling. *Polymer Testing*, 61:46–56, 2017.

[17] Norsok M-710. qualification of non-metallic sealing materials and manufactures, 2001.

[18] R. Mody, D. Gerrard, and J. Goodson. Elastomers in the oil field. *Rubber Chemistry and Technology*, 86(3):449–469, 2013.

[19] N. S. Baranov, V. E. Sokolov, and A. I. El'kin. Contact leaks through flange joints sealed by circular and square-section rubber seals (in russian). *Kauchuk and Rezina*, (8 , 1982):25–28, 1982.

[20] B. Alcock, T. A. Peters, R. H. Gaarder, and J. K. Jørgensen. The effect of hydrocarbon ageing on the mechanical properties, apparent crosslink density and CO_2 diffusion of a hydrogenated nitrile butadiene rubber (HNBR). *Polymer Testing*, 47:22–29, 2015.

[21] H. P. Weise, H. Kowalewsky, and R. Wenz. Behaviour of elastomeric seals at low temperature. *Vacuum*, 43(5):555–557, 1992.

[22] M. Salita. Simple finite-element model of O-Ring deformation and activation during squeeze and pressurization. *Journal of Propulsion and Power*, 4(6): 497–511, 1988.

[23] Ronald D. Stevens, Eric W. Thomas, James H. Brown, and William N. K. Revolta. Low temperature sealing capabilities of fluoroelastomers. In *SAE Technical Paper*. SAE International, 1990.

[24] S. G. Burnay and K. Nelson. Leakage of transport container seals during slow thermal cycling to -40-degrees-C. *International Journal of Radioactive Materials Transport, Vol 2, Nos 1-3, 1991*, pages 91–96, 1991.

[25] G. Streit, M. Achenbach, and A. Kanters. Sealability of O-Rings at low-temperatures .1. Sealability without media influence at low-temperatures. *Kautschuk Gummi Kunststoffe*, 44(9):866–870, 1991.

[26] K. W. Taylor. Performance characteristics of oilfield proven elastomers in low-temperature seal applications. In *Offshore Technology Conference*, 1991.

[27] Peter Warren. Low temperature sealing capability of elastomer O-rings. *Sealing Technology*, 2008(9):7–10, 2008.

[28] M. Jaunich, K. von der Ehe, D. Wolff, H. Voelzke, and W. Stark. Understanding low temperature properties of elastomer seals. *Packaging, Transport, Storage & Security of Radioactive Material*, 22(2):83–88, 2011.

[29] T. Grelle, D. Wolff, and M. Jaunich. Temperature-dependent leak tightness of elastomer seals after partial and rapid release of compression. *Polymer Testing*, 48:44–49, 2015.

[30] B. Omnes and P. Heuillet. Leak tightness of elastomeric seal at low temperature: Experimental and FEM-simulation. In *Constitutive Models for Rubber IX - Proceedings of the 9th European Conference on Constitutive Models for Rubbers, ECCMR*, pages 609–614, 2015.

[31] B. Zhang, M. Yu, and H. Y. Yang. Leakage analysis and ground tests of the O-type rubber ring seal applied in lunar sample return devices. *Proceedings of the Institution of Mechanical Engineers Part G-Journal of Aerospace Engineering*, 229(3):479–491, 2015.

[32] T. Grelle, D. Wolff, and M. Jaunich. Leakage behaviour of elastomer seals under dynamic unloading conditions at low temperatures. *Polymer Testing*, 58:219–226, 2017.

[33] X. Chen, J. Bartos, H. Salem, and R. Zonoz. Elastomers for high pressure low temperature HPLT sealing. volume 5, pages 3828–3842, 2016.

[34] Bob Flitney. How should we rate the temperature capabilities of elastomers? *Sealing Technology*, 2007(11):6–9, 2007.

[35] A. Douglas, O. Devlen, M. Mitchell, D. Edwin-Scott, and M. Neal. Development of a procedure to accurately measure the low-temperature operating limits of elastomeric seals. *Sealing Technology*, 2016(9):7–12, 2016.

[36] B. Alcock and J. K. Jørgensen. The mechanical properties of a model hydrogenated nitrile butadiene rubber (HNBR) following simulated sweet oil exposure at elevated temperature and pressure. *Polymer Testing*, 46(0): 50–58, 2015.

[37] A. G. Akulichev, B. Alcock, A. Tiwari, and A. T. Echtermeyer. Thermomechanical properties of zirconium tungstate/hydrogenated nitrile butadiene rubber (HNBR) composites for low-temperature applications. *Journal of Materials Science*, 51(24):10714–10726, 2016.

[38] L. Mullins. Effect of stretching on the properties of rubber. *Rubber Chemistry and Technology*, 21(2):281–300, 1948.

[39] L. R. G. Treloar. *The physics of rubber elasticity*. Oxford classic texts in the physical sciences. Oxford University Press, Oxford, New York, 3rd edition, 2005.

[40] G. Marckmann and E. Verron. Comparison of hyperelastic models for rubber-like materials. *Rubber Chemistry and Technology*, 79(5):835–858, 2006.

[41] O. H. Yeoh. Developments in finite element analysis. In *Engineering with Rubber*, pages 345–364. Carl Hanser Verlag GmbH & Co. KG, 2012.

[42] *Abaqus/CAE user's guide. Ver. 6.14*. Providence, RI, 2014.

[43] B. N. J. Persson. Theory of rubber friction and contact mechanics. *Journal of Chemical Physics*, 115(8):3840–3861, 2001.

[44] B. N. J. Persson, O. Albohr, C. Creton, and V. Peveri. Contact area between a viscoelastic solid and a hard, randomly rough, substrate. *Journal of Chemical Physics*, 120(18):8779–8793, 2004.

[45] B. N. J. Persson, O. Albohr, U. Tartaglino, A. I. Volokitin, and E. Tosatti. On the nature of surface roughness with application to contact mechanics, sealing, rubber friction and adhesion. *Journal of Physics: Condensed Matter*, 17(1):R1, 2005.

[46] C. Yang and B. N. J. Persson. Contact mechanics: contact area and interfacial separation from small contact to full contact. *Journal of Physics: Condensed Matter*, 20(21):215214, 2008.

[47] B. N. J. Persson and C. Yang. Theory of the leak-rate of seals. *Journal of Physics: Condensed Matter*, 20(31):315011, 2008.

[48] B. Lorenz and B. N. J. Persson. Leak rate of seals: Comparison of theory with experiment. *EPL (Europhysics Letters)*, 86(4):44006, 2009.

[49] B. Lorenz and B. N. J. Persson. Leak rate of seals: Effective-medium theory and comparison with experiment. *The European Physical Journal E*, 31(2): 159–167, 2010.

[50] B. N. J. Persson. Fluid dynamics at the interface between contacting elastic solids with randomly rough surfaces. *Journal of Physics: Condensed Matter*, 22(26):265004, 2010.

[51] A. G. Akulichev, B. Alcock, and Echtermeyer A. T. Compression stress relaxation in carbon black reinforced HNBR at low temperatures. *Polymer Testing*, 63:226–235, 2017.

[52] M. L. Williams, R. F. Landel, and J. D. Ferry. Mechanical properties of substances of high molecular weight .19. the temperature dependence of relaxation mechanisms in amorphous polymers and other glass-forming liquids. *Journal of the American Chemical Society*, 77(14):3701–3707, 1955.

[53] T. Tada, K. Urayama, T. Mabuchi, K. Muraoka, and T. Takigawa. Nonlinear stress relaxation of carbon black-filled rubber vulcanizates under various types of deformation. *Journal of Polymer Science Part B: Polymer Physics*, 48(12):1380–1387, 2010.

[54] J. Glucklich and R. F. Landel. Strain energy function of styrene butadiene rubber and the effect of temperature. *Journal of Polymer Science: Polymer Physics Edition*, 15(12):2185–2199, 1977.

[55] J. D. Ferry. *Viscoelastic properties of polymers*. Wiley, New York, 1980. 3rd ed.

[56] N. W. Tschoegl. *The phenomenological theory of linear viscoelastic behavior: an introduction*. Springer-Verlag, Berlin ; New York, 1989.

[57] S. W. Park and R. A. Schapery. Methods of interconversion between linear viscoelastic material functions. Part I-a numerical method based on Prony series. *International Journal of Solids and Structures*, 36(11):1653–1675, 1999.

[58] K. L. Johnson, K. Kendall, and A. D. Roberts. Surface energy and the contact of elastic solids. *Proceedings of the Royal Society of London A: Mathematical, Physical and Engineering Sciences*, 324(1558):301–313, 1971.

[59] J. A. Greenwood and K. L. Johnson. The mechanics of adhesion of viscoelastic solids. *Philosophical Magazine A*, 43(3):697–711, 1981.

[60] D. Maugis and M. Barquins. Fracture mechanics and the adherence of viscoelastic bodies. *Journal of Physics D: Applied Physics*, 11(14):1989, 1978.

[61] M. K. Chaudhury, T. Weaver, C. Y. Hui, and E. J. Kramer. Adhesive contact of cylindrical lens and a flat sheet. *Journal of Applied Physics*, 80(1):30–37, 1996.

[62] A. Tiwari, L. Dorogin, A. I. Bennett, K. D. Schulze, W. G. Sawyer, M. Tahir, G. Heinrich, and B. N. J. Persson. The effect of surface roughness and viscoelasticity on rubber adhesion. *Soft Matter*, 13:3602–3621, 2017.

[63] B. N. J. Persson and E. A. Brener. Crack propagation in viscoelastic solids. *Phys. Rev. E*, 71(3):036123, 2005.

[64] B. N. J. Persson, O. Albohr, G. Heinrich, and H. Ueba. Crack propagation in rubber-like materials. *Journal of Physics: Condensed Matter*, 17(44):R1071, 2005.

[65] J. A. Greenwood. The theory of viscoelastic crack propagation and healing. *Journal of Physics D: Applied Physics*, 37(18):2557, 2004.

[66] J. A. Greenwood. Viscoelastic crack propagation and closing with lennard-jones surface forces. *Journal of Physics D: Applied Physics*, 40(6): 1769, 2007.

[67] J. A. Greenwood, K. L. Johnson, S. H. Choi, and M. K. Chaudhury. Investigation of adhesion hysteresis between rubber and glass using a pendulum. *Journal of Physics D: Applied Physics*, 42(3):035301, 2009.

[68] A. G. Akulichev, A. Tiwari, L. Dorogin, A. T. Echtermeyer, and B. N. J. Persson. Rubber adhesion below the glass transition temperature: role of frozen-in elastic deformations. *Submitted*, 2017.

[69] R. Hornig, J. Sunder, and B. Herr. Static cold sealing force behaviour of amorphous hnbr materials. *International Polymer Science and Technology*, 39(11):T1–T14, 2012.

[70] A. G. Akulichev, A. T. Echtermeyer, and B. N. J. Persson. Interfacial leakage of elastomer seals at low temperatures. *Submitted*, 2017.

[71] S. N. Shubin, A. B. Freidin, and A. G. Akulichev. Elastomer composites based on filler with negative thermal expansion coefficient in sealing application. *Archive of Applied Mechanics*, 86(1-2):351–360, 2016.

[72] T. A. Mary, J. S. O. Evans, T. Vogt, and A. W. Sleight. Negative thermal expansion from 0.3 to 1050 kelvin in ZrW2O8. *Science*, 272(5258):90–92, 1996.

[73] R.A. Schapery. Thermal expansion coefficients of composite materials based on energy principles. *Journal of Composite Materials*, 2(3):380–404, 1968.

[74] E. H. Kerner. The elastic and thermo-elastic properties of composite media. *Proceedings of the Physical Society. Section B*, 69(8):808, 1956.

[75] U. Bianchi. Pressure Effects on glass transition in polymers. *Journal of physical chemistry*, 69(5):1497–1504, 1965.

[76] N.W. Tschoegl, W. G. Knauss, and I. Emri. The effect of temperature and pressure on the mechanical properties of thermo- and/or piezorheologically simple polymeric materials in thermodynamic equilibrium – a critical review. *Mechanics of Time-Dependent Materials*, 6(1):53–99, 2002.

[77] K. Koperwas, A. Grzybowski, K. Grzybowska, Z. Wojnarowska, J. Pionteck, P. Sokolov, and M. Paluch. Pressure coefficient of the glass transition temperature in the thermodynamic scaling regime. *Physical Review E*, 86 (4, 1), 2012.

[78] B. Lorenz and B. N. J. Persson. Fluid squeeze-out between rough surfaces: comparison of theory with experiment. *Journal of Physics: Condensed Matter*, 23(35):355005, 2011.

[79] B. N. J. Persson, N. Prodanov, B. A. Krick, N. Rodriguez, N. Mulakaluri, W. G. Sawyer, and P. Mangiagalli. Elastic contact mechanics: Percolation of the contact area and fluid squeeze-out. *The European Physical Journal E*, 35 (1):1–17, 2012.

[80] W. Miller, C. W. Smith, D. S. Mackenzie, and K. E. Evans. Negative thermal expansion: a review. *Journal of Materials Science*, 44(20):5441–5451, 2009.

[81] K. Takenaka. Negative thermal expansion materials: technological key for control of thermal expansion. *Science and Technology of Advanced Materials*, 13(1), 2012.

Appendix A

Enclosed papers

A.1 Paper I

Compression stress relaxation in carbon black reinforced HNBR at low temperatures

A.G. Akulichev, B. Alcock, A.T. Echtermeyer.

Polymer Testing. 2017;63:226-235

Paper I

Polymer Testing 63 (2017) 226–235

Contents lists available at ScienceDirect

Polymer Testing

journal homepage: www.elsevier.com/locate/polytest

Material Behaviour

Compression stress relaxation in carbon black reinforced HNBR at low temperatures

Anton G. Akulichev [a, *], Ben Alcock [b], Andreas T. Echtermeyer [a]

[a] The Norwegian University of Science and Technology, Department of Mechanical and Industrial Engineering, Richard Birkelands Vei 2 B, 7034 Trondheim, Norway

[b] SINTEF Materials and Chemistry, Forskningsveien 1, 0373 Oslo, Norway

ARTICLE INFO

Article history:
Received 24 June 2017
Received in revised form
16 August 2017
Accepted 17 August 2017
Available online 19 August 2017

Keywords:
Stress relaxation
Rubber
Low-temperature
Viscoelastic properties
Glass transition
HNBR

ABSTRACT

Findings of a study of stress relaxation behaviour of hydrogenated nitrile butadiene rubber (HNBR) at nominal compressive strains up to 0.4 and temperatures above and below the glass transition temperature T_g are reported. Two formulations of a model HNBR with 36% acrylonitrile content and carbon black (CB) loading of 0 and 50 phr were investigated. The relaxation function of HNBR is found to be independent of strain at temperatures right above the T_g or at times longer than 10^{-3} s for the deformations employed. CB imparts higher long-term stiffness and also larger relaxation strength at times longer than 10^{-4} s to the HNBR, but it does not affect the relaxation behaviour of the rubber in the time span from $10^{-3} - 10^{4}$ s. In addition, the relationship between the strain energy function of HNBR and temperature is demonstrated to have a complex concave-downward shape which is affected by two competing contributions of entropy elasticity and the stress relaxation.

1. Introduction

The mechanical behaviour of elastomers is known [1] to be affected by temperatures due to their entropic nature. In fact, from the Gaussian theory of rubberlike elasticity it follows that the strain energy function (W) of a deformed elastomer proportionally increases with temperature. For instance, the theory entails the following expressions for the strain energy function and the nominal stress S in uniaxial loading [1]:

$$W = \frac{1}{2}nkT\left(\lambda^2 + 2\lambda^{-1} - 3\right) = \frac{1}{2}G\left(\lambda^2 + 2\lambda^{-1} - 3\right) \quad (1)$$

$$S = nkT\left(\lambda - \frac{1}{\lambda^2}\right) = G\left(\lambda - \frac{1}{\lambda^2}\right) \quad (2)$$

where $\lambda = 1 + \varepsilon$ is the stretch ratio, n is the number of network chains per unit volume, k is the Boltzmann constant, T is temperature, and G is the shear modulus.

On the other hand, elastomers also exhibit a viscoelastic behaviour [2]. At temperatures far above the glass transition temperature, the viscoelastic contribution to the strain energy is small and often negligible, and the stress-strain response of elastomers is well described by hyperelastic models. As the temperature approaches the glass transition region, the viscoelasticity begins to play a greater role. One of the practically important consequences, especially for sealing applications, is stress relaxation (SR). When an elastomer is subjected to a specified constant deformation the stress in the material will decay. For a sealing material, SR results in a decrease of contact pressure potentially leading to reduced sealing capability. SR also correlates well with the compression set in elastomer seals [3].

Stress relaxation is rather extensively studied in industrially important elastomers at temperatures above T_g in connection with their aging and chemical degradation, e.g. in Refs. [4–10]. However, there are few studies dedicated to SR at low temperatures, specifically near the glassy region, even though some industrial equipment with elastomer components can be permanently or periodically exposed to such temperatures [11,12]. Neglecting the effect of SR at these low temperatures may lead to catastrophic consequences [13].

Early attempts to understand and characterize SR at low temperatures were undertaken in the 1940s [14–16]. Some of the most

* Corresponding author.
E-mail address: anton.akulichev@ntnu.no (A.G. Akulichev).

http://dx.doi.org/10.1016/j.polymertesting.2017.08.023
0142-9418/

comprehensive investigations of the phenomenon in the glassy and transition regions were made in Refs. [17–20] on polyisobutylene and other amorphous polymers. The authors also demonstrated the equivalence of time and temperature effects on the relaxation behaviour of these materials which is now known as the time-temperature superposition (TTS) principle. The superposition in its simplest form is performed by means of horizontal translation of a viscoelastic quantity along the logarithmic time axis (the time scale becomes reduced by a shifting factor a which is a function of temperature). It was later shown that the temperature variation of the horizontal shifting factor is independent of strain [21,22].

Various aspects of low-temperature SR were subsequently reported in literature [21–32]. Particularly, Bartenev and colleagues [26,27] assert that elastomers exhibit unique relaxation mechanisms with relatively low activation energy when subjected to low strains in the glass transition region. The relaxation process occurs in elastomers held in the temperature region near T_g and is believed to be caused by breakage of ordered supramolecular microdomains formed at low temperatures. These domains create apparent cross-links between the polymer chains at low temperatures and, thus, are responsible for the observed increase in the material stiffness [26,27]. This assertion is in line with the recent work on polymer blends of polybutadiene and styrene butadiene rubber [33] that suggests that rubber-like and glassy-like domains coexist in elastomers exposed to temperatures near the glass transition. The authors [33] concluded that the glassy domains progressively form with cooling in the glass transition region, and, as a result of their formation, the segmental movements of the polymer chains become more and more constrained.

Another important question is whether the strain and the state of strain have any effect on the relaxation function of elastomers at low temperatures. Assuming the total deviatoric stress response of a deformed elastomer consists of the contributions of the long-term hyperelastic stress component $S_{eq}(\lambda)$ and the viscoelastic (time-dependent) stress component $S_{VE}(\lambda,t)$, the time and strain effects on the stress response are separable if

$$S_{VE}(\lambda, t) = S(\lambda)\psi(t) \tag{3}$$

Where $\psi(t)$ is the relaxation function. The separability of time and strain is typically evident from a parallel nature of relaxation curves taken at various strains. Glucklich and Landel [22] demonstrated in their short-term relaxation experiments in uniaxial and biaxial extension of styrene-butadiene rubber (SBR) at temperatures down to −45 °C (about 15 °C above the T_g) that the time and strain effects on the material strain energy function are separable. However they predicted that the invariance would not hold at temperatures far below the minimum used in their experiments. The topic of strain invariance of the relaxation behaviour was later investigated by Tada et al. [34] who employed 3 modes of deformation and confirmed the separability of time and strain effects using both carbon black filled and unfilled SBR in the rubbery region. It is also worth noting that many studies [22,32,34,35] conclude that the SR behaviour in filled and unfilled elastomers is independent of the state of strain (with an exception of volumetric compression).

The research activities in the aforementioned literature have only concentrated on relatively short-term SR with a major focus on the rubbery region, while the region near T_g is often unexamined. It remains inconclusive whether the strain-time separability holds in elastomers cooled down to their glass transition temperature and below. Hence, the primary objective of this work is to study the finite-strain relaxation behaviour of a model hydrogenated nitrile butadiene rubber (HNBR) compound under ambient and sub-ambient conditions near the T_g. The data at some temperatures below the glass transition were also collected and reported here. However, these results are given less attention because of their limited practical importance. The relaxation properties at elevated temperatures are also of interest, especially for carbon black reinforced elastomers, and therefore high-temperature physical stress relaxation is also covered in this work.

The secondary objective of this work is to elucidate the effect of carbon black on the relaxation dynamics and the relaxation strength of the HNBR. The third objective is to verify that TTS can be applied to form SR master curves and identify viscoelastic material parameters required for modelling in FEA software. The lack of available the physical relaxation data for HNBR was also a motivation for this work, although some short-term compression stress relaxation results for an HNBR compound have recently become available [36].

2. Materials and experimental procedure

2.1. Materials and processing

A typical elastomer formulation widely used in demanding sealing applications is studied. The composition is based on hydrogenated nitrile butadiene rubber with 96% saturated polybutadiene with 36% acrylonitrile content and varied carbon black (CB) content of either 0 or 50 phr. The compound formula is detailed in Table 1.

These two compounds are further designated as filled and unfilled HNBR for simplicity. The compounds (except the peroxide) were first combined in an internal mixer and then mixed with the peroxide in a two roll mill. Compression moulding and vulcanization in a press at 170 °C for 20 min was then followed. Finally, a post-curing operation at 150 °C for 4 h in an oven was carried out. More information about the processing and the basic material test data is available in a previous publication [37].

As with all polymers, HNBR shows changes in structure and mechanical performance over time in service, depending on factors such as the local chemical environment and temperature, and previous works have described some of these changes [38,39]. However, all the tests reported in this paper were performed on materials in an unaged state, i.e. soon after manufacture.

The materials have a T_g of about −16 °C as determined by the position their DMTA tan delta peaks [3,38] measured at 1 Hz frequency or −23 °C as determined from DSC results (the heating rate was 20 °C/min) [37].

2.2. Test methods

A test series was developed to measure stress relaxation behaviour at temperatures from −40 °C up to +110 °C. The relaxation testing was done in compression, while uniaxial tensile testing was employed in order to observe the basic changes in the mechanical behaviour with cooling and define the temperature limits of rubberlike elasticity of the compounds.

Table 1
Composition of the elastomers used in this work.

Component	Content, parts per hundred rubber (phr)
HNBR	100
Antioxidant	3
Stearic acid	0.5
Zinc oxide	5
Magnesium oxide	10
Plasticizer	20
Peroxide	10
N-330 HAF carbon black	0 or 50

2.2.1. Uniaxial tensile test

The stress-strain behaviour in quasi-static uniaxial extension was investigated using a Zwick universal testing machine equipped with a thermal chamber, a contact extensometer and a 1 kN load cell. The specimen geometry was in accordance with ISO 37 type 2. Each specimen was fixed in the machine by mechanical grips and pre-loaded to 0.5 N before stretching. The specimens were exposed to the testing temperature for 30 min prior to the commencing the test. All tensile tests were carried out at a strain rate of 0.025 s^{-1}.

2.2.2. Compression stress relaxation (CSR)

Sub-zero compression stress relaxation (CSR) experiments were carried out on a special test rig illustrated in Fig. 1 (hereafter called the "manual method"). The main principle is that a specimen is manually compressed between lubricated steel plates by a screw to a predefined deformation. The applied deformation was controlled by means of the screw rotation. The specimens were maintained at the constant strain and temperature while the force was recorded. Test times were chosen to observe stress decay preferably until attaining the equilibrium where possible. The times were, thus, between 3 h and 15 days.

Prior to loading the rigs, the specimens were positioned in a freezing cabinet and kept there at the desired temperature for at least 12 h. The temperature fluctuations inside the freezing cabinet were ±0.4 °C; the values reported in the paper are mean values. The experiments at most conditions except for temperatures lower than −20 °C were repeated to ensure reproducibility.

The accuracy of the experimental data obtained by compressing specimens using the "manual method" was checked for a few cases by a more conventional test method using the universal testing machine. The discrepancy between these two set-ups was ≤ ca. 3%. This small discrepancy is believed to be caused by the imperfect control of the loading rate in the "manual method".

CSR at temperatures above 0 °C was performed using a Netzsch-Gabo Eplexor 150 DMTA machine with a 1.5 kN load cell and parallel plate specimen holders, operating in compression mode.

The compression specimens had a cylindrical shape with 20 mm nominal diameter and 10 mm height. For measurements below −20 °C, smaller specimens of 10 mm diameter and 6 mm height were used due to the increased level of stiffness of the material and the limited capacity of the force sensors.

The investigated range of nominal compressive strains ε was 10–40% which is relevant for elastomer seals. The loading and subsequent relaxation was performed stepwise with a nominal strain step length of 5%. The maximum degree of compression at temperatures near and lower than the T_g was, however, reduced to 15–30% due to the high stiffness of the materials in the glassy state. Prior to the relaxation experiments, the specimens were pretreated with 4 full deformation cycles in order to minimise the Mullins effect [40]. Pre-studies (not presented here) showed that the data were inconsistent without this pre-treatment, specifically for the carbon black containing material. The specimens were left unloaded to recover their original shape for at least 48 h after the pre-treatment and prior to each test.

3. Results and discussion

3.1. The effect of low temperatures

The quasi-static uniaxial tensile test data, illustrated in Fig. 2, demonstrate the influence of sub-zero temperatures on the stress-strain behaviour of the HNBR compounds.

Exposure to low temperatures generally leads to an increase of the stiffness of HNBR. The low-temperature effect on the elastic modulus is more pronounced at small strains. The large initial modulus is not sustained during further extension. It gradually declines with strain and takes values that are an order of magnitude lower (which are much closer to the modulus data observed in the rubbery state) than that at the initial loading. The increase of stiffness at small strains in the transition region (ca. −16 to −23 °C) is more pronounced in the filled HNBR, while the small-strain tensile behaviour at −40 °C is rather similar in both elastomers.

The most drastic difference is observed between the curves at and below the T_g, especially at small strains (<0.05). A yielding phenomenon is quite apparent at −40 °C in both compounds while it does not seem to occur at the higher temperatures used in the experiment. This complicated behaviour is alike that observed in other glassy polymers, such as PMMA. Therefore, the SR at temperatures below −25 °C will not be evaluated in detail. The ultimate failure strain was not attained in HNBR stretched to 50% at −40 °C at the strain rate of 0.025 s^{-1}. It is likely that the brittleness limit of HNBR at this strain rate lies at an even lower temperature. The material becomes softer with larger extensions and is capable to deform more due a phenomenon of stress-induced or "forced"

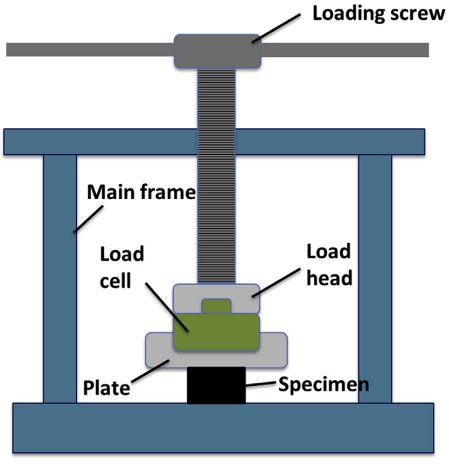

Fig. 1. Schematic of the compression rig used in the "manual method".

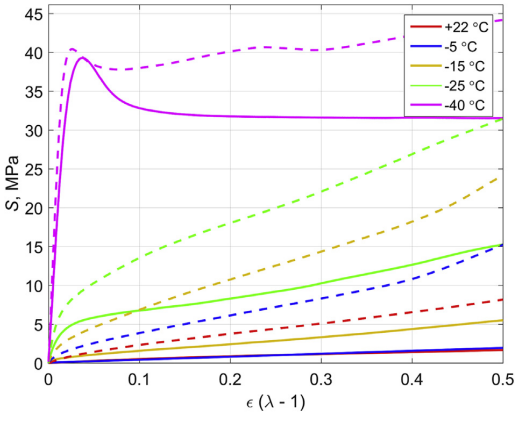

Fig. 2. Representative nominal tensile stress-strain curves of the unfilled (solid lines) and filled (dashed lines) HNBR at the indicated temperatures.

elasticity [41] and also likely due to adiabatic heating, see e.g. Ref. [33]. Bukhina and Kurlyand [41] discuss in more detail the various factors affecting the loading response of elastomers in the glassy region.

It is interesting to note that the difference between the curves at +22 and −5 °C of the unfilled HNBR is small enough that they almost overlap. This rather small difference in the material tension behaviour can mislead to a conclusion of an insignificant temperature dependency of the material stiffness in this temperature region. This, however, is not the case, and the apparent similarity is a result of 2 competing effects: a change of stiffness due to its explicit temperature relation owing to its entropic origin and the stress relaxation processes occurring simultaneously with the deformation. The relaxing part of stress appears to grow with cooling which will be demonstrated in details further here, while the temperature effect on the entropic elasticity will be taken into account in section 3.2.

The effect of temperature on the relaxation behaviour of the unfilled HNBR compound is shown in Fig. 3.

As expected, the cold environment leads to stiffening of HNBR which is manifested in an increase in the instantaneous compressive stress. This is followed by a rapid drop of the stress. The relaxation curves behave qualitatively in agreement with those reported for polyisobutylene [20]. It is possible to identify 3 characteristic regions: the rubbery, the transition and the glassy region. The rubbery region exhibits the lowest rates of relaxation and the material reaches the equilibrium state much faster than in the other regions. At this temperature polymer molecules are believed to have a greater ability to move, and most relaxation processes occur almost instantaneously with deformation. Hence, the relaxation is not as pronounced as when under sub-ambient conditions.

The time window of the compression experiment becomes comparable with the relaxation times in the HNBR exposed to lower temperatures, which is manifested in the observed increase of the relaxation rates. The transition region is, thus, characterized by the most marked SR with the greatest relaxation rates near T_g (the curves at −14.8 °C, −19.8 °C and −25.3 °C). Despite the sharp stress decay at short times, the cooled elastomer in this region requires much more time to achieve the equilibrium state than at ambient temperature. Nevertheless the stress values at longer times are comparable with those in the rubbery state. Furthermore, the HNBR might even have a lower stress magnitude at long times (lower long-term stiffness) in the sub-zero conditions than at ambient or elevated temperatures due to the entropic nature of the material.

Although the curves in the glassy region have somewhat lower rates of relaxation, noticeable stress decay is also observed. The SR results at the lowest temperature of about −40 °C are rather surprising as the material exhibits a reduction of the initial stress by a factor of 2 after 10^3 s and by a factor of 3 after 10^6 s (ca. 12 days). The result may suggest that the molecular motion in the glassy state is not completely frozen and some rearrangement of the deformed polymer chains still occur in spite of the imposed freezing conditions. This observation cannot be explained by the adiabatic heating during the load ramp phase since the relaxation rate keeps on being rather high over the whole time span of the experiment. A

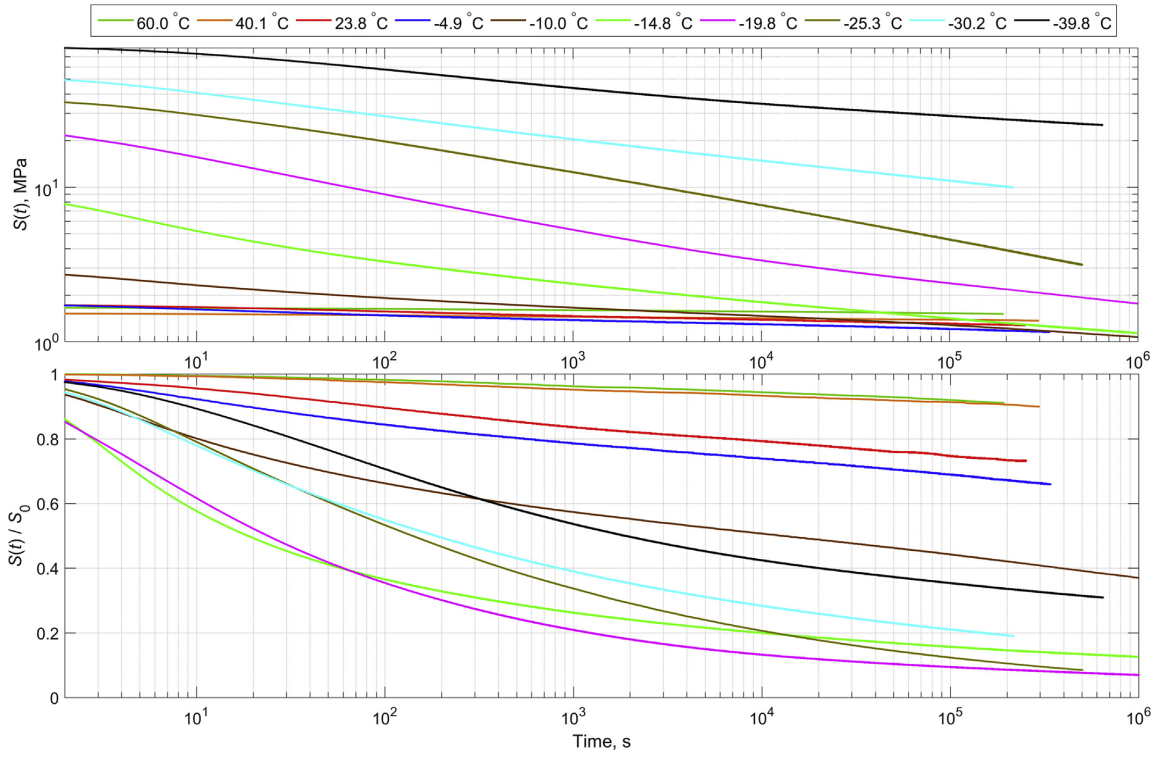

Fig. 3. CSR curves of unfilled HNBR at 20% nominal compression at the indicated temperatures. Top – logarithmic plot of the nominal stress as a function of time; bottom – semi-logarithmic plot of the nominal stress normalized by the maximum (instantaneous) stress value as a function of time.

potential explanation can be as the following. The HNBR investigated here is a copolymer of saturated and unsaturated butadiene units with acrylonitrile units with the ratio between butadiene and acrylonitrile (64:36). It seems likely that there must be some butadiene rich regions which may be mobile down to below −100 °C [33,42], therefore they can still allow some stress relaxation activity below the apparent T_g of the material. It should be noted that the unloaded specimens fully recovered their original height after their warming up (within the accuracy of a calliper measurement).

The effect of temperatures on the stress relaxation in the carbon black reinforced compound is illustrated in Fig. 4. As expected and reported elsewhere [43] carbon black imparts greater long-term stiffness on the elastomer. The impact of low temperatures on the relaxation behaviour is qualitatively similar to the unfilled rubber. The instantaneous stress response of the reinforced HNBR increases with cooling, however the relaxation processes in the reinforced material take much more time. The relaxation rates seen in the transition and glassy regions of the filled HNBR are smaller than those observed in the unfilled compound near T_g. For instance, the average relaxation rate in the unfilled HNBR at −20 °C is approximately 16% per decade, whereas it decreases to approximately 12.6% per decade in the filled HNBR at the same temperature. This is believed to be due to the impeded segmental mobility of the macromolecular chains in the vicinity of the carbon black particles. As a consequence, the filled compound requires much more time to approach the equilibrium state. Nevertheless, the stress decay in the reinforced HNBR is prominent even below the glass transition temperature. The latter, for instance, exhibits a double decrease in the compressive stress approximately after 10^4 s of the experiment at −39.3 °C.

3.2. The effect of temperature on the strain energy function and long-term stiffness

Before further analysis of the relaxation behaviour of HNBR, the aforementioned temperature dependence of the material stiffness will be addressed. The strain energy function of deformed elastomers is often modelled with viscoelastic (transient) and hyperelastic contributions. The latter, as explained in the introduction, is affected by temperature due to its entropic origin [1]. As such, a temperature raise would result in a proportional increase of the strain energy function and the stiffness of the elastomer. On the other hand, the material stiffness at short and intermediate times increases with cooling as, for example, demonstrated in Figs. 3 and 4. Therefore, these competing temperature effects should be clearly distinguished from each other.

Fig. 5(a–b) depict the step strain stress relaxation response at various temperatures and Fig. 5(c–d) show a surface plot of the normalized strain energy density computed by integrating the isochronal stress-strain data. It is quite evident that the long-term stiffness of the base HNBR is temperature dependent in accordance with the established basics of rubber elasticity. The minimal strain energy density is observed at −10 °C after about 3 h of stress

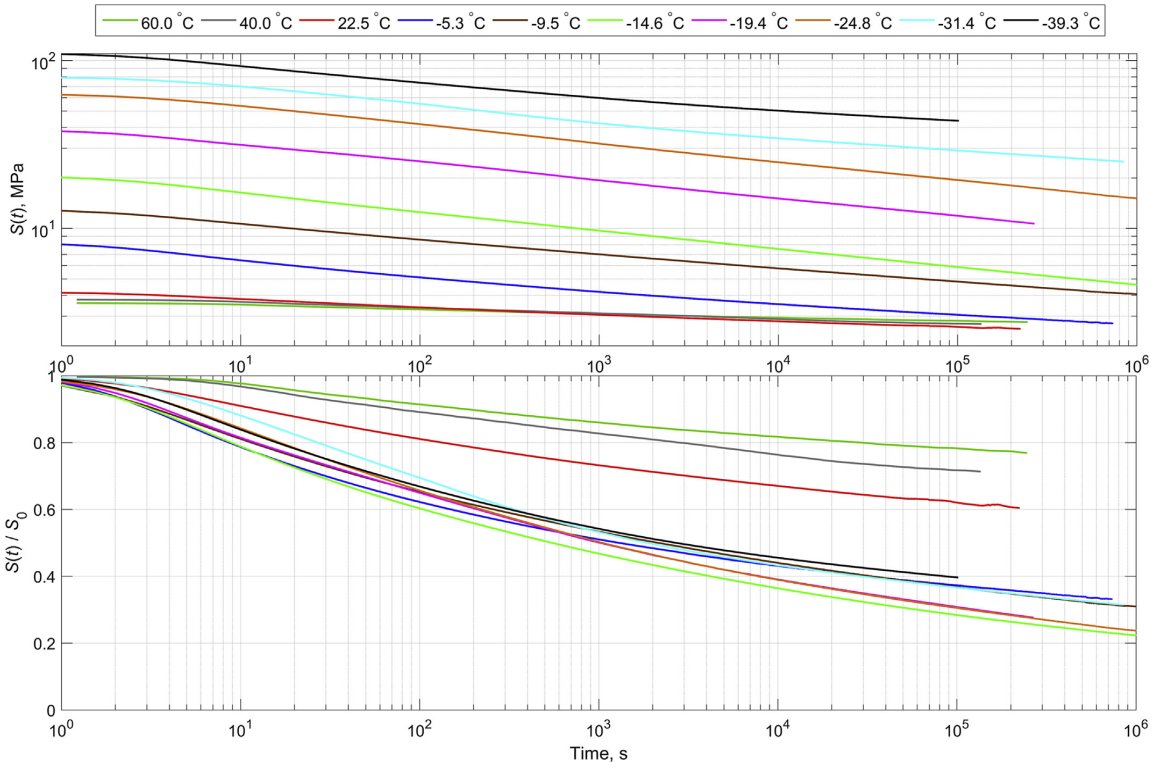

Fig. 4. CSR curves of filled HNBR at 20% nominal compression at the indicated temperatures (the CSR data at −39.3 °C was measured at 15% compression and scaled to 20%). Top – logarithmic plot of the nominal stress as a function of time; bottom – semi-logarithmic plot of the nominal stress normalized by the maximum (instantaneous) stress value as a function of time.

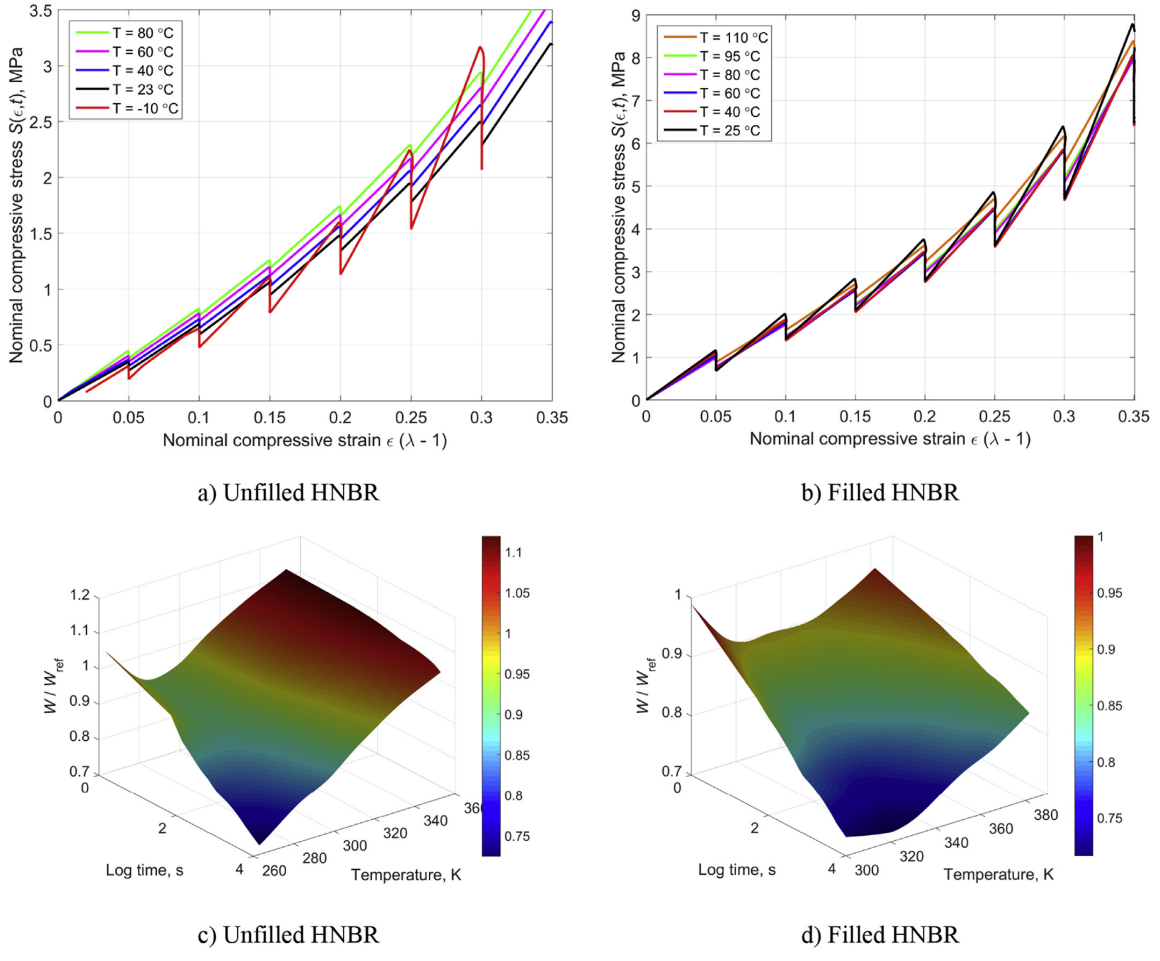

Fig. 5. (a–b) Effect of temperature on the step strain CSR response (Eplexor data plotted using linear interpolation between points, the strain rate here is approximately 0.005 s^{-1}) and (c–d) the time-temperature contour plot of the corresponding strain energy density function for the indicated compounds. The strain energy density data are interpolated by cubic splines and normalized by the values of the instantaneous strain energy density obtained at ambient temperature.

relaxation. The temperature behaviour of the material at shorter times is more complicated due to a noticeable transient component of stress which increases with further cooling. There exists a local minimum of the short-time strain energy density at about 10 °C, below which it steeply increases owing to a growing contribution of the relaxing part. Above 10 °C, it becomes steadily larger with temperature.

The difference between stress-strain curves of the reinforced HNBR at various temperatures is not as clear as in the unfilled rubber. Certainly, the viscous contribution to the instantaneous stress response is much stronger in the filled elastomer than in the unfilled elastomer. The filled elastomer exhibits the highest strain energy density at the ambient temperature in the temperature range depicted in Fig. 5. It is believed that this large transient component masks the entropic contribution the material stiffness. The entropic part, on the other hand, is seen to dominate at elevated temperatures and at long times (Fig. 6). A local minimum of the strain energy function at short times is also observed in the reinforced HNBR, however it is shifted to about 80 °C. Similar temperature relations of the material stress response which had concave-downward shapes with inflection points lying within 70–120 °C were observed in carbon black filled SBR compounds [44]. The inflection point is also evident here at longer times, although it is shifted to lower temperatures (approximately 50 °C).

The effect of temperature on the long-term strain energy functions of both compounds is compared in Fig. 6.

The change from entropic elasticity to the internal energy elasticity at longer times occurs quite abruptly in the unfilled HNBR in the vicinity of T_g, whereas the transition region in the filled compound is more smooth and, as pointed out above, shifted to higher temperatures if compared to the unfilled HNBR. The variation of the material strain energy function with temperature in the entropy-dominated elasticity region is quite well described by a linear relation in both compounds. However, the slope of this relation is higher in the unfilled HNBR than in filled HNBR. The difference can be explained by the presence of carbon black (50 phr which is equivalent to 20.4 vol %) which has a non-entropic origin and softens with temperature. In addition, the tightly bound

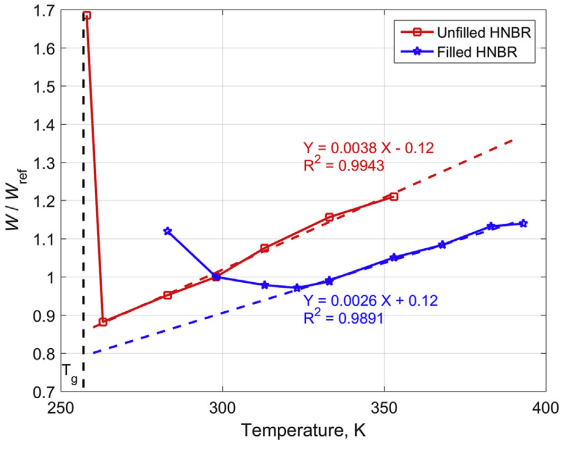

Fig. 6. 10000-sec isochrones of the normalized strain energy density having the same significance as in Fig. 5 plotted as functions of absolute temperature. The data are corrected accounting for the thermal dilatation [37]. The coloured dashed lines represent linear fit in the range of 263–353 K and 333–393 K for the unfilled and filled HNBR respectively.

regions of HNBR [43] local to the surface of the CB particles might contribute to the difference.

Fig. 7 summarises the findings in this section.

The strain energy function of HNBR has a complex concave-downward shape when plotted against the temperature. The position of the minimum strain energy on the temperature scale T' is defined by the experiment relaxation time (or the strain rate), but it cannot be lower than the T_g. Below this point the temperature-dependent stress response of HNBR is presumed to be governed by the internal energy based mechanisms, while the long-term response might still be hyperelastic and follow the entropic temperature relation if temperatures above T_g are considered. It is likely that the volume fraction of glassy-like domains becomes high enough to make the internal energy contribution stronger here. The entropy elasticity, on the other hand, begins to dominate at temperatures above the inflection point T'. The position of T' can also be shifted to higher temperatures by addition of filler as observed in the carbon black reinforced HNBR. Therefore, the temperature effect on the instantaneous response of filled rubber might be masked by a considerable transient stress component at shorter times, since this has a tendency to increase with cooling.

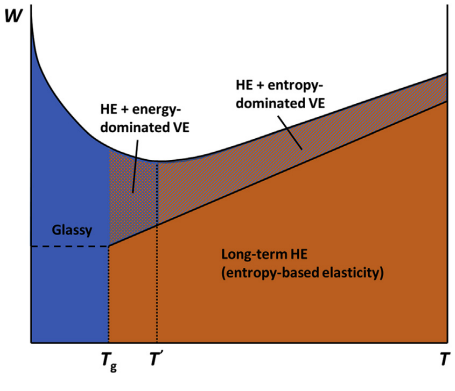

Fig. 7. Schematic of the temperature variation of the strain energy function of HNBR which is composed of hyperelastic (HE) and viscoelastic (VE) parts.

3.3. Time-temperature superposition

The obtained CSR data and shape of the overlapping parts of the segments at and above T_g suggests that a master curve of $S(t)$ or $E(t)$ can be constructed using the TTS principle and assuming that the materials are thermo-rheologically simple, i.e. their viscoelastic response can be translated along the log time scale with temperature. In addition, it is assumed that the relaxation at moderate temperatures is governed only by the physical mechanisms, but not by any chemical changes. The results collected at temperatures below −25 °C were not used in TTS.

An approach allowing for unrestricted horizontal and vertical shifting of the time segments [45] was utilized and implemented in MATLAB as a minimization problem. The following function was minimized with respect to the horizontal and vertical shifting parameters $a(T)$ and $b_{num}(T)$ for each isothermal time segment being shifted:

$$err = \frac{1}{n}\sum_{i=1}^{n}\frac{\left(y_i(t_i) - \hat{y}_i(a(T), b_{num}(T), t_i)\right)^2}{(y_i(t_i))^2}$$

Here y_i are the experimental values of stress S at times t_i, $\hat{y}_i$ are the values of the stress relaxation function interpolated by a polynomial and n is the number measurement points in each segment. The effects of entropy-elasticity as well as the density change associated with cooling or heating are taken into account using values of the vertical shifting factor $b(T)$ obtained from the slopes of the relationships in Fig. 6, i.e. 0.0038 and 0.0026 per degree Kelvin for unfilled and filled compounds respectively. The numerical vertical shifting factor $b_{num}(T)$ bears no physical significance and is used in the optimisation routine merely to obtain smoother master curves. Therefore, the values of $b_{num}(T)$ which were between 0.98 and 1.02 are not reported here. Short-time CSR data corresponding to 15× the loading ramp time in each segment were ignored in order to minimise the errors associated with the ramp effect [46]. In spite of the simplifications mentioned, this approach, as demonstrated in Fig. 8 and Fig. 9, yields a decent

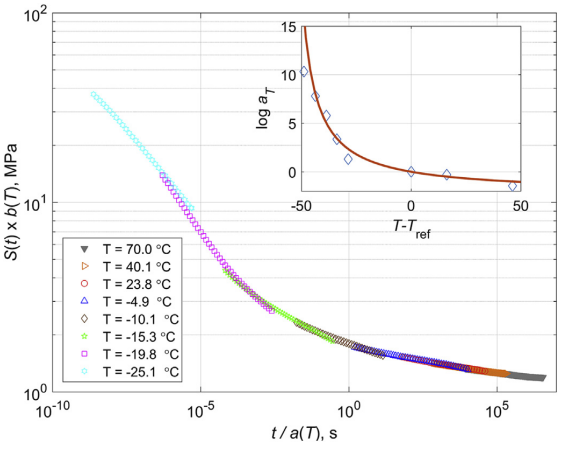

Fig. 8. Representative CSR master curve for the unfilled HNBR. 20% nominal compression and T_{ref} = 23.8 °C. The inset depicts the variation of the horizontal shifting factor with temperature and its fitting by the WLF equation (solid line).

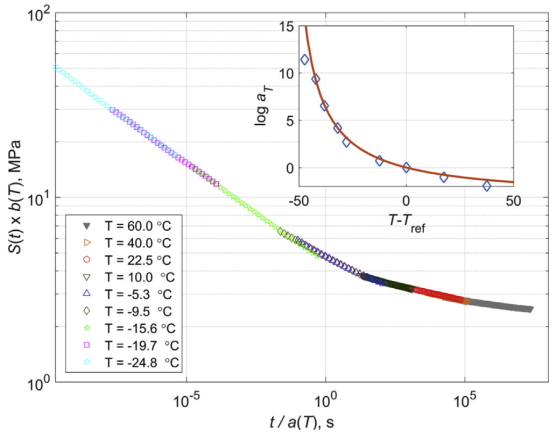

Fig. 9. Representative CSR master curve for the carbon black filled HNBR. 20% nominal compression and T_{ref} = 22.5 °C. The inset depicts the variation of the horizontal shifting factor with temperature and its fitting by the WLF equation (solid line).

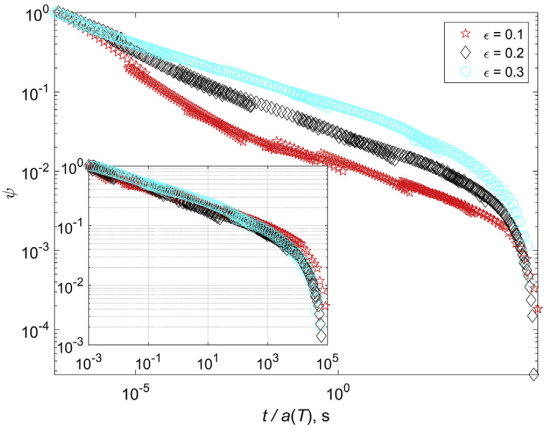

Fig. 10. The relaxation functions of the unfilled HNBR at the indicated nominal compressive strains (short-time cut-off at 10^{-7} s). The inset shows the same at times $\geq 10^{-3}$ s.

representation of the relaxation functions of the filled and unfilled elastomers over a large time span.

3.4. The effect of strain

The master curves are further used to evaluate the effects of strain and filler on the relaxation behaviour of HNBR. The effect of strain is analysed here while the effect of the filler is considered in the next section.

Tada et al. [34] suggest that the relaxation functions of rubber compounds should be analysed and compared after subtracting the equilibrium stress values. Taking this into consideration, a relaxation function $\psi(t)$ is introduced and computed as follows:

$$\psi(t) = \frac{S(t) - S_{eq}}{S(t_1 = t_{\min}) - S_{eq}} \tag{4}$$

where S_{eq} is the equilibrium (long-term) stress, $S(t)$ is the stress at time t.

The effect of strain on the relaxation function of HNBR is illustrated in Fig. 10. It is evident that at times $\geq 10^{-3}$ s the relaxation dynamics of HNBR are not influenced by the compressive strain imposed in the experiment. This time threshold corresponds to approximately between T_g+1 and T_g+8 °C depending on method used to define the T_g [37,38]. Hence, it is fair to state the relaxation behaviour of HNBR held at above the glass transition temperature is to a good approximation independent of strain in the range of deformations experienced in sealing applications. That results in an important conclusion that the strain and time effects can be separated if the elastomer is maintained at temperatures above T_g. This, in turn, entails a simpler analysis and model implementation into FEA software.

However, the separability of time and strain does not hold when the material is cooled down to or below the glass transition temperature. Indeed, the relaxation functions at shorter ($<10^{-3}$ s) experimental times exhibit different shapes, as shown in Fig. 10. The deviation between the relaxation curves progressively grows with reduction of the time scale of the experiment. This mismatch between the curves is not surprising taking into account that the mechanical behaviour of elastomers in the glassy and near-glassy state becomes much more complex and includes yielding phenomena, as mentioned before or studied in more detail elsewhere [33]. Furthermore, it seems from the shape evolution of the relaxation curves that each strain step incurs a shift from the glassy (or the transition) to rubbery region. This might indicate that strain can probably be utilized as a reduced variable for the glassy and transition regions of rubber, however a larger data set would be required to confirm this.

3.5. The effect of carbon black

The effect of carbon black on the relaxation behaviour of the HNBR is illustrated in Fig. 11.

Carbon black imparts higher stiffness to the HNBR, but it is seen that it does not yield much impact on the relaxation behaviour of the polymer in its rubbery region. The relaxation functions for the reinforced and non-reinforced compounds are in very good agreement with each other in a time interval from 10^{-3} to about 10^4 s which supports the results presented elsewhere for SBR [34]. Therefore, it can be concluded that the carbon black does not affect

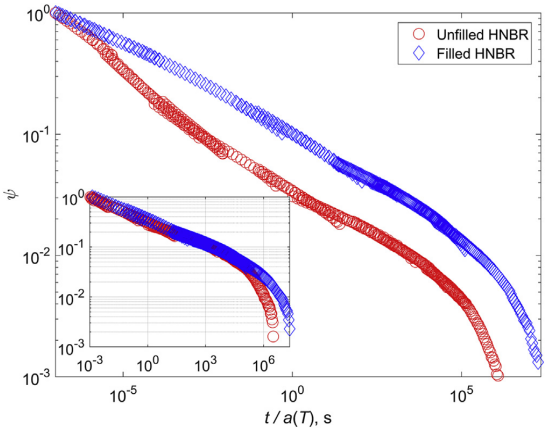

Fig. 11. The relaxation functions $\psi(t)$ of filled and unfilled HNBR at 20% nominal compression (short-time cut-off at 10^{-7} s). The inset shows the same at times $\geq 10^{-3}$ s.

the relaxation dynamics of the studied HNBR in the mentioned time span or at temperatures above the T_g.

The relaxation functions at short ($<10^{-3}$ s) and long ($>10^4$ s) times, on the contrary, deviate substantially. At long times (or at high temperatures) the unfilled HNBR attains the equilibrium state faster than the carbon black reinforced counterpart, which results in lower rates of the stress decay until they diminish to nearly zero. At short times (or as mentioned before at low temperatures in the vicinity of T_g) carbon black seems to hinder the relaxation processes in the polymer, and they occur at a lower rate in the unfilled HNBR.

Finally, the relaxation spectra of the materials are compared. The relaxation spectrum is a very useful characteristic of an elastomer that enables the prediction of other viscoelastic characteristics, e.g. the compression set [3]. The generalized Maxwell model is deployed to fit the CSR master curves using the sign control method (SCM) [47] and obtain the viscoelastic parameters for both compounds. The model used has the following discrete form:

$$S = \varepsilon\left(E_{eq} + \sum_{i=1}^{n} E_i e^{-t/\tau_i}\right)$$

where τ_i are the relaxation times, E_i are the spectral strengths, E_{eq} is the equilibrium modulus. The relaxation spectra are depicted in Fig. 12.

It is apparent that the carbon black filled HNBR exhibits higher relaxation strengths in its relaxation spectrum at intermediate and long times (approximately higher than 10^{-4} s) if compared to the relaxation spectrum of the unfilled rubber at the same temperature. At the glass transition and below it, the effect of carbon black on the relaxation strength of HNBR becomes negligible.

4. Conclusions

The experimental measurements successfully showed changes of the stiffness of carbon black filled (50 phr) and unfilled hydrogenated nitrile butadiene rubber (HNBR) due to stress relaxation at temperatures below and above the T_g. It is experimentally demonstrated that the elastomers can attain the equilibrium state even near the glass transition temperature provided there is enough time for the relaxation to take place.

The stress relaxation significantly affects the mechanical behaviour of HNBR at low temperatures. It is demonstrated that the stiffness of the material at temperatures above the glass transition and at moderate strains is determined by two phenomena which have opposing impacts on it. The first effect is related to the entropic nature of rubber elasticity, and, thus, manifested in a decrease of the modulus with temperature reduction down to the T_g. The second effect consists of a steady increase of the transient component of stress (or the time-dependent part of the modulus) with cooling. As a result of these two competing processes, the temperature variation of the strain energy function of the HNBR has a complex concave-downward shape with an inflection point above the T_g. Generally, HNBR exhibits relaxation-dominated stiffness below the inflection point of the strain energy curve and the entropy-dominated stiffness above. The inflection point is shifted to higher temperatures in the carbon black reinforced HNBR.

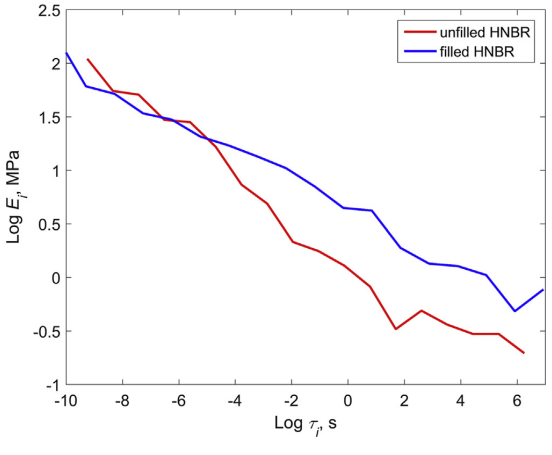

Fig. 12. The effect of carbon black on the relaxation spectrum of HNBR at 20% nominal compression.

The stiffness changes with time and temperature cannot be fully predicted by simple time temperature superposition. Due to the entropic elasticity effect, a temperature correction factor (vertical shifting) needs to be introduced for a more accurate application of the time-temperature superposition principle. These vertical correction factors are found to relate with temperature as 0.0038 and 0.0026 per degree Kelvin for the unfilled and carbon black filled HNBR compounds respectively when the reference temperature is taken as 298 K (+25 °C).

Carbon black is shown to impart greater long-term stiffness and also larger relaxation strength to the HNBR at times longer than 10^{-4} s. On the other hand, the relaxation dynamics of HNBR at times from 10^{-3}–10^4 s are found to be unaffected by the addition of carbon black. At the T_g or deeper into the glassy region, the relaxation rates are found to be lower in the carbon black filled HNBR than in the unfilled HNBR. On the contrary, the relaxation rates in the filled HNBR appeared greater at elevated temperatures (or at times $> 10^4$ s).

From the analysis of the normalized relaxation functions of HNBR at different compression ratios, it is evident that the strain and time effects in HNBR are uncoupled at times longer than 10^{-3} s (which corresponds to a temperature of $T_g + 1 \div 8$ °C in the relaxation experiment). The results, thus, confirm that the time-strain separability in elastomer mechanical behaviour might extend to down to T_g which was not apparent from the earlier publications on the subject [22,34]. This can greatly simplify the analysis of the elastomers and has a large impact on the modelling of elastomer articles (e.g. seals) in practice. Generally, the obtained results can help designers and material engineers to implement temperature-dependent material models in their analysis problems and build better rubberlike material constitutive relationships which include temperature and time as variables.

Declaration of interest

The authors declare that they have no conflict of interest.

Acknowledgments

This work is part of the collaborative project “Thermo Responsive Elastomer Composites for cold climate application” with the industrial partners FMC Kongsberg Subsea AS, STATOIL Petroleum AS, The Norwegian University of Science and Technology (NTNU) and the research institute SINTEF Materials and Chemistry. The authors would like to express their thanks for the financial support by The Research Council of Norway (Project 234115 in the Petromaks2 programme).

References

[1] L.R.G. Treloar, The Physics of Rubber Elasticity, third ed., Oxford University Press, Oxford, New York, 2005.
[2] C.M. Roland, Viscoelastic Behavior of Rubbery Materials, Oxford University Press, Oxford ; New York, 2011.
[3] A.G. Akulichev, B. Alcock, A.T. Echtermeyer, Elastic recovery after compression in HNBR at low and moderate temperatures: experiment and modelling, Polym. Test. 61 (2017) 46–56.
[4] F. Bjork, O. Dickman, B. Stenberg, Long-term studies of rubber materials by dynamic mechanical-stress relaxation, Rubber Chem. Technol. 62 (3) (1989) 387–425.
[5] F. Björk, B. Stenberg, Stress relaxation of a nitrile rubber surrounded by an oil that increases the network density, Polymer 31 (9) (1990) 1649–1657.
[6] S. Ronan, T. Alshuth, S. Jerrams, N. Murphy, Long-term stress relaxation prediction for elastomers using the time–temperature superposition method, Mater Des. 28 (5) (2007) 1513–1523.
[7] B. Slay, W. Webber, Stress relaxation of elastomer compounds, Seal. Technol. 2011 (2) (2011) 9–12.
[8] J.H. Zhao, R. Yang, R. Iervolino, B. van der Vorst, S. Barbera, The effect of thermo-oxidation on the continuous stress relaxation behavior of nitrile rubber, Polym. Degrad. Stab. 115 (2015) 32–37.
[9] W. Zheng, X.Y. Zhao, Q.G. Li, T.W. Chan, L.Q. Zhang, S.Z. Wu, Compressive stress relaxation modeling of butadiene rubber under thermo-oxidative aging, J. Appl. Polym. Sci. 134 (12) (2017).
[10] A. Kommling, M. Jaunich, D. Wolff, Revealing effects of chain scission during ageing of EPDM rubber using relaxation and recovery experiment, Polym. Test. 56 (2016) 261–268.
[11] K.W. Taylor, Performance characteristics of oilfield proven elastomers in low-temperature seal applications, in: 23rd Annual Offshore Technology Conference, Offshore Technology Conference, Houston, Texas, 1991, pp. 193–206.
[12] J. Goodson, T. Tilton, Effects of low temperatures on elastomeric sealing elements in downhole completion tools, Proceedings of the International Offshore Mechanics and Arctic Engineering Symposium, 1992, pp. 231–240.
[13] D. Baker, Why challenger failed, New Sci. 1525(Sep. 11) 52 (1986) 54–56.
[14] J.R. Beatty, J.M. Davies, Time and stress effects in the behavior of rubber at low temperature, Rubber Chem. Technol. 23 (1) (1950) 54–66.
[15] J.R. Beatty, A.E. Juve, Stress relaxation of some rubber and synthetic rubber vulcanizates in compression, Rubber Chem. Technol. 23 (4) (1950) 786–802.
[16] G. Allen, G. Gee, B.E. Read, Stress relaxation in elastomers by visco-elastic mechanisms .1. Natural rubber at high rates of strain and low temperatures, Trans. Faraday Soc. 55 (9) (1959) 1651–1659.
[17] G.M. Brown, A.V. Tobolsky, Elastoviscous properties of polyisobutylene. II. Relaxation of stress in whole polymers of different molecular weights at low temperatures, J. Polym. Sci. 6 (2) (1951) 165–176.
[18] A.V. Tobolsky, J.R. McLoughlin, Elastoviscous properties of polyisobutylene. V. The transition region, J. Polym. Sci. 8 (5) (1952) 543–553.
[19] E. Catsiff, A.V. Tobolsky, Stress-relaxation of polyisobutylene in the transition region (1, 2), J. Colloid Sci. 10 (4) (1955) 375–392.
[20] A.V. Tobolsky, E. Catsiff, Elastoviscous properties of polyisobutylene (and other amorphous polymers) from stress–relaxation studies. IX. A summary of results, J. Polym. Sci. 19 (91) (1956) 111–121.
[21] T.L. Smith, R.A. Dickie, Effect of finite extensibility on the viscoelastic properties of a styrene–butadiene rubber vulcanizate in simple tensile deformations up to rupture, J. Polym. Sci. Part A-2 Polym. Phys. 7 (4) (1969) 635–658.
[22] J. Glucklich, R.F. Landel, Strain energy function of styrene butadiene rubber and the effect of temperature, J. Polym. Sci. Polym. Phys. Ed. 15 (12) (1977) 2185–2199.
[23] Y. Takano, Y. Suzuki, T. Kurihara, The stress relaxation of some rubber vulcanizates at low temperatures (in Japanese), Nippon. Gomu Kyokaishi 39 (9) (1966) 674–682.
[24] R.A. Dickie, T.L. Smith, Viscoelastic properties of a rubber vulcanizate under large deformations in equal biaxial tension, pure shear, and simple tension, T Soc. Rheol. 15 (1) (1971) 91–110.
[25] G.M. Bartenev, Y.V. Zelenev, Low-temperature relaxation processes in rubberlike polymers, in Russian, Dokl. Akad. Nauk. Sssr 154 (3) (1964) 661–664.
[26] G.M. Bartenev, A.M. Kucherskii, Low temperature relaxation phenomena in rubber-like polymers at low deformations, in Russian, Vysokomol. Soedin. A 12 (4) (1970) 794–801.
[27] G.M. Bartenev, A.M. Kucherskii, G.I. Radaeva, Influence of deformation rate on low-temperature relaxation processes in elastomers, in Russian, Vysokomol. Soedin. B 19 (8) (1977) 564–567.
[28] L.A. Akopyan, G.M. Bartenev, M.V. Zobina, B.K. Avrushchenko, Temperature-dependence of contributions of discrete relaxational processes in elastomers, in Russian, Vysokomol. Soedin. B 28 (4) (1986) 301–303.
[29] G.M. Bartenev, A.M. Kucherskii, G.I. Radayeva, Relaxational processes in elastomers at small strains according to data of relaxational spectrometry, stress-strain and thermomechanical curves, in Russian, Vysokomol. Soedin. A 23 (2) (1981) 283–290.
[30] M.V. Karasev, G.M. Bartenev, Relaxation transitions in linear and cross-linked cis-polyisoprene above the glass-transition temperature, Plaste Kautsch 33 (2) (1986) 55–57.
[31] G.M. Bartenev, S.V. Baglyuk, V.V. Tulinova, Relaxational transitions in poly(butadiene-acrylonitriles) above glass-transition temperature, in Russian, Vysokomol. Soedin. A 30 (4) (1988) 821–828.
[32] G.M. Bartenev, A.G. Barteneva, Relaxation Properties of Polymers, in Russian, “Khimiya” Publishers, Moscow, 1992.
[33] P. Shi, H. Montes, F. Lequeux, R. Schach, E. Munch, Linear and Non Linear Mechanical Properties of Miscible Polymer Blends Near Glass Transition, Université Pierre et Marie Curie, Paris VI, 2013.
[34] T. Tada, K. Urayama, T. Mabuchi, K. Muraoka, T. Takigawa, Nonlinear stress relaxation of carbon black-filled rubber vulcanizates under various types of deformation, J. Polym. Sci. Part B Polym. Phys. 48 (12) (2010) 1380–1387.
[35] L.A. Akopyan, G.M. Bartenev, M.V. Zobina, Relaxation processes at various types of the stressed state, in Russian, Vysokomol. Soedin. B 26 (9) (1984) 694–697.
[36] F. Rouillard, P. Heuillet, B. Omnes, Viscoelastic Characterization at Low Temperature on an HNBR Compound for Sealing Applications, Constitutive Models for Rubber VIII, CRC Press, 2013, pp. 591–594.
[37] A.G. Akulichev, B. Alcock, A. Tiwari, A.T. Echtermeyer, Thermomechanical properties of zirconium tungstate/hydrogenated nitrile butadiene rubber (HNBR) composites for low-temperature applications, J. Mater Sci. 51 (24) (2016) 10714–10726.
[38] B. Alcock, J.K. Jørgensen, The mechanical properties of a model hydrogenated nitrile butadiene rubber (HNBR) following simulated sweet oil exposure at elevated temperature and pressure, Polym. Test. 46 (0) (2015) 50–58.
[39] B. Alcock, T.A. Peters, R.H. Gaarder, J.K. Jørgensen, The effect of hydrocarbon ageing on the mechanical properties, apparent crosslink density and CO2 diffusion of a hydrogenated nitrile butadiene rubber (HNBR), Polym. Test. 47 (2015) 22–29.
[40] L. Mullins, Effect of stretching on the properties of rubber, Rubber Chem. Technol. 21 (2) (1948) 281–300.
[41] M.F. Bukhina, S.K. Kurlyand, Low-temperature Behaviour of Elastomers, VSP, Leiden ; Boston, 2007.
[42] C.M. Roland, K.L. Ngai, Segmental relaxation and molecular-structure in polybutadienes and polyisoprene, Macromolecules 24 (19) (1991) 5315–5319.
[43] J.L. Leblanc, Filled Polymers : Science and Industrial Applications, CRC Press, Boca Raton, 2010.
[44] X. Li, Y. Dong, Z.R. Li, Y.M. Xia, Experimental study on the temperature dependence of hyperelastic behavior of tire rubbers under moderate finite deformation, Rubber Chem. Technol. 84 (2) (2011) 215–228.
[45] J. Honerkamp, J. Weese, A note on estimating mastercurves, Rheol. Acta 32 (1) (1993) 57–64.
[46] A. Flory, G.B. McKenna, Finite step rate corrections in stress relaxation experiments: a comparison of two methods, Mech. Time-Depend Mat. 8 (1) (2004) 17–37.
[47] R.D. Bradshaw, L.C. Brinson, A sign control method for fitting and interconverting material functions for linearly viscoelastic solids, Mech. Time-Depend Mat. 1 (1) (1997) 85–108.

A.2 Paper II

Elastic recovery after compression in HNBR at low and moderate temperatures: Experiment and modelling

A.G. Akulichev, B. Alcock, A.T. Echtermeyer.

Polymer Testing. 2017;61:46-56

Paper II

Polymer Testing 61 (2017) 46–56

Contents lists available at ScienceDirect

Polymer Testing

journal homepage: www.elsevier.com/locate/polytest

Material Properties

Elastic recovery after compression in HNBR at low and moderate temperatures: Experiment and modelling

Anton G. Akulichev [a, *], Ben Alcock [b], Andreas T. Echtermeyer [a]

[a] The Norwegian University of Science and Technology, Department of Mechanical and Industrial Engineering, Richard Birkelands vei 2 B, 7034 Trondheim, Norway

[b] SINTEF Materials and Chemistry, Forskningsveien 1, 0373 Oslo, Norway

ARTICLE INFO

Article history:
Received 27 February 2017
Received in revised form
1 May 2017
Accepted 4 May 2017
Available online 5 May 2017

ABSTRACT

Elastic recovery after compression or compression set is one of the key indicators of elastomer performance in sealing applications, such as O-rings in flange joints. In this work, findings of a study of the compression set property of a hydrogenated nitrile butadiene rubber (HNBR) at temperatures above and below the glass transition temperature T_g are presented. The compression set in the elastomer is found to increase with cooling up to 100% at the glass transition temperature and decrease with time after unloading even at temperatures below T_g. The effects of reinforcing filler (carbon black) and the initial compression time are also considered. Equivalence of time and temperature effects on the compression set of the elastomers is then demonstrated. A viscoelastic model describing the time-temperature variation of the compression set is proposed and verified by finite element analysis (FEA) and experimental results. It is shown that modelling captures well the experimental behaviour of the elastic recovery of the studied HNBR at ambient and low temperatures.

1. Introduction

Rubbers or elastomers typically exhibit high resilience properties which make these materials almost ideal candidates for pressure sealing applications. The excellent elastic recovery or low compression set enables the rubber seals to compensate for any movements of the sealed parts, e.g. the sealing gap growth caused by pressure peaks. However the sealing performance is often jeopardized by freezing conditions since rubbers become much less resilient at low temperatures near their glass transition point. This effect is schematically illustrated in Fig. 1.

In reality the contact of rubber seal and its counter surface might be much more complicated on different length scales including micrometer and sub-micrometer ranges [1]. Nevertheless even a sudden microscopic separation can promote leakage if the seal material exhibits no or negligible elastic recovery as depicted in Fig. 2. Therefore understanding the effect of cold environments on the recovery properties of elastomer compounds is of high interest for a number of branches of industry which use machinery operated under high pressure and exposed to low temperatures.

Despite its importance in many practical applications, the elastic recovery or set properties at low temperatures are covered rather scarcely in academic literature. Morris et al. [2] reported high compression set values for several rubber systems exposed to cold environment and noticed that the set effect is reversible upon warming to the ambient temperature. Similar effects of low temperatures on the elastic recovery in styrene butadiene rubber (SBR) and nitrile butadiene rubber (NBR) were later described in Ref. [3]. The same authors reported the effect of crystallization in natural rubber (NR) on the elastic recovery [4]. Baranov and Elkin [5] investigated the development of the elastic recovery and the contact area of elastomeric ring seals with gradual temperature reduction down to −70 °C. They found the recovery was uneven along the contact width of the compressed seals and it was also stress dependent. Bukhina and Parizenberg [6] applied the time temperature superposition (TTS) principle to the rubber recovery at different temperatures and constructed the recovery master curves for several compounds. Jaunich et al. [7,8] recently investigated low-temperature recovery of various rubber compounds by a modified compression set method using a dynamic mechanical analysis (DMA) machine and demonstrated effects of temperature, elastomer nature, the degree of compression, and the machine contact pressure on the compression set development over time.

* Corresponding author.
E-mail address: anton.akulichev@ntnu.no (A.G. Akulichev).

http://dx.doi.org/10.1016/j.polymertesting.2017.05.003
0142-9418/

Fig. 1. Schematic of compressed O-ring seal (black) in a flange: a) at ambient temperature; b) upper part lift-off at low temperature and leakage due to "frozen" seal.

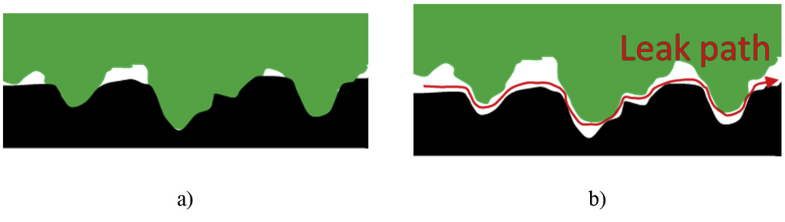

Fig. 2. Schematic magnified view of rubber seal surface (black) in contact with a rigid counter surface: a) at ambient temperature; b) rigid surface lift-off and leakage at low temperatures.

Summing up the available publications, there exists very few reports and experimental studies of the cold recovery of elastomers and particularly no data on hydrogenated nitrile butadiene rubber (HNBR) was found even though this material is of great importance for the oil and gas industry. The main objectives of this work are therefore to study the low-temperature strain recovery property of a model HNBR compound and to elucidate the effect of carbon black as a reinforcing filler on this property. In addition, the recovery behaviour at various temperatures is modelled based on the established mathematical concepts for viscoelastic materials.

2. Materials and experimental procedure

2.1. Materials and processing

A typical rubber formulation widely used in seals in the oil and gas industry was tested. The composition is based on hydrogenated nitrile butadiene rubber with 96% saturated polybutadiene with 36% acrylonitrile content and varied carbon black (CB) content from 0 to 50 phr (parts per hundred rubber). For ease of description, the formulation without carbon black is hereafter referred to as "unfilled" HNBR, while the formulation contained 50 phr carbon black is referred to as "filled" HNBR. The compound formulae are detailed in Table 1.

Table 1
Composition of the generic HNBR used in this study.

Component	Content, phr
HNBR	100
Antioxidant	3
Stearic acid	0.5
Zinc oxide	5
Magnesium oxide	10
Plasticizer	20
Peroxide	10
N-330 HAF carbon black	0 or 50

The compounds (except the peroxide) were combined in an internal mixer to yield a single HNBR masterbatch which was then mixed with the peroxide in a two roll mill. Compression moulding and vulcanization in a press at 170 °C for 20 min followed. Finally, a post-curing operation at 150 °C for 4 h in an oven was carried out. More information about the processing and the basic material test data is available in our previous publication [9]. The vulcanised unfilled HNBR has Shore A hardness of 70 ± 5, while the carbon black filled material has Shore A hardness of 85 ± 5.

2.2. Test methods

2.2.1. Dynamic mechanical thermal analysis

Dynamic mechanical thermal analysis (DMTA) was carried out on a Netzsch-Gabo Eplexor 150 DMTA machine equipped with a 150 N load cell and a thermal chamber. A temperature sweep was performed using the tension loading mode and the testing frequency of 1 Hz. Specimens for the experiments were nominally 8 mm wide and 2 mm thick moulded-to-shape bars. The temperature was swept in the range of −60 to 120 °C. For each temperature step, the specimens were pre-loaded to 0.05% of the initial length on top of which a cycling strain with the amplitude of 0.02% was applied. The specimen was unloaded each time before moving to a new temperature step to reflect changes in the specimen length.

2.2.2. Compression strain recovery

At least 2 standardised methodological approaches to measure elastic recovery of rubber materials in compression at low temperatures exist. The first method is based on compression set (CS) measurements and described in ISO 815-2 [10], while the other is called elastic rebound after compression and implemented in Russian GOST 13808-79 [11]. The principal formulae for calculation of the recovery parameters and the essential testing conditions are summarized in Table 2.

The compression set approach was followed in this study. Nevertheless, as it is immediately deduced from the equations,

Table 2
Comparison between ISO 815-2 and GOST 13808-79.

Test conditions	ISO 815-2	GOST 13808-79
Initial compression	25% for hardnesses below 80 IHRD 15% for hardnesses between 80 and 89 IHRD 10% for hardnesses above 90 IHRD	20 ± 2%
Specimen geometry	A: Ø 29 × 12.5 mm B: Ø 13 × 6.3 mm	Ø 10 × 10 mm
Test duration (cold exposure)	24 or 72 h	5 min
Specimen recovery time	30 ± 3 min	3 min
Principal equation	$CS = \frac{h_0 - h(t)}{h_0 - h_c}$	$K_r = \frac{h(t) - h_c}{h_0 - h_c}$
The principal equation in terms of engineering strain	$CS = \frac{\varepsilon(t)}{\varepsilon_0}$	$K_r = 1 - \frac{\varepsilon(t)}{\varepsilon_0}$

Here CS is the compression set parameter; K_r is the coefficient of elastic recovery; h_0 is the initial thickness of the specimen; $h(t)$ is the thickness after recovery time t; h_c is the compressed thickness of the specimen.

$\varepsilon_0 = \frac{\Delta h}{h_0} = \frac{h_0 - h_c}{h_0}$ is the initial compressive strain; $\varepsilon(t) = \frac{h_0 - h(t)}{h_0}$ is the strain after recovery time t.

these two recovery metrics are related if we assume equal testing conditions (i.e. specimen geometry, initial compression, duration of the experiment and the elapsed time t at the property measurement).

The strain recovery tests were carried out using the same Eplexor 150 DMTA machine using a 1500 N load cell and parallel plate compression holders. The specimens were cylindrical with 10 mm nominal diameter and 6 mm height. The testing procedure in this work was somewhat different with the major change being the duration of the holding time under the freezing conditions which was set to 30 min as compared to 24 h in the ISO standard. The procedure illustrated in Fig. 3 was automatized in the machine. First a rubber specimen was compressed to 85% of its initial height (step I) and left to relax at room temperature for 6 h (step II). This is to reflect the practical application in which rubber seals are rarely pressurized or exposed to the service environment immediately after installation. Nevertheless the impact of the duration of the compression step was also included into the investigation. After the compression step, the rubber specimen was exposed to the required temperature and held under load over 30 min (steps III and IV). Then the compression load was quickly removed keeping, however, 2 N compressive force in order to maintain the contact with the specimen. The specimen height change was recorded over time starting from the point of unloading (step V). The compression set values reported hereafter correspond to the time of 30 min after unloading (as in ISO 815-2) unless stated otherwise or designated by the time.

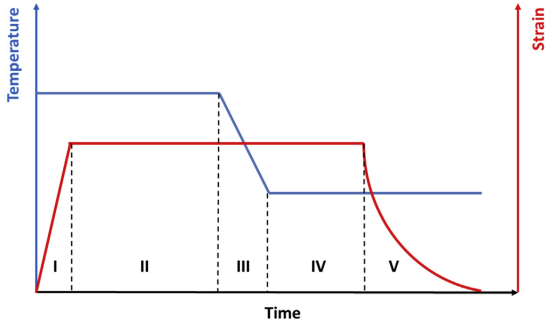

Fig. 3. Schematic of the low-temperature strain recovery test procedure: I – loading step; II – stress relaxation step; III – cooling (heating) step; IV – temperature conditioning period; V – recovery step (load released).

3. Results

3.1. Dynamic mechanical thermal analysis

Fig. 4 depicts the outcome of DMTA for both HNBR compounds (i.e. unfilled and filled with 50 phr carbon black). As expected, the addition of carbon black results in a significant increase of the dynamic moduli [12,13]. In contrast with the material stiffness, the filler does not produce a noticeable impact on the glass transition temperature which is determined from the tan delta peak maximum to be about −16 °C for 1 Hz testing frequency in both cases.

3.2. Strain recovery and compression set

Preliminary compression set (CS) experiments in a freezing cabinet indicate that the studied HNBR demonstrates almost no elastic recovery already at −25 °C, only a few degrees below T_g. Moreover, if the elastomer is sufficiently compressed against a rough surface, such as sand paper in Fig. 5, the counter-surface topography is mirrored on the elastomer specimen surface after unloading in a freezing environment. The observed set is not permanent. As already noticed by Morris et al. [2], putting the cold CS specimens back to the ambient condition leads to relatively quick (10–20 min) restoration of the major portion of their original shapes.

More quantitative CS experiments at various temperatures down to −30 °C followed. The processed strain recovery data is plotted in Fig. 6 as a variation of compression set with time and temperature for both studied HNBR compounds. The compression set is seen to increase with cooling below the ambient temperature, and it rises steeply near the glass transition point. This is in line with the previous observations in other elastomers [3,4,6–8]. At the temperature of −30 °C, both compounds lose their resilience completely and do not regain their undeformed shapes as demonstrated by their compression set values of 95–100% at the short times. As expected, the compression set in HNBR has also a strong time-dependent nature. It gradually decreases as the recovery time progresses at all temperatures. Even at the lowest temperature some recovery is evident but it occurs at a very slow rate.

It is noteworthy that the filled HNBR has inferior compression set characteristics at sub-ambient temperatures above the glass transition point if compared to the unfilled HNBR, even though they exhibit close magnitudes of compression set at room and elevated temperatures. This result is in good agreement with the CS measurements carried out using zirconium tungstate filled HNBR [9] where a noticeable increase of CS in the filled rubber was also

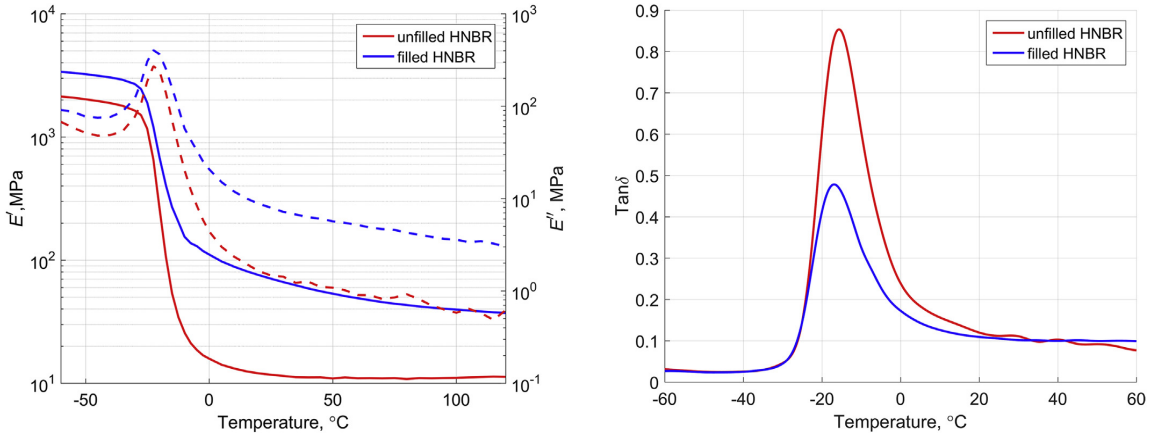

Fig. 4. DMTA testing results taken at 1 Hz frequency: a)Storage (solid line) and loss (dashed line) moduli as a function of temperature; b)Tan delta as a function of temperature. Spline interpolated data.

observed. The difference in CS between the carbon black filled and the virgin compound enlarges with temperature reduction peaking near the T_g region, which is seen in Fig. 6 and more clearly in Fig. 7.

Fig. 8 demonstrates how the initial compression time at room temperature influences the compression set property at room temperature and at T_g. The room temperature CS clearly increases with the duration of the initial squeeze, while the results at T_g show no considerable effect of the compression time on the recovery of HNBR. Therefore keeping the CS specimens over a long time interval under compression at temperatures near or below T_g (as for example stated in ISO 815-2) may not be necessary, unless secondary low temperature effects such as crystallization are to be investigated at the same time.

3.3. Compression set master curves

Since the compression set in the studied materials has a clear viscoelastic origin at low and moderate temperatures, and the neighbouring time segments have similar shapes and overlap quite well near their edges, the postulate of time and temperature equivalence can be applied to construct compression set master curves. A specific shifting routine was implemented in MATLAB in order to obtain a smooth master curve following the approach suggested in Ref. [14]. The following function was minimized with respect to the horizontal shifting parameter $a(T)$ for each isothermal time segment being shifted:

Here y_i are the experimental values of the compression set at times t_i, $\overline{y_i}$ are the values of the compression set function approximated by a polynomial, and n is the number measurement points in each time segment. Since the machine unloading time is finite and affects the measurements at short times, the initial period of 100 s in each segment was ignored. The obtained master curves are presented in Fig. 9.

A plot of the shifting factors versus temperature is presented in Fig. 10. The figure also demonstrates that the relation between the horizontal shifting factors and temperature can be well described by the WLF equation expressed as [15,16].

$$\log_{10}(a_T) = \frac{-C_1\left(T - T_{ref}\right)}{C_2 + T - T_{ref}}$$

It is evident that the carbon black does not have much influence on the temperature variation of the shifting factor, and the discrepancy between the curves for the filled and unfilled HNBR is probably within the experimental and computing errors in shifting and model fitting. It is also interesting to note that the values of the WLF parameters obtained in both compounds are similar to the "universal" constants for polymers ($C_1 = 17.44$ and $C_2 = 51.6$ K) reported in Ref. [15].

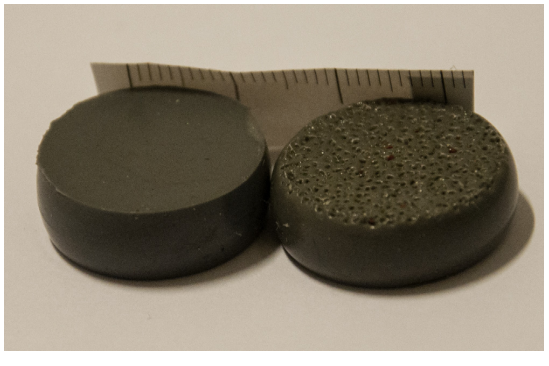

Fig. 5. Unfilled HNBR CS specimens photographed 3 min after load release at −25 °C. 20% nominal compression was imposed, and the specimen on the right was compressed against sandpaper (photo courtesy of Natalia Akulicheva). The scale bar behind the specimens indicates mm.

4. Modelling of the recovery experiment

4.1. Viscoelastic modelling

The recovery after compression should be a viscoelastic process and it should be possible to model the recovery based on the viscoelastic characteristics of the rubber materials. The modelling approach presented here is based on the linear viscoelasticity principles and inspired by Ref. [17]. We begin with the Boltzmann

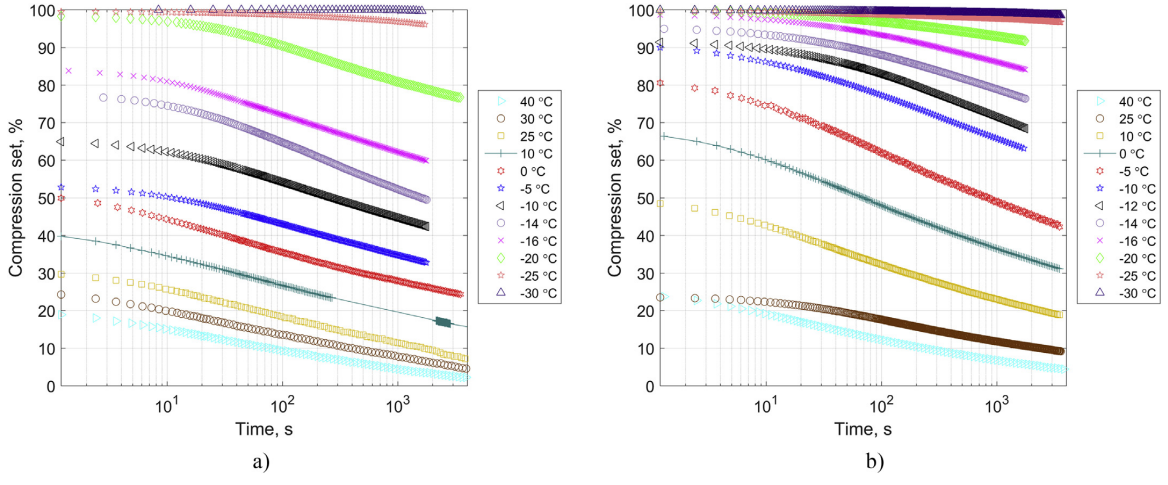

Fig. 6. Compression set as a function of time at the indicated temperatures.

superposition principle which yields the following equation for creep strain at time t [16,17]:

$$\varepsilon(t) = \int_{-\infty}^{t} D(t-u)\frac{d\sigma(u)}{du}du, \tag{1}$$

where $D(t)$ is the creep compliance and $\sigma(t)$ is the stress acting on the material. Since ε and σ are defined from $t = 0$ the integral can be rewritten to get

$$\varepsilon(t) = \frac{\sigma}{E_0} + \int_{0}^{t} D(t-u)\frac{d\sigma(u)}{du}du \tag{2}$$

Here E_0 is the instantaneous modulus corresponding to the initial elastic response. The compression set test is basically carried out in 2 phases: compression (stress relaxation) phase with duration t_c with no changes in strain and the recovery phase when the load is removed ($\sigma = 0$). We also assume that the initial compression strain ε_0 is known and constant and the unloading step is momentary. Therefore the expression is changed to

$$\varepsilon(t) = \varepsilon_0 + \int_{t_c}^{t} D(t-u)\frac{d\sigma(u)}{du}du \tag{3}$$

Integration by parts knowing $\sigma(t)_{t>t_c} = 0$ gives

$$\varepsilon(t) = \varepsilon_0 - \sigma(t_c)D(t-t_c) \tag{4}$$

It is quite common that the mechanical response of a viscoelastic solid material is successfully modelled by phenomenological approaches using elastic springs and dashpots in series or parallel. To model a stress relaxation process, the generalized Maxwell model consisting of an elastic spring representing equilibrium (long-term) response and m Maxwell elements is typically used [16,18]:

$$\sigma(t) = \varepsilon_0\left[E_\infty + \sum_{i=1}^{m} E_i e^{-(t/\rho_i)}\right], \tag{5}$$

where E_∞ is the equilibrium elastic modulus, E_i are the relaxation strengths and ρ_i are the corresponding relaxation times. The series expression for the Maxwell elements is described mathematically as a Prony series [18]. Although equation (5) is strictly valid only for small strain linear viscoelasticity problems, it is found to approximate the rubber relaxation behaviour relatively well for the moderate strains (up to 15%) used in the compression set experiments reported here. The creep compliance of a viscoelastic solid material is often modelled by the generalized Voigt model with n Voigt elements having the following expression [16,18]:

$$D(t) = D_g + \sum_{j=1}^{n} D_j\left(1 - e^{-(t/\tau_j)}\right) \tag{6}$$

where D_j are the retardation strengths and τ_j are the corresponding retardation times. D_g is the glassy compliance found by

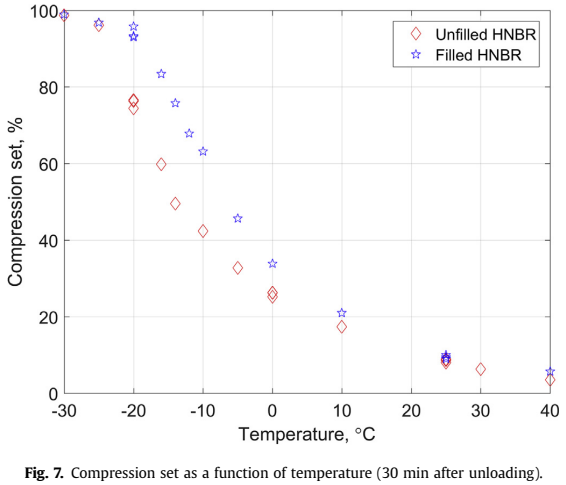

Fig. 7. Compression set as a function of temperature (30 min after unloading).

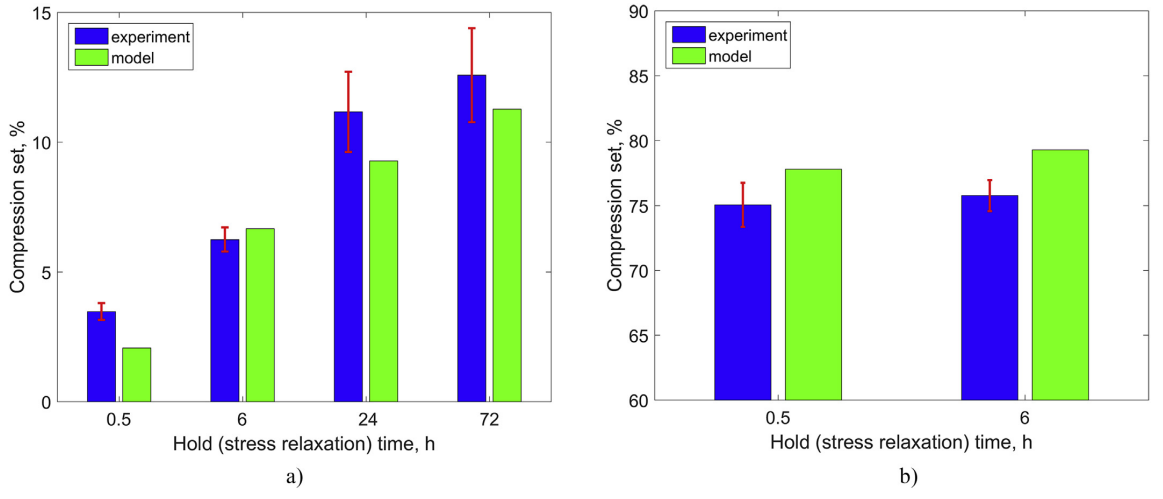

Fig. 8. Effect of the hold time (step II) at room temperature on the compression set of the unfilled HNBR: a) at room temperature and b) at −20 °C. The error bars indicate the standard deviation. The data for 24 and 72 h hold time are taken from the previous study [9]. The modelling approach and the predictions are to be described in sections 4.1 and 4.3.

$$D_g = \frac{1}{E_\infty + \sum_{i=1}^{m} E_i} \tag{7}$$

Incorporating (5) and (6) into (4) one may arrive at

$$\varepsilon(t) = \varepsilon_0 \left(1 - \left(E_\infty + \sum_{i=1}^{m} E_i e^{-(t_c/\rho_i)}\right)\left[D_g + \sum_{j=1}^{n} D_i \left(1 - e^{-\left(\frac{t-t_c}{\tau_i}\right)}\right)\right]_{t \geq t_c}\right) \tag{8}$$

The expression consists of two terms in the parentheses. The first of which accounts for the compression stress relaxation history while the second determines the actual recovery behaviour. Despite a potentially large number of material parameters in the Prony series coming into the formula, it can be easily programmed to supply any number of the Prony elements. After computing the strain recovery, the compression set or the recovery coefficient are calculated in accordance with the equations in Table 2. A permanent strain term could be added if justified by the experimental data, however this was not considered necessary in this work.

If the recovery test is performed at a temperature T different from the ambient T_c, then the recovery term in the equation has to be evaluated at the temperature of interest. This can be achieved using a physical test or using TTS by shifting the whole retardation spectrum along the time scale by the superposition factor $a_T(T)$ if there is an established and proven relation between a_T and temperature. The equation for the strain recovery at an arbitrary temperature T is, thus, generalized to

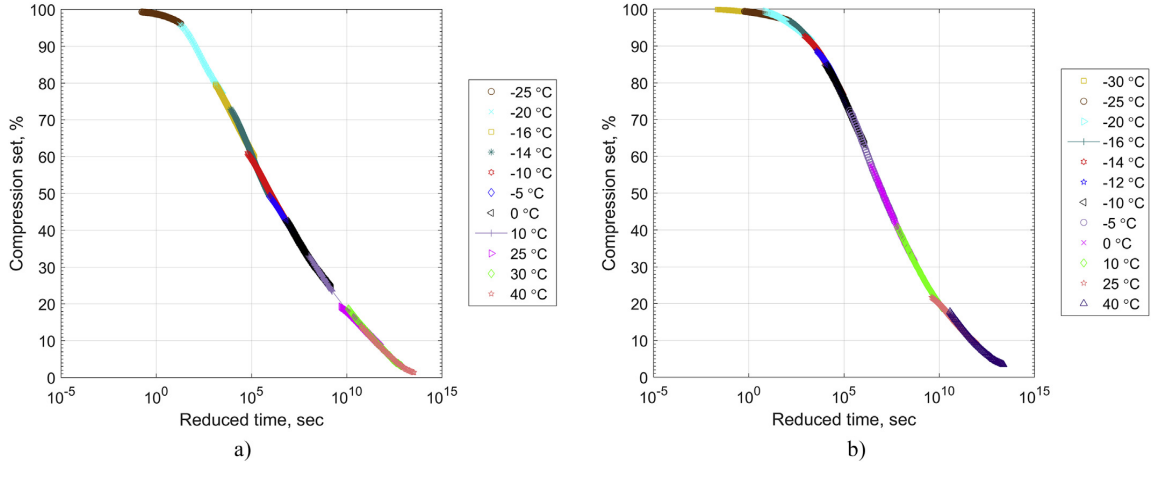

Fig. 9. Master curves of the compression set property of the studied HNBR compounds with $T_{ref} = -20$ °C. No correction for thermal shrinkage (vertical shifting) was applied.

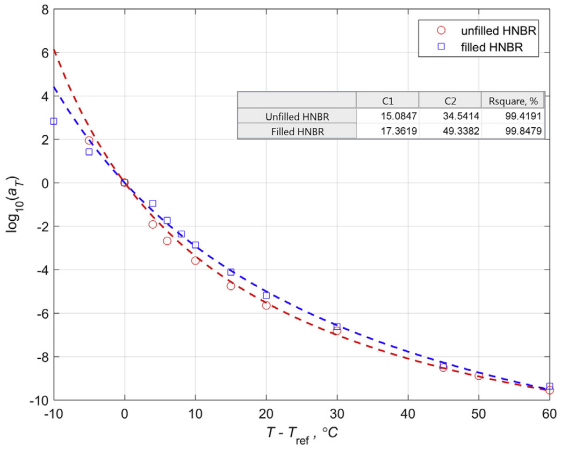

Fig. 10. Horizontal shift factor as function of temperature at $T_{ref} = -20$ °C. The dashed lines represent WLF fit made in the range of −20 to +40 °C.

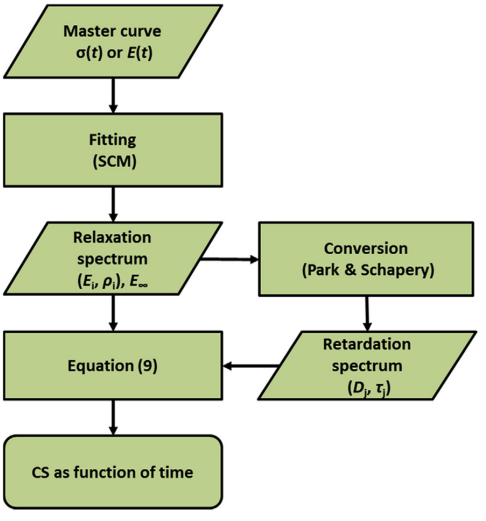

Fig. 12. Compression set computation workflow.

$$\varepsilon(t,T) = \varepsilon_0\left(1 - \left(E_\infty + \sum_{i=1}^{m} E_i e^{-(t_c/\rho_i)}\right)\left[D_g + \sum_{j=1}^{n} D_j\left(1 - e^{-\left(\frac{t-t_c}{a_T(T)\tau_j}\right)}\right)\right]_{t\geq t_c}\right) \quad (9)$$

In practice, it is rather common that only a relaxation or retardation spectrum is available, and therefore a conversion method that is favourable to the user has to be employed. The numerical method proposed by Park and Schapery [19] was used in this work due to its straightforward implementation in MATLAB.

The test data used were quasi-static compression stress relaxation (CSR) master curves measured for these materials [20,21]. The data were fitted to equation (5) using the sign control method [22] (SCM). An example showing the relaxation data, the fit curves and the obtained relaxation spectra are depicted in Fig. 11. It should be noted that the carbon black filled HNBR exhibits higher relaxation strengths in its relaxation spectrum at intermediate and long times if compared to the relaxation spectrum of the unfilled rubber at the same temperature. This effect determines the higher relaxing component of stress and higher CS values observed in the filled rubber during the recovery experiments at temperatures above T_g.

The full procedure for compression set calculation is illustrated in Fig. 12. A comparison of the predictions using this model with experimental data will be discussed below and is shown in Figs. 15 and 16.

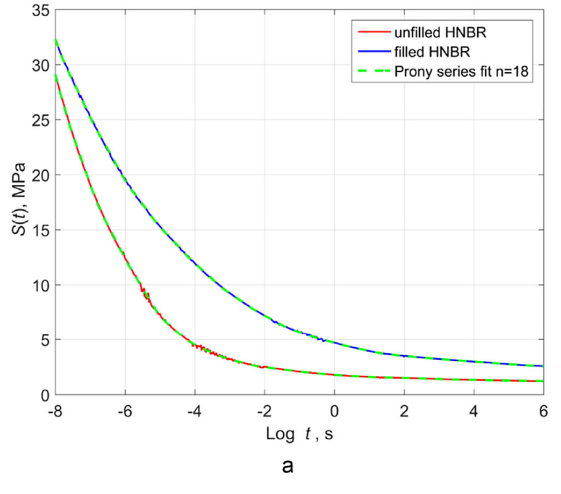

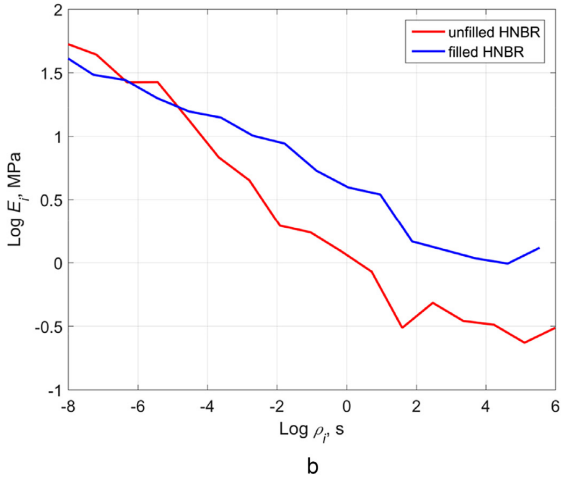

Fig. 11. a) CSR master curves (solid lines) with $T_{ref} = +23$ °C [20,21] and their fitting (dashed lines) by SCM; b) the computed relaxation spectra of the studied HNBR compounds.

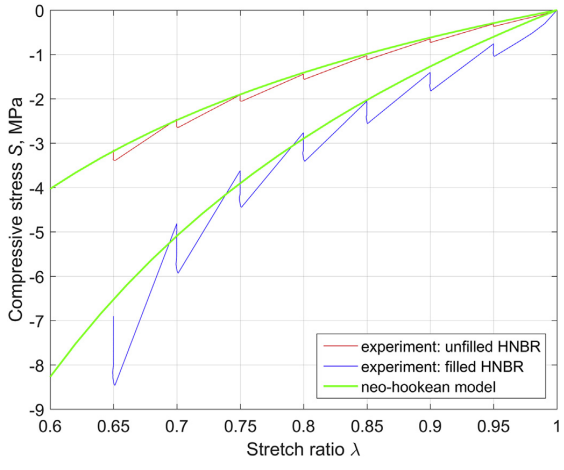

Fig. 13. Step strain CSR response at +40 °C as function of stretch ratio and fitting of the relaxed (long-term) stress data by the neo-hookean model. Cylindrical specimens were compressed in the Eplexor machine using the same compression holder. A silicone grease was applied to minimise barrelling. The strain rate here is approximately 0.005 sec^{-1}. The strain step length is 0.05, and linear interpolation is used between the measurement points.

Table 3
Long-term material properties used in FEA.

Parameter	Unfilled HNBR	Carbon black filled HNBR
C_{10}, MPa	0.92	1.89
D_1, MPa^{-1}	0.001	0.00087

4.2. FEA modelling

An alternative way to model the shape recovery of the rubber specimens with time is to use finite element analysis (FEA) using the viscoelastic data of the HNBR rubber system. Generally, finite element analysis is a preferable way to determine the behaviour of industrial seals, as they might have intricate cross section geometries and various inserted elements. In this work, Abaqus software (v. 6.14) was used to simulate the performed compression set experiments and verify the proposed model. The FEA model of a cylindrical rubber block compressed by rigid surfaces was made in the axisymmetric setting using CAX4RH linear hybrid elements. The friction coefficient for the rubber block and the mating rigid surfaces was set to 0.2, although this value was found not to significantly affect the results.

The FEA material model consists of two parts: the first is to model the hyperelastic behaviour and the second is for the viscoelastic behaviour with the temperature relation of the superposition factor provided by the WLF equation. The neo-hookean form of the strain energy density function was chosen as a hyperelastic material model for the FEA since only moderate strains are of concern in the current investigation. The strain energy density function for a compressible neo-hookean material is typically formed of the deviatoric and the volumetric terms [23,24] and expressed as:

$$W = C_{10}(\bar{I}_1 - 1) + D_1(J-1)^2$$

where C_{10} and D_1 are material parameters representing the resistance to shear and the compressibility of the material respectively; $\bar{I}_1 = J^{-2/3}I_1$ is the first deviatoric strain invariant; $J = \lambda_1\lambda_2\lambda_3$ and $I_1 = \lambda_1^2 + \lambda_2^2 + \lambda_3^2$ is the first strain invariant expressed in terms of the principal stretch ratios λ_i. The parameter C_{10} is found from fitting of the corresponding long-term compression stress-stretch data demonstrated in Fig. 13, while the compressibility was measured earlier [9]. The model adequately fits the uniaxial compression data sets for both compounds yielding only a slightly higher fitting error than the models with larger number of material parameters [21].

The material model parameters used in the FEA are listed in Table 3.

The viscoelastic material behaviour is modelled by the Prony series in dimensionless form as required by Abaqus. The same CSR data sets were used to identify the viscoelastic material parameters for the FEA. The number of Prony series terms was, however, reduced to 13 to comply with the limitation of the software.

An example of the visualization output of the performed FEA is shown in Fig. 14.

4.3. Comparison with experimental data

The experimental CS data for the unfilled HNBR and filled HNBR are plotted in Figs. 15 and 16 respectively together with the modelling results.

Both models predict the elastic recovery of HNBR quite well at ambient temperature (+25 °C) and acceptably at around the glass

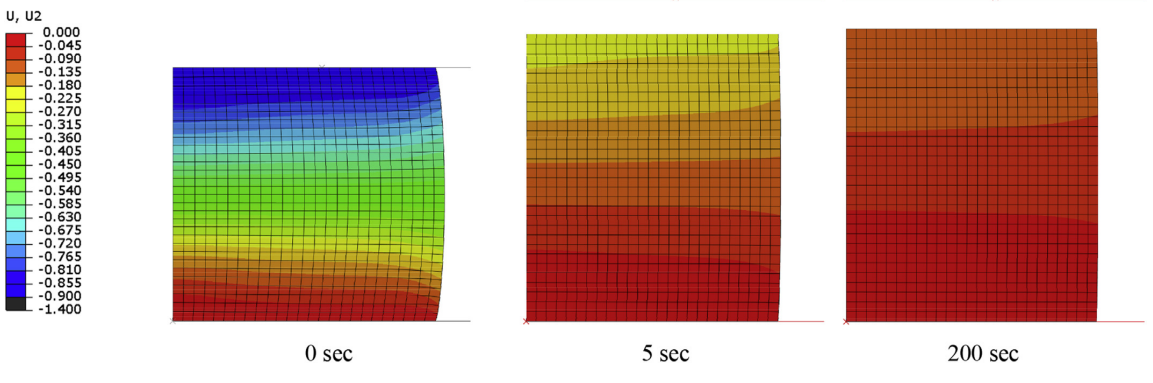

Fig. 14. Images of the simulated compression set test at the ambient temperature. The times indicated are after the load is released.

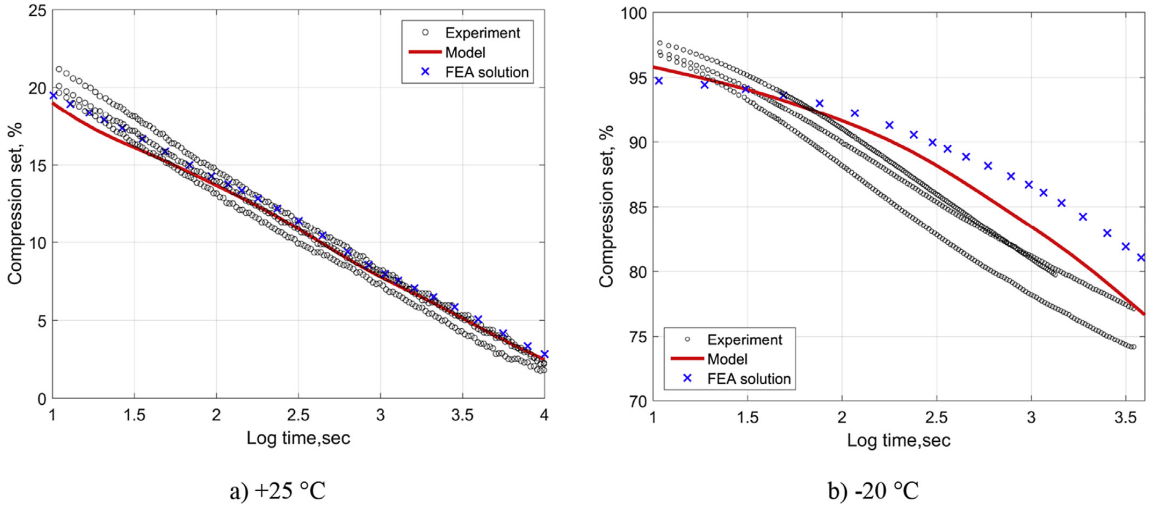

Fig. 15. Experimental and modelling results of the compression set as function of time for the unfilled HNBR at a) 25 °C and b) −20 °C. The data in b) are corrected for the thermal contraction.

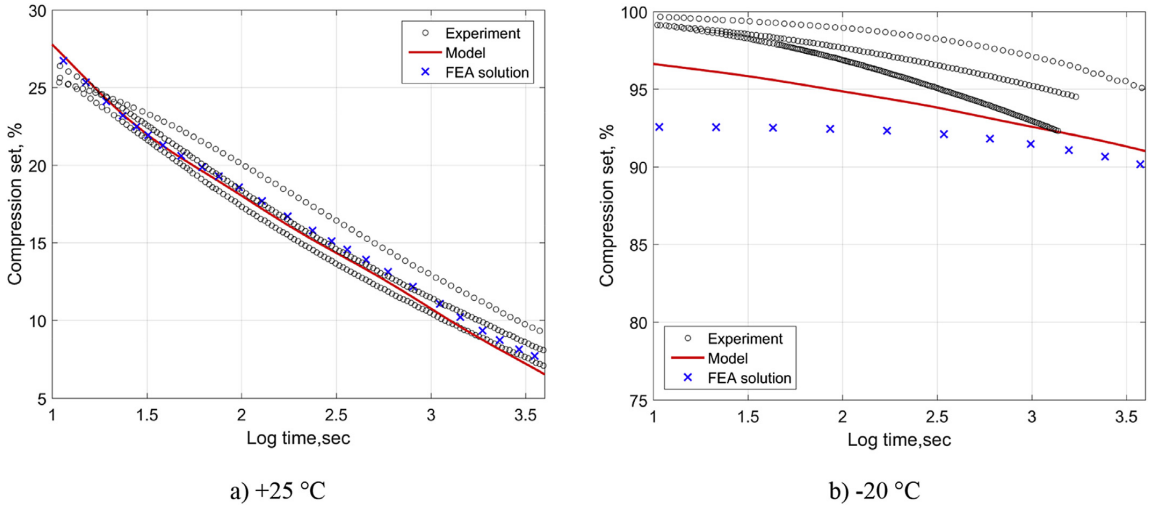

Fig. 16. Experimental and modelling results of the compression set as function of time for the carbon black filled HNBR at a) 25 °C and b) −20 °C. The data in b) are corrected for the thermal contraction.

transition temperature (−20 °C). The deviation between the FEA solution and the proposed model is rather small and presumably related to the difference in fitting of the relaxation data and the limited number of the Prony elements in Abaqus as described above. Another potential source of this small discrepancy is the necessary use of the hyperelastic material model in FEA dictated by the finite strains in the model.

The largest differences between the experiment and modelling results of about 5% are observed close to T_g in both compounds. In general, the thermo-mechanical behaviour of rubber becomes more complex in the vicinity of T_g, and there can be several reasons for the noticeable deviation. The first potential explanation is the known temperature dependency of the rubber modulus which has not been not accounted for in the modelling approach (it directly affects the compression history term). Therefore, for more accurate results in the case of large temperature differences a correction factor, e.g. a vertical shifting factor $b_T(T)$, should be introduced. Furthermore, the cooling (or heating) process takes time during which some incomplete relaxation processes may still take place at rates varying with the temperature. This effect is, however, not considerable at T_g as evident from the experiments with varying initial compression times (Fig. 8b).

The mechanical behaviour of rubber at finite strains in the glassy state or on the upper shelf of the transition region might no longer be correctly described by the simple models used in this work. As such, both FE and analytical approaches might fail to give accurate

estimates of CS below T_g. Nonetheless, as demonstrated by this work and many other experiments [3,4,6–8], rubber at these temperatures exhibits no or very limited recovery manifested in CS values of about 100%.

The modelling approach could also be extended to predict CS in rubber exposed to elevated temperatures. The necessary condition for the utilization is that the stress relaxation at these temperatures is governed only by physical mechanisms and that there is a complete relaxation data set (a relaxation or retardation spectrum) available at short and long times. If the physical relaxation is augmented with some chemical relaxation processes, the approach will most likely stop yielding adequate estimates of CS. The variation of the horizontal shifting factor with temperature, if used, should be well characterized since low accuracy in its temperature relation might also be a significant source of error in the CS estimation.

The modelling approach can also help explain the noticeable difference in CS values demonstrated in Fig. 8 when the initial compression is applied with various durations. In the case of a short compression relaxation period (the relaxation processes in the rubber are incomplete) the compression history term in equation (9) is high and facilitates the strain recovery to proceed much faster. If the compression relaxation time is much longer, the contribution of the compression history term decreases, approaching the equilibrium state at long times (E_∞) and, thus, the computed recovery rate is much smaller and in accordance with the experimental observations. In contrast to the ambient conditions, the CSR term becomes negligible at, and below, T_g in comparison with the recovery term at the same temperature. Hence, the recovery rate is mostly governed by the retardation spectrum at these temperatures.

5. Conclusions

The following conclusions can be drawn based on the experimental results and the subsequent modelling:

1. The studied HNBR compounds (with and without the addition of 50 phr carbon black) possess rather poor recovery at low temperatures at and near the glass transition region demonstrated by large compression set (CS) values of 70–100% at these temperatures. Nevertheless, the compression set might approach zero even at low temperatures near T_g provided there is substantial time for the shape recovery;
2. The duration of the initial compression has a significant effect on the elastic recovery in the CS experiments conducted at ambient temperature, while the effect becomes minimal at sub-zero conditions once the glass transition region is reached;
3. Carbon black as a filler imparts inferior low temperature recovery properties to HNBR compared to the unfilled HNBR, although the negative effect is not substantial at ambient conditions. The largest difference of about 20% between the property values in the filled and unfilled HNBR is observed near the T_g region. Below this temperature both compounds demonstrate no or minimal elastic recovery;
4. The time-temperature superposition principle is found to be applicable to the HNBR compression set data measured at various temperatures, since the neighbouring isothermal time segments overlap quite well. The variation of the horizontal shifting parameter a_T with temperature is well fitted by the WLF expression with the parameters being similar to the "universal" values for polymers regardless of if the HNBR compound is reinforced or not.
5. A viscoelastic model for prediction of the time variation of the strain recovery is proposed. The model links the basic relaxation characteristics of a rubbery material, such as the relaxation spectrum obtained from stress relaxation experiments, with the compression set in the material. It is demonstrated that the model prediction matches the FEA modelling output and it successfully captures the recovery behaviour of the studied HNBR at ambient temperature.
6. The modelling approach can also be used to predict rubber recovery at low and moderately elevated temperatures provided that only physical relaxation processes occur in the studied material and the temperature relation of time-temperature superposition factor a_T is available.

Declaration of interest

The authors declare that they have no conflict of interest.

Acknowledgments

This work is part of the collaborative project "Thermo Responsive Elastomer Composites for cold climate application" with the industrial partners FMC Kongsberg Subsea AS, STATOIL Petroleum AS, The Norwegian University of Science and Technology (NTNU) and the research institute SINTEF Materials and Chemistry. The authors would like to express their thanks for the financial support by The Research Council of Norway (Project 234115 in the Petromaks2 programme).

References

[1] B.N.J. Persson, O. Albohr, U. Tartaglino, A.I. Volokitin, E. Tosatti, On the nature of surface roughness with application to contact mechanics, sealing, rubber friction and adhesion, J. Phys. Condens. Matter 17 (1) (2005) R1.
[2] R.E. Morris, J.W. Hollister, P.A. Mallard, The cold-compression sets of natural and synthetic vulcanizates, Rubber Chem. Technol. 19 (1) (1946) 151–162.
[3] B.M. Gorelik, M.F. Bukhina, Effect of degree of compression of rubber on strain recovery and contact pressure, in Russian, Kauchuk i Rezina 9 (1961) 22–26.
[4] B.M. Gorelik, M.F. Bukhina, Crystallization of rubber at low temperatures in compression, in Russian, Kauchuk i Rezina 11 (1961) 11–15.
[5] N.S. Baranov, A.I. El'kin, Loss of resilience of rubber seals at low temperatures, in Russian, Kauchuk i Rezina 5 (1974) 33–37.
[6] M.F. Bukhina, M.D. Parizenberg, Temperature-strain superposition of elastomer properties near the transition from rubberlike into glassy state, in Russian, Vysokomol. Soedin. B 23 (6) (1981) 456–460.
[7] M. Jaunich, W. Stark, D. Wolff, A new method to evaluate the low temperature function of rubber sealing materials, Polym. Test. 29 (7) (2010) 815–823.
[8] M. Jaunich, W. Stark, D. Wolff, Comparison of low temperature properties of different elastomer materials investigated by a new method for compression set measurement, Polym. Test. 31 (8) (2012) 987–992.
[9] A.G. Akulichev, B. Alcock, A. Tiwari, A.T. Echtermeyer, Thermomechanical properties of zirconium tungstate/hydrogenated nitrile butadiene rubber (HNBR) composites for low-temperature applications, J. Mater Sci. 51 (24) (2016) 10714–10726.
[10] ISO 815–2: Rubber, Vulcanized or Thermoplastic - Determination of Compression Set - Part 2: at Low Temperatures, The International Organization for Standardization, 2008.
[11] GOST 13808-79. Method for Determination of Low Temperature Resistance According to Elastic Rebound after Compression, Standards Publisher, Moscow, 1988.
[12] G. Kraus, Reinforcement of elastomers by carbon black, Rubber Chem. Technol. 51 (2) (1978) 297–321.
[13] J.L. Leblanc, Filled Polymers : Science and Industrial Applications, CRC Press, Boca Raton, 2010.
[14] J. Honerkamp, J. Weese, A note on estimating mastercurves, Rheol. Acta 32 (1) (1993) 57–64.
[15] M.L. Williams, R.F. Landel, J.D. Ferry, Mechanical properties of substances of high molecular weight .19. The temperature dependence of relaxation mechanisms in amorphous polymers and other glass-forming liquids, J. Am. Chem. Soc. 77 (14) (1955) 3701–3707.
[16] J.D. Ferry, Viscoelastic Properties of Polymers, Wiley, New York, 1980.
[17] C. Joubert, A. Michel, L. Choplin, P. Cassagnau, Influence of the crosslink network structure on stress-relaxation behavior: viscoelastic modeling of the compression set experiment, J. Polym. Sci. Part B Polym. Phys. 41 (15) (2003) 1779–1790.
[18] N.W. Tschoegl, The Phenomenological Theory of Linear Viscoelastic Behavior : an Introduction, Springer-Verlag, Berlin ; New York, 1989.

[19] S.W. Park, R.A. Schapery, Methods of interconversion between linear viscoelastic material functions. Part I—a numerical method based on Prony series, Int. J. Solids Struct. 36 (11) (1999) 1653–1675.
[20] A.G. Akulichev, A. Echtermeyer, B. Alcock, Stress relaxation in HNBR at low temperatures, The International Rubber Conference 2016 (IRC2016), Kitakyushu, Japan, 2016.
[21] A. Akulichev, A. Echtermeyer, B. Alcock, Compression stress relaxation in carbon black reinforced HNBR at low temperatures. To be published.
[22] R.D. Bradshaw, L.C. Brinson, A sign control method for fitting and interconverting material functions for linearly viscoelastic solids, Mech. Time-Depend Mat. 1 (1) (1997) 85–108.
[23] O.H. Yeoh, Developments in Finite Element Analysis, Engineering with Rubber, Carl Hanser Verlag GmbH & Co. KG2012, pp. 345–364.
[24] Abaqus/CAE User's Guide. Ver. 6.14,, Dassault Systèmes, Providence, RI, 2014.

A.3 Paper III

Rubber adhesion below the glass transition temperature: role of frozen-in elastic deformations

A.G. Akulichev, A. Tiwari, L. Dorogin, A.T. Echtermeyer, and B.N.J. Persson.

Submitted

Paper III

Rubber adhesion below the glass transition temperature: role of frozen-in elastic deformation

A.G. Akulichev,[1,2] A. Tiwari,[1,2] L. Dorogin,[2,3,4] A.T. Echtermeyer,[1] and B.N.J. Persson[2,5]

[1]*Department of Mechanical and Industrial Engineering (MTP), Norwegian University of Science and Technology, Richard Birkelandsvei 2B, N-7491 Trondheim, Norway*
[2]*PGI-1, FZ Jülich, Germany, EU*
[3]*Leibniz Institute for Polymer Research Dresden, P.O. Box 120 411, D-01005 Dresden, Germany*
[4]*ITMO University, Kronverskiy pr. 49, 197101, Saint Petersburg, Russia*
[5]*www.MultiscaleConsulting.com*

We have studied how the adhesion between rubber and a flat counter surface depends on temperature. When the two solids are separated at room temperature negligible adhesion is detected, which is due to the elastic deformation energy stored in the rubber, which is given back during pull-off and help to break the adhesive bonds. When the system is cooled down below the glass transition temperature, the elastic deformation imposed on the system at room temperature is "frozen-in" and the stored-up elastic energy is not given back during separation at the low temperature. This results in a huge increase in the pull-off force. This study is crucial for many applications involving rubber at low temperatures, e.g., rubber seals for cryogenic or space applications.

Introduction – Most surfaces of solid objects have surface roughness on many length scales[1], which has a crucial influence on the contact between elastic solids[2–11]. Surface roughness is the main reason for why adhesion (manifested as a pull-off force), is usually not observed at the macroscopic length scale[12–27]. Solids can interact and form bonds only when separated at atomistic distances (nanometer or less), and in order to make contact the solids must deform at the interface. For elastically "hard" solids this results in a very small contact area which reduces the adhesion. More important, the elastic deformation of the solids at the interface (as a result of the adhesive forces) leads to stored-up elastic energy. During separation this elastic energy is given back, and helps to break the atomic bonds, and results in the vanishing pull-off force observed in most cases. Thus adhesion is only observed for either extremely smooth surfaces (as in wafer bonding[28]), or when at least one of the solids is elastically very soft[29, 30].

At room temperature rubber-like materials are soft with a Young's modulus of order a few MPa for most types of engineering rubber, such as rubber for seals, tires or wiper blades, and even much less for the weakly cross-linked rubber used, e.g., for pressure sensitive adhesives (which can have Young's modulus as low as 1 kPa)[30]. However, when rubber materials are cooled below the glass transition temperature the Young's modulus typically increases by a factor of ∼ 1000 (and sometimes much more) to several GPa. Thus if a rubber object is moved in contact with another solid at low temperature no adhesion force will be detected in most cases, even if the adhesion would be strong at room temperature. However, here we will show that if a rubber object is squeezed into contact with a counter object at room temperature and then cooled down below the glass transition temperature, an extremely strong adhesive bond can form. This results from the frozen-in elastic deformation field (see Fig. 1), and from the high effective Young's modulus in the glassy state. As will be discussed below, these phenomena have important technological implications, and if not properly accounted for, can result in expensive or disastrous consequences, such as the Challenger catastrophe [31].

Experimental – We have performed two types of experiments (schematically shown in Fig. 2(a) and 2(b)) to study how the adhesion between rubber and a counter surface depends on the temperature. We have used unfilled hydrogenated nitrile butadiene rubber (HNBR). The material composition and the processing details were reported elsewhere [32, 33]. The first set of experiments used a rubber half-cylinder (radius R = 1.5 cm, length L = 7 cm) confined between two flat, smooth, and parallel Polymethylmethacrylat (PMMA) surfaces at a separation about 10% – 20% smaller than the radius of the rubber cylinder. This resulted in a rectangular region of (apparent) Hertz-like contact with the width $2a \approx 1$ cm (see Fig. 1). The system was kept at room temperature for about 12 hours before put in a cold room with temperature −40 C. After staying in the cold room for about 12 hours we removed the rubber-PMMA contact and observed frozen-in elastic deformation (see Fig. 1b). Similar observations were made in [33] for button-shaped HNBR specimens exposed to temperatures below the glass transition temperature T_g.

For the second set of adhesion experiments we have used a Dynamic Mechanical Analysis (DMA) apparatus (Netzsch-Gabo Eplexor 150 machine with a thermal chamber and a 150 N force transducer). The machine was operated in the compression mode. The compression holders were cleaned with ethanol prior to each experiment. For the experiment, cylindrical specimens of 2.4 – 2.8 cm length were cut from rubber O-rings having a nominal cross section diameter of $2R \approx 0.53$ cm.

FIG. 1: Demonstration of frozen-in elastic deformation. Picture of a rubber half-cylinder at (a) room temperature and (b) at $T = -40°C$, after the cylinder was squeezed at room temperature against a sandpaper surface, and then cooled down. Note in (b) the rectangular (nominal flat) strip of frozen-in rubber deformation (Hertz-like contact). The magnification picture (right) shows that the (nominal flat) contact area has frozen-in surface roughness inherited from the surface roughness of the sandpaper. The frozen-in deformation of the rubber cylinder stays unchanged as long as the rubber is kept at $T = -40°C$, but disappears when the rubber sample is kept for some time at a temperature above the rubber glass transition temperature, e.g., at room temperature.

The cylindrical specimens were compressed in the radial direction by the DMA machine and let relax for 1000 s under the constant deformation. Then the chamber was cooled down to -50 °C keeping the displacement constant. The force, clamp separation and the chamber temperature were recorded during the experiment. At some temperature, below the glass transition point of the rubber, the compressive force gradually decreased down to zero (due to the frozen-in deformation field and the thermal contraction of the material; see below), and even to negative values due to the adhesive strength of the rubber-steel contact; see Fig. 3. Once the tensile stress in the rubber near the interface reached the rubber-steel bond strength, breakage of the adhesive bonds (opening crack propagation) occurred, and the force vanished abruptly. We performed several experiments with different compression of the rubber O-ring, and for smooth and rough rubber surfaces.

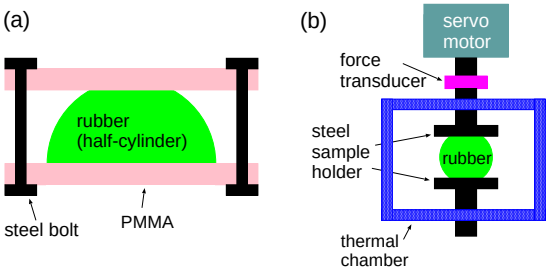

FIG. 2: Schematics of the two set-ups used for studying adhesion at low temperatures.

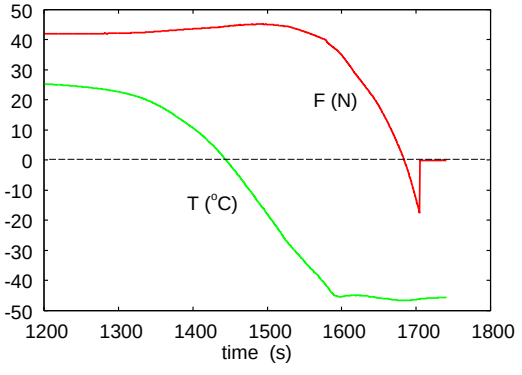

FIG. 3: The rubber O-ring with smooth surface initially compressed 10% and cooled down. The compressive force acting on the steel plate (red line) and the temperature (green line) as a function of time is depicted. Note that the temperature plot indicates the temperature inside the chamber, but not the rubber O-ring internal temperature.

We also performed some pull-off experiments with the system at room temperature. In this case we obtained the pull-off force (at the pull-off speed $v_z = 140$ μm/s): 0.9 ± 0.2 N for the smooth, clean rubber O-ring and 0.015 ± 0.015 N for the roughened rubber O-ring. These values should be compared to the 20.4 N and 4.8 N observed during (the thermal contraction-induced) pull-off when the system temperature is below the rubber glass transition temperature; see Table I for a summary.

Adhesion in a room temperature contact – The adhesive interaction between an elastic cylinder and a flat surface is a straightforward extension of the classical theory of the interaction between a spherical body and a flat surface known as Jonson-Kendel-Roberts (JKR) theory[34]. If the applied pull-off force is orthogonal to the flat contact region, the pull-off force per unit length is given by[35–37]

$$f_c = -\frac{3\pi E_0^* a_c^2}{4R},$$

TABLE I: The change in the force (pull-off force) during the abrupt detachment, induced by the thermal contraction of the rubber at low temperature (LT), and due to pull-off (at speed v_z = 140 μm/s) at room temperature (RT). In the first case the system is prepared at room temperature and then cooled down to −50°C in ≈ 300 s (see Fig. 3). The pull-off force was measured for 10% and 20% compression of the rubber O-ring, and for all surfaces cleaned by ethanol. We show results for smooth rubber and roughened rubber surface.

surface condition	10% compression	20% compression
smooth, LT	20.4 ± 3.0 N	31.4 ± 8.8 N
rough, LT	4.8 ± 0.2 N	..
smooth, RT	0.9 ± 0.2 N	..
rough, RT	0.015 ± 0.015 N	..

where the half-width of the the rectangular contact region at the pull-off instability is given by

$$a_c = \left(\frac{2wR^2}{\pi E_0^*}\right)^{1/3},$$

and the effective low-frequency Young modulus $E_0^* = E_0/(1-\nu^2)$,where E_0 and ν are the rubber low-frequency Young modulus and Poisson ratio, respectively. For HNBR rubber against smooth glass surface, for an opening crack at the pull-off velocity ≈ 1 μm/s we have measured the work of adhesion $w \approx 0.1$ J/m^2 [21]. However, the pull-off velocity in our experiments is ∼ 100 times higher and theory predicts for this case a ∼ 10 times higher work of adhesion because of the viscoelastic enhancement factor (see Ref. [38–43]). Assuming $w \approx 1$ J/m^2 for HNBR rubber against the steel surface (at the pull-off speed ≈ 100 μm/s) we get $a_c \approx 0.1$ mm and the pull-off force $F_c/L = f_c = 40$ N/m or for our $L = 2.6$ cm long rubber cylinder, about $F_c \approx 1$ N. This low pull-off force is close to our measured pull-off force at room temperature (0.9 ± 0.2 N).

Adhesion in a cooled contact – For the system which was cooled below the rubber glass transition temperature we observed very strong adhesion (see above). This can be understood qualitatively as follows. First note that the adhesion observed at room temperature is so small as a result of the elastic energy stored at the interface during the compression of the rubber cylinder. That is, during removal of the steel (or PMMA) sheet, the elastic energy stored at the interface helps to break the adhesive bonds and result in the small pull-off force observed. Now when the (compressed) system is cooled to $T = -50$°C (or $T = -40$°C as in the first experiment), which is way below the rubber glass transition temperature ($T_g \approx -23$°C), the elastic deformation field is frozen-in and not given back during the pull-off. This frozen-in deformation field can be clearly seen in Fig. 1(b) where a flat rectangular region is observed on the top of the rubber cylinder. As the rubber heats up, this flat region disappears, and the rubber regains its original perfect cylinder shape with half-circular cross section. However, a very large pull-off force is necessary to separate the rubber and a rigid counter-surface if the rubber is below the glass transition temperature. Consider, for example, the limiting case where the rubber surface within the rectangular contact region (width $2a$) can be considered to be in full contact with the countersurface, and assume that *no elastic energy is given back during pull-off*. In this case, using the theory of cracks, we estimate the force needed for pull-off when the applied force is orthogonal to the flat contact region:

$$f_{\rm pull-off} \approx (2\pi w a E_1^*)^{1/2},$$

where E_1^* is the (effective) elastic modulus of the rubber in the glassy response region (or high-frequency modulus), which is of order several GPa. Using that $a \approx (R\delta)^{1/2}$ (where δ is the penetration) we get for ∼ 10% compression (i.e. $\delta = 0.1R$) $a \approx 0.5$ mm. Thus with $L = 2.6$ cm and $E_1^* = 2$ GPa, we get the pull-off force $F = Lf \approx 17$ N, which is close to what we observe for the smooth clean rubber O-ring section (see Table I). Here we have assumed[44] $w = 0.07$ J/m^2 because when the rubber is in the glassy region it behaves as an elastic solid, and there is no viscoelastic enhancement factor. If the contact is incomplete within the nominal contact area, the work of adhesion and, hence, the calculated pull-off force is smaller.

When the rubber surface was roughened with sandpaper the pull-off force at low temperature did not decrease as one would expect based on experiments at room temperature. This is due to the fact that the elastic deformation field imposed on the asperity contact regions during the contact formation at room temperature, is frozen-in when the temperature is lowered to $T = -50$°C (or to $T = -40$°C in the first experiment), and hence no elastic asperity deformation energy is given back during pull-off at $T = -50$°C. Table I shows that the pull-off force at low temperature on the roughened surface is a factor 4.8/20.4 ∼ 0.24 smaller than for the smooth rubber surface. We interpret this as reflecting a change in the contact area: if we assume the work of adhesion w is proportional to the contact area we get a decrease by a factor of $(4.8/20.4)^2 \approx 0.06$ in the contact area upon roughening of the rubber surface. In particular, if the relative contact area $A/A_0 = 1$ for the smooth rubber surface we get $A/A_0 = 0.06$ for the roughened surface. The pull-off force at room temperature scales with w as $w^{2/3}$, so if the change in the contact area would be the only reason for the drop in adhesion at room temperature, one would expect the pull-off force at room temperature to be (0.9 N) × $(0.06)^{2/3} \approx 0.14$ N. However, the observed pull-off force is 0.015 ± 0.015 N. This shows, as already pointed out, that the main reason for the low adhesion

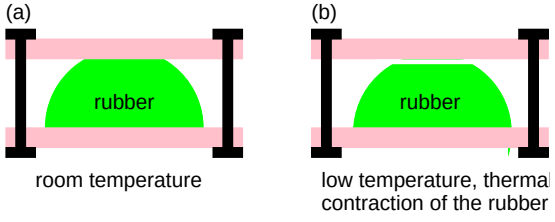

FIG. 4: (a) When the confined rubber cylinder is cooled below the rubber glass transition temperature, the deformation field imposed at room temperature becomes frozen-in. (b) If the system is cooled further below the glass transition temperature, the surfaces may separate at the adhering interface because of the thermal contraction mismatch. This assumes that the thermal contraction of the rubber compound is larger than the thermal contraction of the "box" containing the rubber cylinder, which is typically the case owing to the relative large thermal expansion coefficients of rubber materials. Considering low-temperature application of rubber seals, this large thermal contraction in combination with the poor shape recovery at and below the glass transition might result in an abrupt increase in the leak rate as the surfaces separate.

observed at room temperature is not the reduction in the contact area, but rather the elastic (asperity) deformation energy stored at the interface.

Discussion – We have studied adhesion between rubber and flat PMMA and steel surfaces when the system is cooled (starting with a contact formed at room temperature) below the rubber glass transition temperature. When the separation between the rubber and the counter surface occurs at room temperature negligible adhesion is detected, which is due to the elastic deformation energy stored at the interface, which is given back during pull-off and helps to break the adhesive bonds resulting in the negligible pull-off force observed in this case. When the system is cooled down below the glass transition temperature, the elastic deformation imposed on the system at room temperature is "frozen-in", and the stored-up elastic energy is not given back during separation at the low temperature. This results in a huge pull-off force. Here we note that this phenomenon is similar to liquid glues which is put between two surfaces and harden with increasing time, e.g., due to formation of cross-links or due to evaporation of a liquid component. This results in a solid in perfect contact with the substrate and without elastic energy stored-up at the interface, at least in the ideal case where no stresses develop in the adhesive during the transformation from the liquid to solid state. Thus, the absence of the elastic deformation energy can result in very strong adhesive bonds. A good example is cyanoacrylate adhesives ("superglues") which cure through reaction with moisture held on the surface to be bonded.

In the second experiment reported on above, the pull-off force resulted from the thermally induced contraction of the rubber as it is cooled to low temperature. The thermal expansion coefficient of most rubber materials is much larger than that of steel and other metals or metal alloys. For example, for carbon steel and the rubber compound at $T = -33°C$, the linear thermal expansion coefficient $\alpha = (dL/dT)/L_0$ (where L_0 is the length of the sample at room temperature) are $\approx 1 \times 10^{-5}$ K^{-1} [45] and $\approx 8 \times 10^{-5}$ K^{-1} [32], respectively. Thus from the glass transition temperature to $T = -50°C$, we expect the rubber to contract with $\approx 0.2\%$, or (for the $2R = 0.53$ cm rubber O-ring) $\Delta R \approx 10$ μm in the radial direction. If no contraction would be possible (e.g., by adhesion to the confining plates), one would instead expect a stress of order $\sigma \approx E_1 \Delta R/R \approx 4$ MPa to develop, and a normal force $F \approx L2a\sigma \approx 100$ N, which is larger than the adhesive force found above. Hence, the adhesive bond will break during the cooling down as indeed observed.

To summarize, when a rubber O-ring is confined between steel surfaces (as in a typical application) if the temperature is lowered below the rubber glass transition temperature, where the rubber deformation field is "frozen-in", the mismatch between thermal expansion of the rubber and the confining box material, may result in a finite surface separation at low temperatures (see Fig. 4). This would result in a dramatic increase of leakage of the seal. In another set of experiments, which we will report elsewhere, we indeed observed an abrupt increase in the gas leakage of rubber O-ring seals at low temperatures, which we interpret as resulting from the combination of the frozen-in rubber deformation field, and the thermal contraction of the rubber O-ring. In this case we measure both the rubber contact force acting on the steel surface, and the gas leakage, which abruptly increased at the same time as the contact force abruptly changed. The observed cold pull-off force for the seal rings in the leakage experiments is consistent with the measurements presented above.

Summary and conclusion – We have studied adhesion between rubber and flat smooth PMMA and steel surfaces, when the system is cooled (starting with a contact formed at room temperature) below the rubber glass transition temperature. When the separation between the rubber and the counter surface occurs at room temperature small (for smooth rubber surface) or no (for roughened rubber surface) adhesion can be detected, which is due to the elastic deformation energy stored at the interface, which is given back during pull-off and help to break the adhesive bonds resulting in the small pull-off force observed in these cases. When the system is cooled down below the glass transition temperature, the elastic deformation imposed on the system at room temperature is "frozen-in" and the stored-up elastic energy is not given back during pull-off at the low temperature. This results in a huge pull-off force. The study above is crucial for

applications involving rubber at low temperatures, e.g., in many applications where rubber seals operate at very low service temperatures, e.g., in some mining and oil-field applications in regions with cold climate or in space applications.

Acknowledgments: This work was performed within a Reinhart-Koselleck project funded by the Deutsche Forschungsgemeinschaft (DFG). We would like to thank DFG for the project support under the reference German Research Foundation DFG-Grant: MU 1225/36-1. This work was also supported by the Research Council of Norway (Project 234115 in the Petromaks2 programme). The research work was also supported by the DFG-grant: PE 807/10-1 and DFG-grant No. HE 4466/34-1. This work is supported in part by COST Action MP1303.

[1] B.N.J. Persson, Tribology Letters **54**, 99 (2004).
[2] E. Gnecco and E. Meyer, *Elements of Friction Theory and Nanotribology*, Cambridge University Press (2015).
[3] J.N. Israelachvili, *Intermolecular and Surface Forces* (Academic, London), 3rd Ed. (2011).
[4] B.N.J. Persson, Surface Science Reports **61**, 201 (2006).
[5] B.N.J. Persson, *Sliding Friction: Physical Principles and Applications*, Springer, Heidelberg (2000).
[6] W.B. Dapp, A. Lucke, B.N.J. Persson and M.H. Müser, Phys. Rev.Lett. **108**, 244301 (2012).
[7] S. Hyun, L. Pei, J.-F. Molinari, and M. O. Robbins. Phys. Rev. E **70**, 026117 (2004)
[8] C. Campana and M. H. Müser, Europhys. Lett. **77**, 38005 (2007)
[9] B.N.J. Persson, Journal of Chemical Physics, **115**, 3840 (2001).
[10] S. Akarapu, T. Sharp and M.O. Robbins, Physical Review Letters **106**, 204301 (2012)
[11] C. Campana, B.N.J Persson, M.H. Müser, Journal of physics: condensed matter **23**, 085001 (2011)
[12] K. Kendall, *Molecular Adhesion and its Applications: The Sticky Universe* (New York: Kluwer Academic, 2001)
[13] K.N.G. Fuller and D. Tabor, Proceedings of the Royal Society of London. A. Mathematical and Physical Sciences **345**, 327 (1975).
[14] B.N.J. Persson, The European Physical Journal E **8**, 385 (2002).
[15] L. Pastewka and M.O. Robbins, Proceedings of the National Academy of Sciences **111**, 3298 (2014).
[16] S. Zilberman and B.N.J. Persson, The Journal of chemical physics **118**, 6473 (2003).
[17] Q. Li and K.-S Kim, Acta Mechanica Solida Sinica **22**, 377 (2009).
[18] N. Mulakaluri and B.N.J. Persson, EPL **96**, 66003 (2011).
[19] G. Carbone, E. Pierro and G. Recchia Physical Review E **92**, 062404 (2015).
[20] M. Müser, Tribology International **100**, 41 (2016)
[21] A. Tiwari, L. Dorogin, A.I. Bennett, K.D. Schulze, W.G. Sawyer, M. Tahir, G. Heinrich and B.N.J. Persson, Soft Matter, 13, 3602-3621 (2017).
[22] B. Lorenz, B.A. Krick, N. Mulakaluri, M. Smolyakova, S. Dieluweit, W.G. Sawyer and B.N.J. Persson, Journal of Physics: Condensed Matter **25**, 225004 (2013).
[23] B.A. Krick, J.R. Vail, B.N.J. Persson and W.G. Sawyer, Tribol Lett **45**, 185 (2012).
[24] B.N.J. Persson and M. Scaraggi, The Journal of Chemical Physics **141**, 124701 (2014).
[25] B.N.J. Persson, I.M. Sivebaek, V.N. Samoilov, K. Zhao, A.I. Volokitin and Z. Zhang, J Phys Condens Matter **20**, 395006 (2008).
[26] G. Carbone, M. Scaraggi and U. Tartaglino, Eur. Phys. J E**30**, 65 (2009).
[27] A. Chateauminois and C. Fretigny, Eur. Phys. J. E **27**, 221 (2008)
[28] U. Gösele and Q.-Y. Tong, Annu. Rev. Mater. Sci. **28**, 215 (1998).
[29] B.N.J. Persson, O. Albohr, C. Creton and V. Peveri, J Chem Phys. **120** 8779 (2004).
[30] C. Creton and M. Ciccotti, Reports on Progress in Physics **79**, 046601 (2016).
[31] R. P. Feynman, *What do you care what other people think?: Further Advances of a Curios Character*, (W.W. Norton & Company, 2001).
[32] A.G. Akulichev, B. Alcock, A. Tiwari and A.T. Echtermeyer, Journal of Materials Science **51**, 10714 (2016).
[33] A. G. Akulichev, B. Alcock, and A. T. Echtermeyer, Polymer Testing, **61**, 46 (2017).
[34] K. L. Johnson and K. Kendall and A. D. Roberts, Proc. R. Soc. London A **324**, 301 (1971).
[35] J. A. Greenwood and K. L. Johnson, Philos. Mag. **43**, 697 (1981).
[36] D. Maugis and M. Barquins, J. Appl. Phys. D **11**, 1989 (1978).
[37] M.K. Chaudhury, T. Weaver, C.Y. Hui and E.J. Kramer, J Appl Phys **80**, 30 (1996).
[38] BNJ Persson, EA Brener, Physical Review E **71**, 036123 (2005).
[39] BNJ Persson, O Albohr, G Heinrich, H Ueba, Journal of Physics: Condensed Matter **17**, R1071 (2005).
[40] Tao Lin Sun, Feng Luo, Wei Hong, Kunpeng Cui, Yiwan Huang, Hui Jie Zhang, Daniel R. King, Takayuki Kurokawa, Tasuku Nakajima, and Jian Ping Gong, Macromolecules **50**, 2923 (2017).
[41] J.A. Greenwood, J. Phys. D: Appl. Phys. **37**, 2557 (2004).
[42] J.A. Greenwood, J. Phys. D: Appl. Phys. **40**, 1769 (2007).
[43] J.A. Greenwood, K.L. Johnson, S.-H. Choi and M.K. Chaudhury, Journal of Physics D: Applied Physics **42**, 035301 (20089).
[44] We estimate the adiabatic (thermal equilibrium) work of adhesion for the steel-rubber interface using $w \approx 2(\gamma_1\gamma_2)$, where γ_1 and γ_2 are the surface energies of the steel and rubber surfaces, respectively [see J.N. Israelachvili, *Intermolecular and Surface Forces* (Academic, London), 3rd Ed. (2011)]. The surface energy of clean steel surfaces is very large, but steel surfaces exposed to the normal atmosphere has strongly bound contamination which cannot be removed with water or organic fluids such as acetone. The measured surface energy of steel surfaces after cleaning with water or acetone is [see M. Mantel and J.P. Wightman, Surfaces and Interfaces **21**, 595 (1994)] about $\gamma_1 \approx 0.04$ J/m^2. Using the surface energy $\gamma_2 \approx 0.03$ J/m^2 for the HNBR rubber this gives $w \approx 0.07$ J/m^2.
[45] R.J. Corruccini and J.J. Gniewek, *Therman Expansion of Technical Solids at Low Temperatures: A Compilation From the Literature*, National Bureau of Standards, NBS

monograph 29 (1961).

A.4 Paper IV

Interfacial leakage of elastomer seals at low temperatures
A.G. Akulichev, A.T. Echtermeyer, and B.N.J. Persson.
Submitted

Paper IV

Interfacial leakage of elastomer seals at low temperatures

A. G. Akulichev[a], A. T. Echtermeyer[a], B. N. J. Persson[b,c]

[a]*Department of Mechanical and Industrial Engineering (MTP), Norwegian University of Science and Technology, Richard Birkelandsvei 2B, N-7491 Trondheim, Norway*
[b]*PGI-1, FZ Jülich, Germany, EU*
[c]*www.MultiscaleConsulting.com*

Abstract

Interfacial leakage of air in hydrogenated nitrile butadiene rubber (HNBR) O-ring seals exposed to sub-ambient temperatures is studied. Flange-type fixtures with sealing surfaces produced by 3 different surface finish processes are used. When the seals are cooled down to temperatures below the elastomer glass transition point T_g of (−23 °C), an abrupt increase of air leakage ($> 10^{-2}$ cm^3/min) is observed. The effects of surface finish conditions, compression ratio, grease lubrication and additions of carbon black in the HNBR on the cold leakage are discussed. Persson's contact mechanics and effective medium leakage theory coupled with finite element analysis (FEA) of the HNBR seals are utilized to capture the changes in the contact area and pressure with cooling and predict the seal failure temperatures. The main cause for the cold seal failures is believed to be the detachment of the elastomer seals from their mating sealing parts due to the elastomer thermal contraction and the negligible recovery of the HNBR in cold environment. In addition, the adhesive rubber-substrate interface influences the detachment and seal failure.

Keywords:
Elastomer, Seals, Leakage, Low-Temperature Extreme

1. Introduction

Elastomeric seals are used in almost any industrial pressure retaining equipment operating at low and high pressure, e.g. in oil and gas, automotive or aerospace applications. These seals usually have excellent flexibility, resilience and elastic recovery properties and do not require very fine surface finish to make a good seal, as, for example, thermoplastic seals would demand. There are, however, factors under which the pressure integrity of elastomeric seals can be compromised. One of these influencing factors is exposure to a cold environment which might, in fact, lead to catastrophic consequences, as, for instance, in the Challenger disaster [1].

Among all fluids, sealing of gases represents the most difficult task for engineers due to their extremely low viscosity. The gas leakage in elastomer seals arises from gas permeation through the materials and from the interfacial (or contact) leakage. The permeation of gases through elastomers is known to decrease with temperature reduction [1, 2, 3] and is, thus, not as significant at low temperatures as the interfacial leaks [2]. The Challenger catastrophe triggered scientists and engineers from a variety of industries to study the low-temperature behaviour of elastomer seals to be used in gas containing systems. As a result of their efforts, some publications appeared [4, 5, 6, 7, 8, 9, 10, 11, 12, 13, 14, 15]. A short summary of the experimental details and findings of the existing literature is given in Table 1.

The sealing experiments undertaken in different conditions and using different equipment show some similarities. Thus, the majority of seals failed at temperatures approximately 10-35 °C below T_g depending on their compression level and the exerted pressure difference. Hence, T_g does not accurately define the low-temperature limit of serviceability of elastomeric seals. Furthermore, T_g can be determined by several methods, which in general do not give the same results.

Another interesting observation can be made considering the effect of gas pressure: high ($\geq$ 100 bar) pressure difference, if applied prior to cooling of the sealed joint, might result in lower leakage temperatures [8, 10]. Higher failure temperatures were obtained in low-pressure ($<$ 100 bar) systems [5, 6, 11, 13], or in high-pressure systems pressurized after the cooling step [10]. Furthermore, there are indications that pressure and temperature cycling from

low to high values might yield increased leak temperatures [16], but not much experimental data are available to public for these cases.

Most of the earlier investigators used commercial seals with scarcely reported low-temperature properties of the seal materials (typically only the glass transition T_g and sometimes 10 % retraction TR-10 temperatures) and the sealed surface properties. Therefore, the mechanisms of cold leakage of elastomeric seals have remained unclear, except for the case where the sealing gap was artificially increased and seals failed due to their slow elastic recovery at low temperatures near their T_g [12, 15, 18]. This is, however, an extreme scenario which will not be considered herein. The main objective of this work is to understand the phenomena governing the leakage of static elastomeric seals in flange-type joints at low temperatures. The effects of filler in the elastomer and lubrication will be considered as well. The most common scenario when seals are mounted in a joint at ambient temperature inside a workshop or an assembly site and then brought to a cold service is followed. Prediction of the temperature at which the particular elastomer seal fails is of the most interest and aimed in this work.

Table 1: Short summary of the low-temperature leak test data. The imposed compression and applied gas pressure difference are given in parentheses; for more details the reader is referred to the indicated publications. ΔT indicates the difference between the measured leakage temperature T_{fail} and the glass transition. Special test conditions are explained in notes

Elastomer type	T_g, °C	TR-10, °C	Typical conditions		Special conditions		Notes
			T_{fail}, °C	ΔT, °C	T_{fail}, °C	ΔT, °C	
Taylor [8] (15% compression / 345 bar)							
Nitrile	-37		-56	-19			
Arctic Nitile	-35	-49	-62	-27			
Camlast 1049	-18	-19	-40	-22			
Aflas	7		-23	-30			
Viton	3		-34	-37			
Burnay and Nelson [6] (1 bar)							
FKM E60C	-18		-30	-12			
Stevens et al [5] (10 /20 % compression / 14 bar)							
FKM E60C	-18		-31	-13			10 % compression
FKM B70	-21		-33	-12			
FKM B600	-13		-26	-13			
FKM GLT	-29		-44	-15			
FKM GLFT	-23		-36	-13			
Weise et al [9] (25 % compression / 1 bar)							
Viton1	-7		-35	-28			
Viton2	1		-20	-21			
Viton3	-6		-31	-25			
Viton5	-23		-44	-21			
EPDM	-30		-61	-31			
Silicone	-31		-63	-32			
Warren [10] (16.6-18.5% compression / 100 (175) bar)							
NHNBR LT	-32	-36	-54	-22	-41	-9	Pressurized after the cooling step
FKM LT	-19	-31	-55	-36	-32 (-40)	-13(-21)	
FKM ULT	-27	-40	-56	-29	-42(-45)	-15(-18)	
Omnés and Heuillet [13] (24 % compression / 5 bar)							
HNBR	-18				-30	-12	Pressurized after the cooling step
Grelle et al [12] (20 % compression / 1 bar)							
FKM	-17		-38	-21	-10	7	Partial release of compression

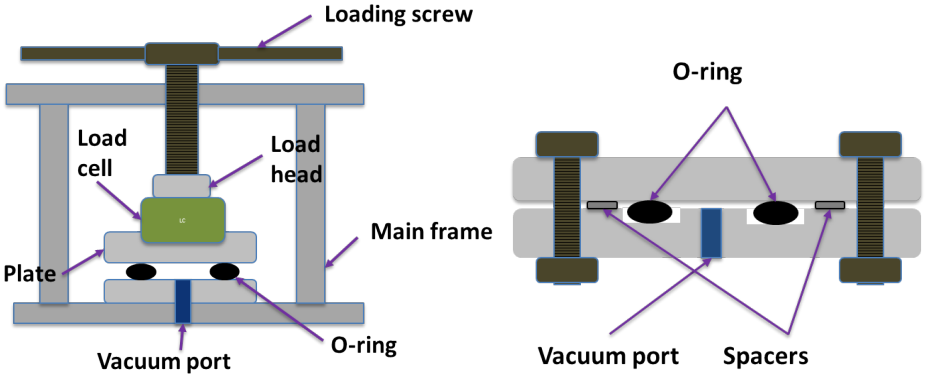

(a) Leak test rig with a load cell.

(b) Leak test flange.

Figure 1: Leak test rigs used in the experiment (schematic).

2. Materials and methods

The cold sealing experiments reported here were performed using a custom-built thermal chamber coupled with heat exchanger piping connected to a recirculating coolant bath manufactured by Julabo. The interiors of the chamber with test rigs can be cooled down to about −52 °C in the experimental set-up.

Two configurations of test rigs were utilized in the experiment. The first one was based on the compression rig concept used in stress relaxation experiments [19] and features compression (sealing) force measurements by a 2.5 kN compression load cell, see Fig. 1a. Pre-defined compression is exerted to an O-ring by a screw in this set-up. The sealing counter-faces have root mean square (RMS) surface roughness of 0.95 µm. The main purpose of the measurements with this rig was to measure the sealing force variation with cooling. Vacuum creates additional compressive force to the seal estimated to be about 800 N leading to lower failure temperatures, especially if the pressure difference is applied at temperatures above the T_g. As a result, another rig was also utilized for measurement of leak rates in cold environment.

The second rig is schematically illustrated in Fig. 1b and represents a simple flange arrangement accommodating an O-ring and exchangeable flange parts having different sealing surface topography as will be described later. A set of spacers was selected to fix the desired seal compression δ. The temperature of the tested O-rings was measured by two thermocouples positioned near the seals; the average values of the thermocouple readings are reported. The sealing surfaces were cleaned with ethanol prior to each test, and the seals were mounted dry at a temperature of 24 ± 1 °C. In addition, several experiments were carried out with application of silicone grease (Molykote 33 Medium).

A vacuum pump connected to the leak port in the test fixtures was used to create a pressure difference between the system and ambient environment. The system (vacuum) pressure and leak rate was continuously measured during each test by a vacuum pressure transducer and supplemented by a flow meter with a resolution of 10^{-3} cm^3/min. The overall system leakage (which includes the leakage in the fittings and air permeation through the polymer parts) was measured to be approximately 2×10^{-3} cm^3/min by the pressure decay method.

Three flange parts with different surface finish were used in the leak measurements. The sealing surfaces were prepared by milling, turning and grinding processes and possess rather different surface roughness. Their surface topography characteristics in the direction orthogonal to the leakage path are summarised in Table 2. The surface roughness of the milled surface finish is somewhat higher than usually specified in engineering documentation, however that was made intentionally to promote leakage. The sealing area topography of the flange parts is depicted in Fig. 2a, while Fig. 2b shows the computed one-dimensional (1D) surface roughness power spectra. It should be noted that the surface roughness is anisotropic in all cases studied here.

Table 2: Surface roughness properties of the sealing surfaces used in the flange experiment. Line scan was performed by stylus profilometer with a lateral resolution of 0.56 µm and track length of 10 mm.

Surface finish	Surface roughness parameters				
	R_a, µm	R_q, µm	R_v, µm	R_p µm	RMS slope
Milling	1.7806	2.1588	-6.189	5.38	0.1807
Turning	0.4081	0.5069	-1.043	1.212	0.0083
Grinding	0.4788	0.6471	-3.812	2.517	0.0928

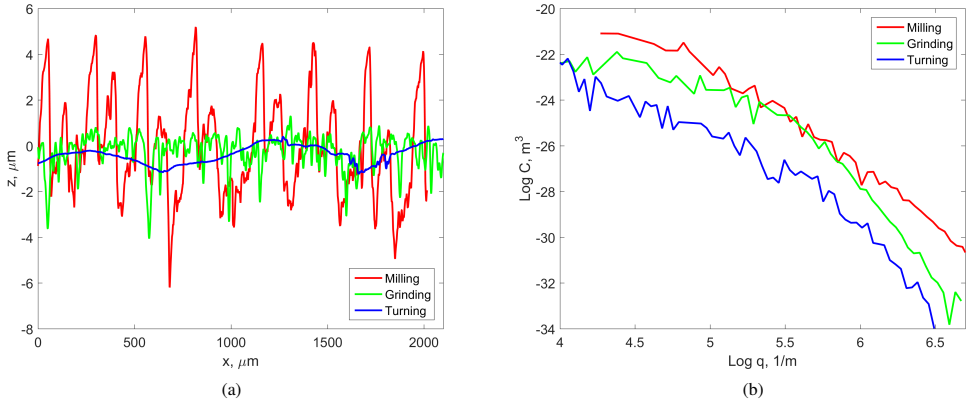

(a) (b)

Figure 2: a) topography measured by stylus profilometer and b) 1D surface roughness power spectra of the indicated sealing surfaces.

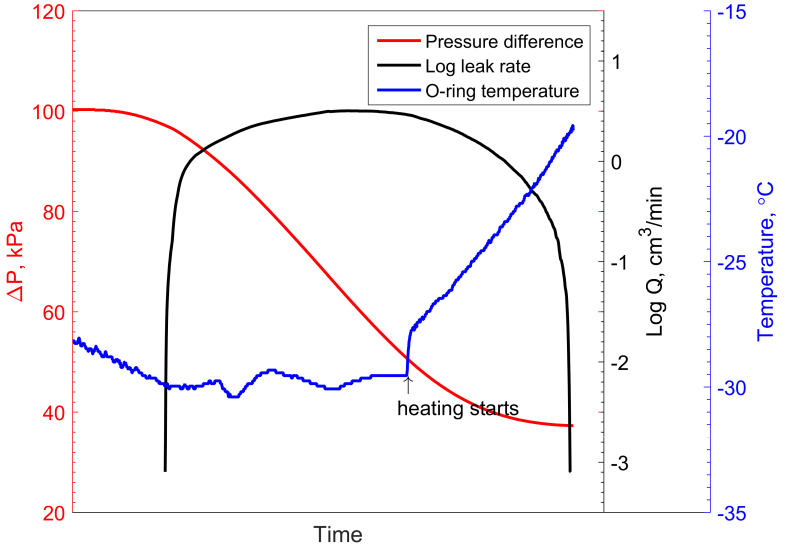

Figure 3: Pressure difference in the system, leak rate and temperature of an unfilled HNBR O-ring subjected to ≈ 8 % compression as function of time (grinding surface finish).

For the experiments hydrogenated nitrile butadiene rubber (HNBR) O-rings of ca. 108 mm inner diameter and 5.3-5.5 mm cross section diameter were manufactured in lab environment by compression moulding. Due to the variance in the cross section diameter of the seals, the attained compression levels in flange-type experiment were somewhat different. The basic material is HNBR having 96 % saturated polybutadiene with 36 % acrylonitrile content. Two formulations were used: one with 20.4 Vol.% N-330 HAF carbon black (CB) loading and the other without it (further referred to as unfilled HNBR). The full description of the material composition, the processing details and the material properties were provided in the previous publications [17, 18, 19]. It is important to mention that the elastomers have a T_g of about −16 °C as determined by dynamic mechanical thermal analysis (DMTA) experiments at the measurement frequency f of 1 Hz [18] or −23 °C as determined from differential scanning calorimetry (DSC) measurements conducted using a heating rate of 20 °C/min [17].

In the flange-based set-up, three O-rings of each compound were tested against each of three sealing surfaces using three different compression ratios, so the total number of leakage tests was 54.

3. Results

The leak rates of the studied seals do not change much with cooling to temperatures approximately above −25 °C. At certain temperatures below it an abrupt increase in the air leakage occurs, as for instance depicted in Fig. 3. This finding is in accordance with the cold seal failures experienced in the past works [2, 6, 9, 11]. We refer to the temperature at which the leak rate abruptly increases ($> 10^{-2}$ cm^3/min) reflecting the seal failure as leakage temperature. In order to stop such large leaks, the seals have to be heated to temperatures several degrees higher then that at the onset of the large leak (see Fig. 3). The variation of the leakage temperature with O-ring compression is shown in Fig. 4a-4c for all studied counter-surfaces.

The leak data feature a wide distribution of leak temperatures depending on the filler content, the sealing surface topography and the seal compression level. The leak temperature of the seals is found to decrease with increase

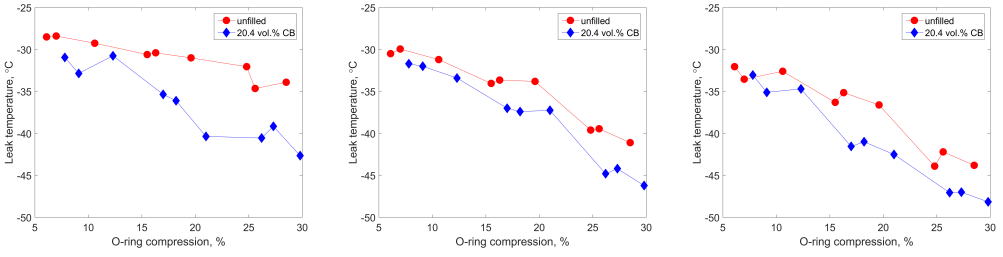

(a) Milling (b) Grinding (c) Turning

Figure 4: Leak temperature as function of seal compression for 20.4 vol.% CB filled and unfilled HNBR seals.

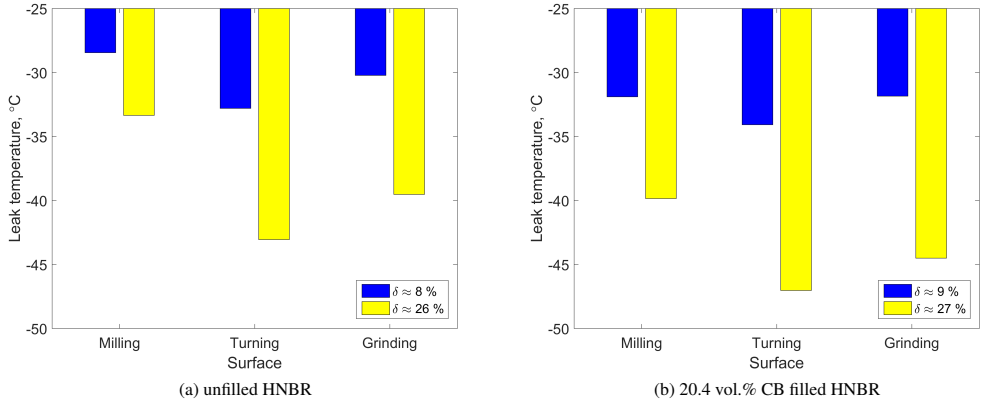

(a) unfilled HNBR (b) 20.4 vol.% CB filled HNBR

Figure 5: The effect of surface finish on leak temperature a) in unfilled HNBR and b) in filled HNBR seals at the indicated seal compression ratio δ.

of O-ring compression for all types of surface finish and regardless of CB content in HNBR. The effect of larger seal compression is, however, more pronounced in the CB filled HNBR seals. Furthermore, the seals made of CB filled HNBR in general demonstrate lower leak temperatures as compared to the unfilled HNBR seals. The highest leak temperature (about $-28\,^{\circ}$C) was observed in the unfilled HNBR seals at $\approx 7\,\%$ compression with the roughest counter-surface, while the lowest leak temperatures below $-45\,^{\circ}$C were found in the filled HNBR seals at $\approx 30\,\%$ compression against the most smooth sealing counter-surface in the experiment.

The variation of the leak leak temperatures with the surface finish conditions is illustrated in Fig. 5a and Fig. 5b for unfilled and filled HNBR respectively. The positive effect of a smoother sealing surface on the seal failure temperature is quite apparent for seals made of both elastomers. However, the effect of roughness at relatively low $(7-10\,\%)$ seal compression ratios is not as significant as at high $(25-30\,\%)$ compression ratios. The plausible reason is related to the strength of adhesion between HNBR and the steel counter-face and will be discussed in the next section.

Another set of experiments was carried out using the rig with the sealing force measurement capability. Low temperatures have a profound effect on the retention of the sealing force of the tested O-rings as depicted in Fig. 6a. The O-ring sealing force decays with cooling to nearly zero at a variable decay rate which reaches a maximum at about $-10\,^{\circ}$C. A similar behaviour of force decline during cooling at low temperatures was noticed earlier in fluoroelastomer [5, 7, 6] and HNBR [20, 13] seals. In addition, experiments were carried out on CB filled O-rings, and the effect of

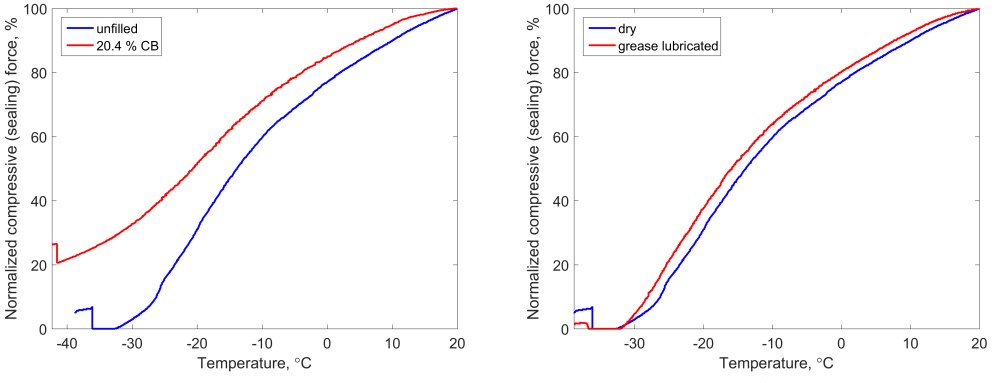

Figure 6: The effect of CB loading in a) and grease lubrication in b) on the temperature variation of the O-ring compressive force normalised to the compressive force at room temperature. The seals were compressed ($\delta = 0.1 \pm 0.005$) and left to relax under the constant strain for approximately 16-17 hours before the cooling step in order to minimise the effect of stress relaxation during the experiment.

filler on the sealing force is quite apparent here. A higher amount of carbon black makes the retention of the sealing force at low temperatures better. This positive effect of the filler is in a good agreement with the results of the flange-based leak experiments and attributed to a lower thermal contraction of the filled elastomers [17] as well as a lower contribution of the entropy elasticity [19]; see also the analysis and discussion below.

Another interesting phenomenon, which was not discovered in the earlier studies, is the abrupt force increase observed in our experiments at temperatures below the glass transition (see Fig. 6a). These force jumps led, in turn, to an drastic increase of the leak rates in every experiment, except for the seals lubricated by a silicone grease. This peculiar effect is believed to be related to breakage of the adhesive bond between the elastomers and the metal substrates at low temperatures as the thermal stresses in the rubber near the interface reach a critical value due to the thermal shrinkage [21]. The effect of adhesion on the cold leakage will be discussed below.

No significant increase of the leak rates was observed in grease lubricated seals, even though the seals detached from the counter-surface manifested in similar force jumps as in the dry O-rings, see Fig. 6b. The silicone grease is likely to fill up the gap between the HNBR and its counter-surface and, thus, impedes the air permeation through the contact.

4. Analysis and discussion

Leakage experiments of HNBR seals exposed to low temperatures at various compression levels were carried out using sealing surfaces with different topography. In order to understand the effects of compression and the counter-surface topography on leakage, a multi-scale approach to the contact mechanics of an elastomer seal ring against a rough rigid substrate has be to undertaken.

Consider a case of an O-ring seal squeezed between flange parts in a tight joint. The seal delimits a high and low pressure regions with the pressure drop ΔP. The nominal contact area A_0 between the O-ring and the rigid counter surface is $L_y \times L_x$ or $\pi D \times 2a$, where D is the seal diameter and a is the half-width of the contact region in the fluid leakage direction. It is well known [22], that most surfaces in engineering applications exhibit surface roughness on a wide range of length scales, which has to be accounted for in the contact studies. As such the contact area, for example, when observed with micro-scale resolution, will be smaller than the nominal one. This is due to the existence of microscopic peaks and valleys in the topography of the surface, even if the looks smooth and flat to the naked eye.

In order to quantify the effect of roughness on different levels mathematically, magnification ζ is introduced according to the Perssons contact theory [23]. The apparent contact area $A(\zeta)$ can be then studied as a function of magnification ζ. The contact between a rubber block and a rigid surface appears to be complete $A(1) = A_0$ at the lowest magnification $\zeta = 1$. At higher magnifications surface roughness can be observed and, thus, the apparent contact area decreases ($A(\zeta) < A_0$). The apparent relative contact area $A(\zeta)/A_0$ at the magnification ζ can be obtained using the Perssons contact theory [23, 22, 24] via

$$\frac{A(\zeta)}{A_0} = \mathrm{erf}\left(\frac{P_0}{2G^{\frac{1}{2}}}\right) \tag{1}$$

where erf(x) is the error function, P_0 is the nominal contact pressure and the function G is expressed as

$$G(\zeta) = \frac{\pi}{4}\left(\frac{E}{1-\nu^2}\right)\int_{q_L}^{\zeta q_L} \mathrm{d}q q^3 C(q) \tag{2}$$

where $C(q)$ is the 2D surface roughness power spectrum, E and ν are the elastomer Youngs modulus and the Poissons ratio, $q = \zeta q_L$ (with $q = 2\pi/\lambda$ and $q_L = 2\pi/L_x$) is the wave vector and λ is the wavelength.

Estimation of the interfacial leak rate through a seal-rigid substrate contact can be done using the critical junction [26, 25] or effective medium theories [27, 28]. The latter is used here since it takes into account the leakage through multiple channels, not only the critical constriction channel as in the former approach. The effective medium theory treats a multi-component medium (e.g. a porous medium in the fluid flow studies) as a single phase medium with effective (averaged) properties. Assuming incompressible and laminar flow, the leak rate is calculated using the effective conductivity of the contact interface σ_{eff} in accordance with [27, 28]

$$Q = \frac{L_y}{L_x}\sigma_{\mathrm{eff}}\Delta P \tag{3}$$

where

$$\frac{1}{\sigma_{\mathrm{eff}}} = \int_1^{\zeta}\left(-\frac{A'(\zeta)}{A_0}\right)\frac{2}{\sigma_{\mathrm{eff}} + \sigma(\zeta)}\mathrm{d}\zeta \tag{4}$$

and

$$\sigma(\zeta) = \frac{[u_1(\zeta)]^3}{12\mu} \tag{5}$$

Here $u_1(\zeta)$ is a function dependent on the average effective separation, μ is the sealed fluid viscosity. For more details on the theoretical foundation of the leak rate calculations, the reader is referred to the original publications [27, 28].

The leak rates for the cases studied here were calculated using the methodology presented above. Fig. 7b depicts the outcome of the leakage calculations with leak rate Q plotted against the normalized contact pressure (P_0/E). The surfaces evidently have different interfacial leakage characteristics. As expected, the milled surface represents the worst leakage case, while the surface produced by turning is characterized by the lowest leak rates. In fact, the real contact area (see Fig. 7a) reaches the percolation threshold (for $A(\zeta)/A_0 \approx 0.42$) at much lower compression than in the other cases which leads to an abrupt decrease of leak rate already at very small contact pressures ($P_0/E \geq 0.005$ or, for instance, $P_0 \geq 0.025$ MPa for the unfilled HNBR). In contrast, the contact pressure required to attain the percolation threshold for the surface after milling is about 16 times higher: $P_0/E \approx 0.08$ or $P_0 \approx 0.4$ MPa for the unfilled HNBR. This will have an effect on the leakage at low temperatures in addition to the other effects. It is noteworthy that the leak rates in Fig. 7b have to be multiplied by a factor of ≈ 1000 coming from the ratio L_y/L_x and even higher as the contact width L_x dramatically reduces with cooling, see the analysis of the contact below. In this study, the roughness of the HNBR O-ring surface is assumed smaller than the counter-surface roughness.

It is quite clear that the seal contact pressure is a very important characteristic for the leak rate in ambient conditions. Changes in the contact pressure with temperature is also likely to define the onset of the observed air breakthrough at temperatures below T_{g}. In order to understand the development of the contact pressure profile across the sealed interface with temperature, a finite element analysis (FEA) approach is utilized. An axisymmetric model of an

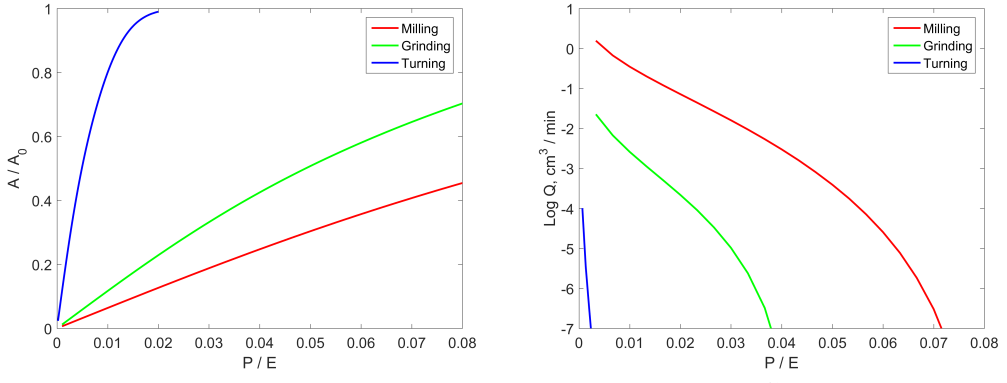

Figure 7: Calculated relative contact area in a) and calculated leak rate Q in b) as functions of the normalized contact pressure at the indicated surface finish. The results were obtained using 1D power spectra depicted in Fig 2b without taking the adhesion and the surface roughness anisotropy into account.

O-ring with a cross section diameter of 5.5 mm was built and analysed using Abaqus software (v. 6.14). For meshing, CAX4RH linear hybrid elements were utilized. Compression of the ring was done by rigid analytical surfaces.

The thermo-mechanical properties of the materials employed were obtained in the previous studies [17, 18, 19]. The thermal dilatation curves of the studied elastomers are depicted in Fig. 8a and implemented into the analysis as temperature dependent functions of the coefficients of thermal expansion. It is worth mentioning that the CB filled HNBR apparently has a lower thermal expansivity than the unfilled material.

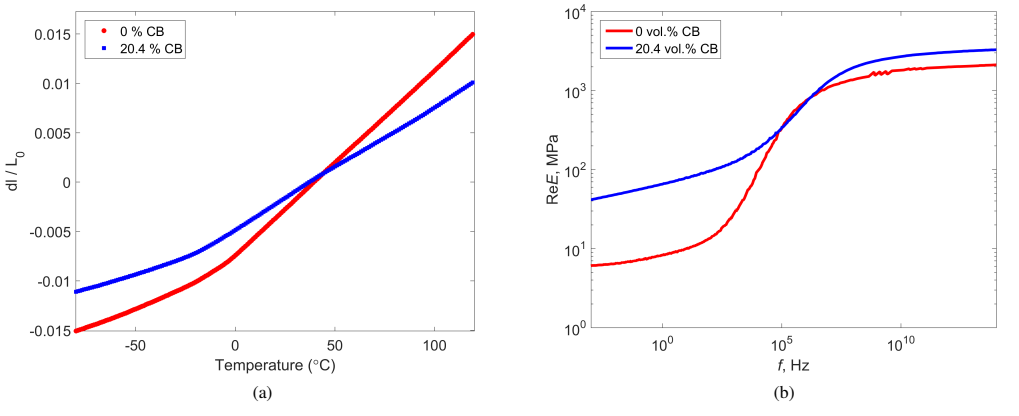

Figure 8: The thermo-mechanical data of HNBR at the indicated CB volume fraction: a) dilatometric curves and b) storage modulus master curves. The dilatometric measurements were carried out using Netzsch DIL402C dilatometer at a heating rate of 2 °C/min [17].

The model takes into account long-term hyperelastic and viscoelastic (time-dependent) responses and finite compressibility of the materials [17, 18]. Modelling the viscoelastic behaviour of the HNBR near the glass transition is not straightforward as it also exhibits an increasing strain dependency at about −15 °C and deeper into the glass transition

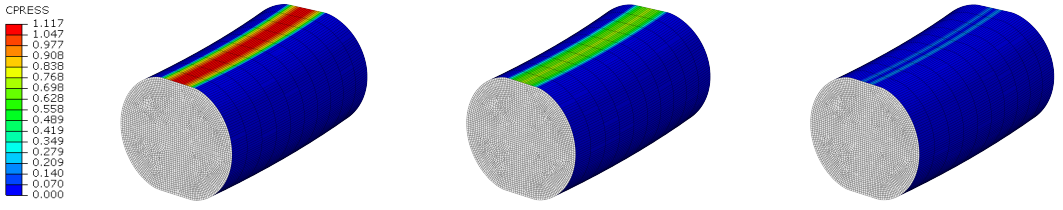

(a) $T = 297K$ (b) $T = 253K$ (c) $T = 243K$

Figure 9: An example of the simulated contact pressure profile along the contact line of an O-ring section subjected to 10 % compression at ambient temperature and cooled down. The contact pressure scale bar is in MPa. The maximum contact pressure at −20 °C (253 K) is about a half of the initial one due to the thermal shrinkage of the HNBR and softening related to the entropic nature of the material. The contact pressure at −20 °C is still sufficient to retain the air tightness at 1 bar pressure difference (see Fig. 9b), whereas at −30 °C (243 K) it diminishes to nearly zero with a minor contact width resulting in leakage. The FEA was performed using a cooling rate of −0.01 °C/s and CoF of 0.5.

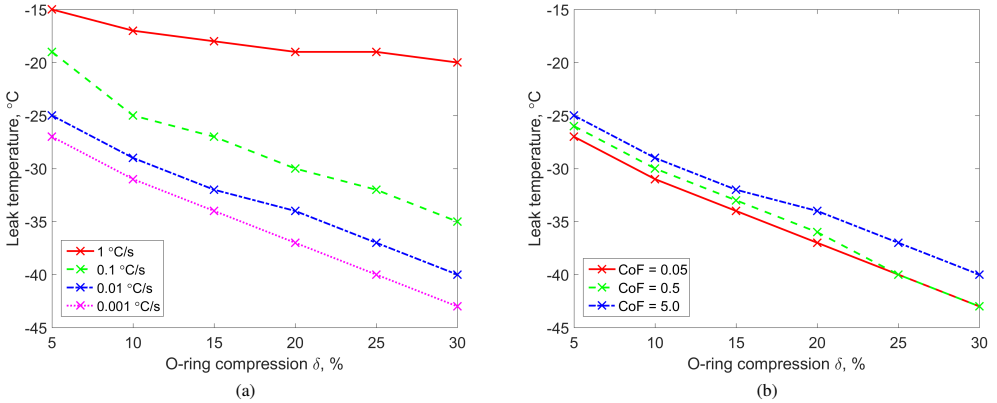

(a) (b)

Figure 10: The effects of cooling rate with CoF = 5 in a) and the coefficient of friction using the cooling rate of −0.01 °C/s in b) on the simulated seal failure temperatures for the unfilled HNBR compound.

[19]. However, considering the initial large-strain field in the seal is essentially frozen-in below the T_g [18, 21], the modelling approach in the first approximation can be considerably simplified focusing only on the thermal shrinkage in the transition and glassy regions which causes small strain changes with each temperature increment ($\approx 0.1 - 0.2$ % over the total temperature range from −20 °C to −40 °C). Therefore, only small-strain viscoelastic material data are needed to get the corresponding Maxwell model parameters. The data were collected during temperature-frequency sweeps using a TA instruments dynamic mechanical thermal analysis (DMTA) apparatus. The data were then used to build master curves depicted in Fig. 8a and compute the viscoelastic parameters to feed the viscoelastic part of the model. All material properties used in the simulation are listed in Appendix A.

An example of the FEA simulation is given in Fig. 9a-9c. The simulated contact pressure steadily decreases with cooling and, at temperatures below the glass transition, abruptly drops to zero. For the counter-surface produced by grinding, microscopic separation of the seal from the counter-part is likely to occur as the maximum contact pressure quickly falls below ≈ 0.25 MPa (or ≈ 0.51 MPa for the 20.4 vol.% CB filled compound). This in turn results in a drastic increase in the air leak rate through the contact. This contact pressure corresponds to the leak rate Q ≈ 10^{-3} cm^3/min estimated by the effective medium leakage theory for this surface (see Fig. 7b).

The simulation results are influenced by non-material parameters. The rate of cooling has a large impact on the

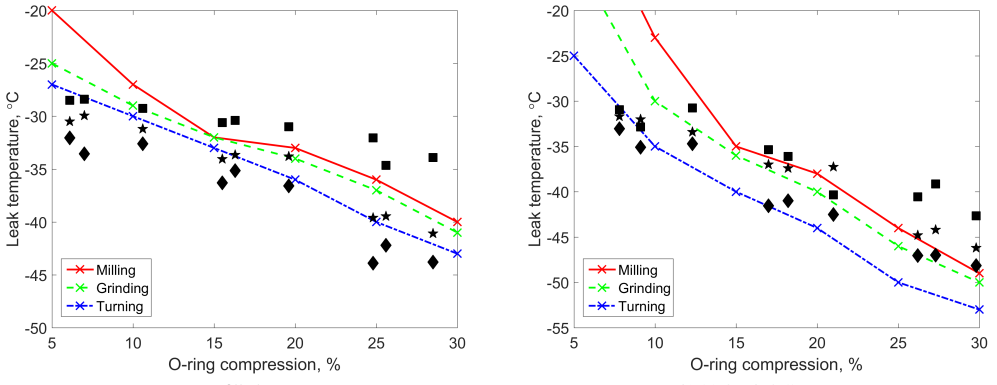

(a) Unfilled HNBR (b) 20.4 vol.% CB HNBR

Figure 11: Simulated and experimental leak temperatures as functions of seal initial compression for sealing surfaces with indicated surface treatment. The experimental data are for surfaces after milling (■), grinding (★) and turning (⧫) listed in the direction of roughness decrease. The FEA was performed using a cooling rate of −0.01 °C/s attained in the flange-based leak tests and CoF = 5.0.

cold seal failures as demonstrated by Fig. 10a built based on FEA simulation with various cooling rates. It is evident that the leakage temperature greatly increases at higher rates of cooling. The seal detaches from its substrate at temperatures above the T_g when the cooling rate of 1 °C/s is applied. It can be understood qualitatively as follows. As the rate of cooling grows, the ability of HNBR to recover and compensate for the thermal shrinkage becomes more and more reduced. The recovery is a time (and temperature) dependent process [18] and the time window required for the seal to recover the thermal contraction becomes smaller and smaller with cooling in the transition and glassy regions. Therefore, the condition for the seal failure would be:

$$\dot{\varepsilon}_r \lessapprox \alpha(T)\dot{T} \tag{6}$$

where ε_r is the recoverable strain. The results of the FEA simulation also depend on the coefficient of friction (CoF) used as demonstrated in Fig. 10b. However, the sensitivity to the variation of CoF is not as substantial as the sensitivity to the cooling rate. Furthermore, a rather high friction is to be expected due to the adhesion and "locking" of the frozen elastomer between the steel asperities, especially in the roughest sealing surface.

The actual cooling rate of −0.01 °C/s achieved in the flange experiments is used in further analysis and comparison with the experimental leak data. The predicted seal failure temperature is plotted against the initial compression of the seal together with the experimental leak data for the 2 studied compounds in Fig. 11a and in Fig. 11b. The simplified FEA model is seen to capture the onset of air leakage in HNBR seals against the surface after grinding at temperatures below the T_g quite well, considering the data scatter and the assumptions used in the modelling approach. The difference between experimental and predicted leakage temperatures can also be attributed to quality of the data fitting with 13 Prony elements (maximum in Abaqus) and also cold adhesion phenomena.

It has been found above and in [21] that the adhesion bond between HNBR seal and its steel substrate might break at low temperatures due to thermal stresses in elastomer at the interface leading to the premature onset of air leakage. The adhesion of the HNBR O-ring compressed at ambient temperature to a rigid substrate is rather small (the pull-off force per unit length $f_{adh} \approx 0.04$ N/mm) at this temperature, however it is found to grow with cooling [21]. The effect is strongest for smooth and clean surfaces, whereas contaminated or rough surface might reduce the adhesion significantly. This difference can reach one order of magnitude (e.g. $f_{adh} \approx 0.2$ N/mm for roughened HNBR vs $f_{adh} \approx 1$ N/mm for clean and smooth HNBR [21]). The thermal stresses are generated in the elastomer rings due to thermal contraction both in radial and circumferential directions (the O-ring cross section and the circumference decrease with cooling). As soon as the normal or shear stresses exceed the adhesion strength at a critical temperature T_{crit}, the detachment of a glassy elastomer takes place. In turn, a large leakage might immediately develop since the

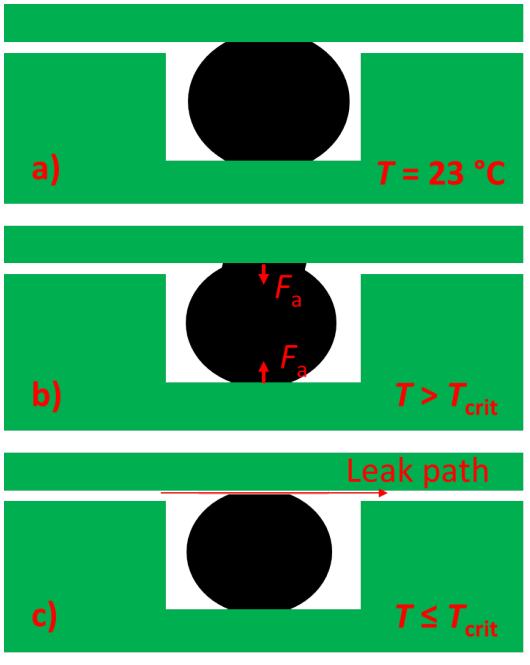

Figure 12: Schematic of the O-ring compressed in a flange joint a) at room temperature, b) cooled down to a low temperature (rubber-steel adhesion increases with cooling down to T_g), c) cooled down to the critical temperature ($T_{crit} < T_g$) at which debonding and subsequent leakage occur.

deformation field in the elastomer seal is frozen-in in the initial compressed state (i.e. it has a negligible recovery), as schematically illustrated in Fig. 12. The leak will be sustained if the seal is not able to recover within the experiment time, as most likely the case for with our leakage tests below T_g. Only external heating can help the elastomer to recover and close up the gap between the HNBR seal and its counter-surface.

A quantitative estimation of the thermal stresses in the direction orthogonal to the contact area and its effect on adhesion-connected seal failure temperatures can be made. The condition for the adhesion bond breakage is

$$S > S_{adh} \tag{7}$$

where the normal thermal stress $S = E\alpha\Delta T$ and the bond strength $S_{adh} = F_{adh}/(2aL_y) = f_{adh}/(2a)$. Hence, the temperature interval that the adhesion bond in glassy elastomer can sustain without failure (assuming no recovery) is

$$\Delta T = \frac{f_{adh}}{2aE\alpha} \tag{8}$$

Consider two limiting cases of weak and strong cold adhesion measured using unfilled HNBR O-ring sections [21], i.e. the pull-off force of 0.2 N/mm and 1 N/mm respectively in the case of 10 % initial compression. Thus, using the glassy modulus E of 2 GPa and $\alpha \approx 8 \times 10^{-5}$ °C^{-1} the lower and upper bounds of ΔT are ≈ 1.2 °C and ≈ 6 °C. Since f_{adh} increases with $\sqrt{a}$ (or $\approx \delta^{1/4}$) [21] while the contact area linearly grows with a (or $\approx \sqrt{\delta}$), it can be concluded that the adhesion bond might fail earlier (at lower ΔT) at higher compression ratios δ. The opposite is of course true at lower δ, e.g. 5 %. Similar observations can be made taking the elastic modulus (f_{adh} scales with $\sqrt{E}$ [21], while the thermal stress has a linear relationship with E).

The results also signify the effect of the thermal contraction of static seal material at the point where the frozen seal cannot recover within the experimental time scale. The importance of the elastomer thermal contraction at and below T_g is much higher than estimated before [29]. It is clear that the CB filled HNBR seals with the coefficient

of thermal expansion $\alpha \approx 6 \times 10^{-5}\,^{\circ}\mathrm{C}^{-1}$ in the glassy state yielded better cold leakage performance than the unfilled counterparts with $\alpha \approx 8 \times 10^{-5}\,^{\circ}\mathrm{C}^{-1}$, in spite of the inferior cold-recovery properties of the filled HNBR [18]. This is also supported by the experimental data of the sealing force decay which is significantly lower in CB filled HNBR seals. Therefore, having an elastomer with a small CTE (ideally $\leq 1 \times 10^{-5}\,^{\circ}\mathrm{C}^{-1}$ for contact with steel counter-parts) would be very beneficial for sealing applications where permanent or periodic exposure to temperatures reaching the glass transition and below is foreseen.

5. Conclusions

Cold performance of hydrogenated nitrile butadiene rubber (HNBR) O-rings at various compression is studied using low (1 bar) pressure difference. When cooling down to temperatures below the glass transition point T_g of HNBR ($-23\,^{\circ}\mathrm{C}$), an abrupt increase of air leakage ($> 10^{-2}\,\mathrm{cm}^3/\mathrm{min}$) is observed. The experimental results demonstrate that the seal failure temperatures are affected by surface finish conditions, variation of the compression ratio of the seals and additions of carbon black (CB) in the HNBR. The seal compression force is also found to decrease with cooling and the rate of the compression force decay depends on the CB content. In addition, an abrupt increase of compression force followed by a sudden increase of the leak rate in HNBR seals was observed at low temperatures $< T_g$. This effect is believed to be caused by failure of the HNBR-substrate adhesion bond induced by thermal shrinkage of the elastomer. The origin and conditions of the cold adhesion and its failure is explained in our separate publication [21].

The main reason for the seal failures is believed to be detachment of the elastomer seals from their mating sealing parts due to a) breakage of the adhesion bond induced by the elastomer thermal contraction in case of a rather strong adhesion bond and negligible recovery of the HNBR below T_g or b) due to the thermal contraction and the negligible recovery when the strong adhesion bond is not formed. It is shown that most of the cold failures can be modelled by the effective medium leakage theory and a simple finite element analysis (FEA) approach using thermo-mechanical material data the most important of which are the thermal expansivity and small-strain viscoelasticity of HNBR. Despite the worse recovery properties, the CB filled HNBR has a lower thermal expansion which results in a better retention of the sealing force and lower leakage temperatures if compared to the seals made of the unfilled HNBR. Hence, it can be inferred that better low-temperature serviceability in static joints can be achieved using elastomer compounds with low coefficients of thermal expansion ideally close to the one of the seal housing material.

No leakage was found in silicone grease lubricated seals which is likely to fill the gap between the HNBR and its counter-surface after the separation of HNBR seal from it in a cold environment. However, the effect of the grease and other industrial lubricants on cold adhesion is unclear and should be studied in more detail. Furthermore, the grease might squeeze out with time or might be washed away by service fluids, and, therefore, a different leakage behaviour should be expected in circumstances other than in this work.

6. Acknowledgement

This work was supported by the Research Council of Norway (Project 234115 in the Petromaks2 programme), FMC Kongsberg Subsea AS and STATOIL Petroleum AS, with the research partners Norwegian University of Science and Technology (NTNU) and SINTEF Materials and Chemistry. This work is also supported in part by EU COST Action MP1303. The authors would like to thank Dr. Peter Köllensperger and Ida Marie Eriksdatter Høiaas for the surface topography measurements at NTNU NanoLab and Boris Lorenz and Avinash Tiwari for DMTA measurements at FZ Jülich.

7. References

[1] Müller HK, Nau BS. Fluid sealing technology : principles and applications. New York: M. Dekker; 1998. viii, 485 p.
[2] Baranov, N. S., Sokolov V.E., Elkin A.I. Contact leaks through flange joints sealed by circular and square-section rubber seals (in Russian). Kauch. & Rezina 1982;8: 25-28.
[3] Alcock B., Peters T.A., Gaarder R.H., Jørgensen J.K. The effect of hydrocarbon ageing on the mechanical properties, apparent crosslink density and CO2 diffusion of a hydrogenated nitrile butadiene rubber (HNBR).Polymer Testing 2015; 47: 22-29.
[4] Salita M. Simple finite-element model of o-ring deformation and activation during squeeze and pressurization. J Propul Power. 1988;4(6):497-511
[5] Stevens RD, Thomas EW, Brown JH, Revolta WNK. Low temperature sealing capabilities of fluoroelastomers. SAE Technical Papers. 1990.

[6] Burnay SG, Nelson K. Leakage of transport container seals during slow thermal cycling to -40-degrees-C. International Journal of Radioactive Materials Transport. 1991;2:91-6.
[7] Streit G, Achenbach M, Kanters A. Sealability of O-rings at low-temperatures .1. Sealability without media influence at low-temperatures. Kaut Gummi Kunstst. 1991;44(9):866-70.
[8] Taylor KW. Performance Characteristics of Oilfield Proven Elastomers in Low-Temperature Seal Applications. 23rd Annual Offshore Technology Conference; 1991/1/1/; Houston, Texas. OTC: Offshore Technology Conference; 1991. p. 193-206.
[9] Weise HP, Kowalewsky H, Wenz R. Behaviour of elastomeric seals at low temperature. Vacuum. 1992;43(5):555-7.
[10] Warren P. Low temperature sealing capability of elastomer O-rings. Sealing Technology. 2008;9:7-10.
[11] Jaunich M, von der Ehe K, Wolff D, Voelzke H, Stark W. Understanding low temperature properties of elastomer seals. Packaging, Transport, Storage & Security of Radioactive Material. 2011;22(2):83-8.
[12] Grelle T, Wolff D, Jaunich M. Temperature-dependent leak tightness of elastomer seals after partial and rapid release of compression. Polymer Testing. 2015;48:44-9.
[13] Omnés B, Heuillet P. Leak tightness of elastomeric seal at low temperature: Experimental and fem-simulation. In:Constitutive Models for Rubber IX. ECCMR 2015: Proceedings of the 9th European Conference on Constitutive Models for Rubbers; 2015, p. 60914.
[14] Zhang B, Yu M, Yang HY. Leakage analysis and ground tests of the O-type rubber ring seal applied in lunar sample return devices. P I Mech Eng G-J Aer. 2015;229(3):479-91.
[15] Grelle T, Wolff D, Jaunich M. Leakage behaviour of elastomer seals under dynamic unloading conditions at low temperatures. Polymer Testing. 2017;58:219-26.
[16] Chen X, Bartos J, Salem H, Zonoz R. Elastomers for high pressure low temperature HPLT sealing. In: Offshore Technology Conference. OTC 2016: Proceedings of the Offshore Technology Conference; 2016, p. 382842.
[17] Akulichev AG, Alcock B, Tiwari A, Echtermeyer AT. Thermomechanical properties of zirconium tungstate/hydrogenated nitrile butadiene rubber (HNBR) composites for low-temperature applications. J Mater Sci. 2016;51(24):10714-26.
[18] Akulichev AG, Alcock B, Echtermeyer AT. Elastic recovery after compression in HNBR at low and moderate temperatures: Experiment and modelling. Polymer Testing. 2017;61:46-56.
[19] Akulichev AG, Alcock B, Echtermeyer AT. *Stress relaxation in carbon black reinforced HNBR at low temperatures* (in press) 2017, https://doi.org/10.1016/j.polymertesting.2017.08.023.
[20] Hornig R, Sunder J, Herr B. Static cold sealing force behaviour of amorphous HNBR materials. International Polymer Science and Technology. 2012;39:T1-T14.
[21] Akulichev AG, Tiwari A, Dorogin L, Echtermeyer AT, and Persson BNJ, *Rubber adhesion below the glass transition temperature: role of frozen-in elastic deformations* (submitted) (2017).
[22] Persson BNJ, Albohr O, Tartaglino U, Volokitin AI, Tosatti E. On the nature of surface roughness with application to contact mechanics, sealing, rubber friction and adhesion. Journal of Physics: Condensed Matter. 2005;17(1):R1.
[23] Persson BNJ. Theory of rubber friction and contact mechanics. J Chem Phys. 2001;115(8):3840-61.
[24] Yang C, Persson BNJ. Contact mechanics: contact area and interfacial separation from small contact to full contact. Journal of Physics: Condensed Matter.
[25] Persson BNJ, Yang C. Theory of the leak-rate of seals. Journal of Physics: Condensed Matter. 2008;20(31):315011.
[26] Bottiglione F, Carbone G, Mantriota G. Fluid leakage in seals: An approach based on percolation theory. Tribology International. 2009;42(5):731-7.
[27] Lorenz B, Persson BNJ. Leak rate of seals: Effective-medium theory and comparison with experiment. The European Physical Journal E. 2010;31(2):159-67.
[28] Persson BNJ. Fluid dynamics at the interface between contacting elastic solids with randomly rough surfaces. Journal of Physics: Condensed Matter 2010;22: 265004.
[29] Shubin SN, Freidin AB, Akulichev AG. Elastomer composites based on filler with negative thermal expansion coefficient in sealing application. Archive of Applied Mechanics. 2016;86(1-2):351-60.

Appendix A. Material properties used in FEA

Appendix A.1. Thermal expansion

Thermal expansion properties

T, °C	α, 1/°C	
	0 vol.% CB	20.4 vol.% CB
-50	0.000131	0.000104
-40	0.000141	0.000112
-30	0.000153	0.000119
-20	0.000167	0.000126
-10	0.00018	0.000129
0	0.000188	0.000131

Appendix A.2. Hyperelastic model parameters

Hyperelastic material model parameters

T, °C	C_{10}, MPa		D_1, MPa^{-1}	
	0 vol.% CB	20.4 vol.% CB	0 vol.% CB	20.4 vol.% CB
-20	0.715	1.595	0.001	0.00087
-10	0.754	1.644	0.001	0.00087
10	0.816	1.743	0.001	0.00087
23	0.863	1.807	0.001	0.00087

Appendix A.3. Viscolastic model parameters

Viscolastic material model parameters

0 vol.% CB		20.4 vol.% CB	
g_i	τ_i	g_i	τ_i
0.016446	3.88E-11	0.0091265	8.13E-15
0.084958	4.05E-10	0.077912	1.90E-13
0.12617	4.23E-09	0.10678	4.44E-12
0.18243	4.42E-08	0.17927	1.04E-10
0.24471	4.62E-07	0.27004	2.42E-09
0.24072	4.82E-06	0.21934	5.66E-08
0.080891	5.04E-05	0.073866	1.32E-06
0.013841	0.00052604	0.02312	3.09E-05
0.003442	0.0054945	0.0095157	0.00072235
0.0010951	0.05739	0.0059176	0.016879
0.00094397	0.59944	0.0046534	0.39441
0.00035235	6.2612	0.0030326	9.2161
0.00058876	65.398	0.011327	215.35

Appendix A.4. Time temperature superposition (WLF) parameters

TTS parameters

Material	T_{ref}	C_1	C_2
0 vol.% CB	293	4.3661	71.1068
20.4 vol.% CB	293	8.41	91.0144

A.5 Paper V

Thermomechanical properties of zirconium tungstate/hydrogenated nitrile butadiene rubber (HNBR) composites for low-temperature applications

A.G. Akulichev, B. Alcock, A. Tiwari, and A.T. Echtermeyer.
Journal of Material Science. 2016;51(24):10714-10726

Paper V

Is not included due to copyright